The momentum spectrum of nuclear active particles in the cosmic radiation

Hook, J. R.

THE MOMENTUM SPECTRUM OF NUCLEAR ACTIVE PARTICLES IN THE COSMIC RADIATION

by

J.R. Hook B.Sc., A.R.C.S.

A thesis submitted to the University of Durham in accordance with the Regulations for admittance to the Degree of Doctor of Philosophy.

Department of Physics
University of Durham

November, 1972

ABSTRACT

This thesis describes studies of nuclear active particles (NAPs) in the cosmic radiation over the momentum range 1-30 GeV/c. Both unaccompanied particles and NAPs in extensive air showers (EAS) are studied near sea level at Durham using an air-gap magnet spectrograph in conjunction with a neutron monitor.

Details are given of the design of the spectrograph, neutron monitor and associated equipment as used for measurements on unaccompanied NAPs (Chapter 2), and the techniques used for derivation of the momentum spectra from the basic data are described in Chapter 3.

The results, in the form of momentum spectra of unaccompanied protons and negative pions, and the limited analysis of NAPs in EAS are presented in Chapter 4 where they are compared with the results of other workers. Measurements of the momentum of NAPs in EAS were found to be difficult and the data are mainly concerned with the response of the neutron monitor to EAS.

A model of the propagation of cosmic rays through the atmosphere, which was mainly intended for predictions of the properties of large EAS, is described and used to predict the momentum spectra of unaccompanied particles at sea level. The results of this prediction are compared with the experimental data (Chapter 5) and the results of other model predictions (Chapter 6). It is shown that no single model, when combined with a reasonable spectrum of primary cosmic rays, can adequately explain all the data on unaccompanied particles at sea level. It is also shown that the spectra of high energy protons and pions are likely to be the sea level measurements which are most sensitive to the form of the primary cosmic ray spectrum.

PREFACE

The work described in this thesis was done by the author when a research student in the Department of Physics of the University of Durham under the supervision of Dr. K.E. Turver.

The author was involved in all aspects of the construction of the equipment and shared responsibility with his colleagues for the collection and initial reduction of the experimental data. The derivation of the momentum spectra of unaccompanied NAPs was done by the author.

Dr. J.C. Earnshaw was responsible for the development of the model used here but the author was entirely responsible for the prediction of the spectra of unaccompanied particles at sea level.

Preliminary results of the experimental measurements have been reported at the International Conferences on Cosmic Rays held in Budapest (1969) and Hobart (1971).

C O N T E N T S

CHAPTER ONE

INTRODUCTION

1.1 General Introduction

The primary cosmic radiation incident on the Earth's atmosphere is now known to consist of atomic nuclei (predominantly hydrogen, but including nuclei of larger atomic mass numbers), electrons and positrons, neutrinos, and electromagnetic radiation covering the whole frequency spectrum from radio-waves to high energy γ-quanta. Studies of these components to date have yielded information on the structure of the Solar System, the Galaxy and the Universe as a whole. The energies of the charged particle component of the primary radiation range from less than 1 GeV up to a maximum, at present, of $\sim 10^{10}$-10^{11} GeV. These charged particles interact with the galactic magnetic field so that all information concerning the original direction of the lower energy particles, and hence their source, is lost; the effect is less important at higher primary energies. An obvious source for these particles is the Sun, and indeed there is a good correlation between the intensity of the low energy nuclei and solar flares, indicating that the Sun is in fact a source of such atomic nuclei. However, no known stellar process can accelerate particles to the highest energies observed, and so there must be some other origin for the nuclei of energy in excess of $\sim$10 GeV.

Various theories, which predict the energy spectrum and mass composition of the primary nuclei, have been proposed to explain the origin of the nuclear component; a recent example being the pulsar model of Gunn and Ostriker, 1971. Hence it is of considerable importance to know these parameters as accurately, and over as wide a range of energy, as possible. Up to energies of $\sim 10^{13}$ eV it is feasible to make direct cmeasurements on the primary nuclei using balloon - or satellite - borne equipment, but at higher energies the flux of particles is so low that the atmosphere must be used to magnify the effect of individual particles by means of the showers of secondary particles produced.

1.2 Cosmic Rays in the Atmosphere.

When a primary nucleus is incident on the Earth's atmosphere it interacts with the nucleus of an "air molecule", breaking up into its constituent nucleons, and loses energy which is used in the production of a number of secondary particles. Although there is evidence for the production of a small proportion of kaons and baryon-anti-baryon pairs, the majority of the particles are charged and neutral pions. These secondary particles, together with the fragments of the primary nucleus, then either decay or interact, leading to a cascade of particles through the atmosphere, giving rise to the various components of the cosmic radiation observed at sea level. Neutral pions decay into two photons which initiate electromagnetic cascades forming the "soft" component (which is strongly attenuated by $\sim$ 10cm of lead), while muons, from the decay of charged mesons, and surviving nuclear-active particles make up the "hard", or penetrating, component. Muons are the most commonly studied sea level particles, mainly because they are the most intense and easily identified component, but more information on the primary radiation should be obtained by studying all types of particles, i.e. muons and nuclear-active particles, together.

During their passage through the atmosphere, and at their point of production, the secondary particles are scattered about the direction of the trajectory of the primary particle. Thus the effect of the primary particle may be detected at large distances from its projected impact point on the Earth's surface although much information concerning the nature of the primary particle is lost.

There are so few surviving particles at sea level from the primary particles of energy less than $\sim 10^4$ GeV that only one will be observed in a detector of a given area. These constitute the "unaccompanied" cosmic rays. If the primary particle is of an energy $\gtrsim 10^4$ GeV, sufficiently large numbers of particles survive so that coincident signals can be obtained from separated charged particle detectors. Such events are known as extensive air showers (EAS), and the collecting area from a small number of reasonably

sized detectors enables the arrival of higher energy primary particles to be detected at acceptable rates.

1.3 Simulations of Cosmic Rays in the Atmosphere

In order to obtain useful information about the primary particles it is necessary to relate the results of observations low in the atmosphere to the energy and type of the primary particle. To do this a model of the propagation of cosmic rays through the atmosphere must be formed and used, together with assumptions about the primary particles, to predict the properties which are measured. Then, on the basis of the comparison between the predictions and the observations, the validity of the assumptions about the primary particles may be checked. The model can be used in this way only if there is confidence in the accuracy of the representation of high energy nuclear interactions. Hence the model must be constructed using the best data currently available on nuclear interactions and then tested as extensively as possible. Some of the data which can be used for testing the model are the sea level momentum spectra of unaccompanied particles and observations on small EAS.

In order to test the model satisfactorily the experimental data on, for example, the unaccompanied cosmic rays at sea level, must be well known. This is so in the case of the momentum spectrum of unaccompanied muons which has been extensively studied, e.g. Hayman and Wolfendale, 1962, Allkofer et al., 1971. However, there have been only two measurements of the spectrum of protons, over a range of momentum at momenta greater than 1 GeV/c (Mylroi and Wilson, 1951, Brooke and Wolfendale, 1964), and only one measurement of charged pions at sea level (Brooke et al., 1964b). This paucity of measurements of these components means that the conclusions from comparisons of the predictions of models with the observed data must be restricted.

Several different models for cosmic ray propagation through the atmosphere have been developed recently, e.g. Bradt and Rappaport, 1967, Jabs, 1968, and O'Brien, 1971. Jabs and O'Brien developed their models

mainly in attempts to explain the observed properties of unaccompanied cosmic rays in the atmosphere, and used numerical techniques to solve the differential equations set up to describe the diffusion of the various components through the atmosphere. O'Brien obtained satisfactory agreement between his predictions and the experimental measurements, but Jabs was unable to explain simultaneously the spectra of muons, protons and pions. Thus there is not, at present, agreement between predictions of the properties of unaccompanied particles from various models, which apparently contain no gross oversimplifications; further, in the case of unaccompanied protons and pions, there is a paucity of experimental data at sea level momenta greater than 1 GeV/c.

Bradt and Rappaport used a Monte Carlo technique to predict the properties of EAS arising from primary particles of energy $> 10^5$ GeV, and did not compare the predictions of their model with the unaccompanied cosmic ray spectra arising from primary particles of lower energy. They obtained reasonable agreement between their predictions and the existing measurements in EAS and also predicted that the ratio of the numbers of pions to protons in the nuclear-active component of an EAS could be related to the atomic mass number of the primary particle, a parameter of considerable importance which is difficult to determine.

1.4 The Present Work.

Following the work of Bradt, La Pointe and Rappaport, 1965, equipment was constructed to attempt to measure the properties of the nuclear-active component of small EAS, in order to estimate the primary mass composition. This proved to be an extremely difficult measurement to make and a brief report of the initial attempt was given by Hook et al., 1970. Since this report the equipment has been extensively modified and used, in addition, for measurements of the momentum spectra of unaccompanied nuclear-active particles near sea level, of which there have been few previous measurements.

At the same time a model of the progapation of cosmic rays through the atmosphere was developed intended mainly for predictions of the

properties of large EAS. However, as a check on the validity of this model, it was also used to predict the momentum spectra of unaccompanied cosmic rays at sea level, for comparison with the spectra measured in the present experiments and the previous predictions from the models of Jabs and O'Brien.

CHAPTER TWO

EXPERIMENTAL EQUIPMENT

2.1 Introduction

Measurements of the momentum spectra of nuclear-active particles (NAPs) in extensive air showers (EAS), and of unaccompanied protons and pions in the cosmic radiation near sea level have similar experimental requirements. A detector of large area and solid angle of acceptance is needed to obtain a useful rate of events, since the intensity of EAS of size $\geq 3 \times 10^5$ charged particles at sea level (of interest in this work) is approximately 2×10^{-7} $m^{-2} sec^{-1} ster^{-1}$, and the density of NAPs of energy >1 GeV at a lateral distance from the shower axis of, say, 10 m is only 0.45 m^{-2} (Greisen, 1960). Similarly, because of the low intensity of unassociated protons, for which previous measurements indicate fluxes at momenta >1 GeV/c of only ~ 1 m^{-2} $sec^{-1} ster^{-1}$, (Brooke and Wolfendale, 1964) and of single pions of $\sim 8 \times 10^{-2} m^{-2} sec^{-1}$ (Brooke et al., 1964a), a large detector is needed for statistically accurate studies of such unassociated NAPs.

A detector has been constructed for which rates of useful NAPs in EAS of ~ 1 day^{-1} and of unaccompanied NAPs of ~ 18 hr^{-1} were expected, neglecting losses due to inefficiencies in the detector. In this instrument the particle momentum was measured by determining the deflection of the particles in the field of a magnet. Since the particles of interest interact strongly, it was essential for the spectrograph to contain as little material as possible, and so an air-gap magnet was used in preference to a thick solid iron magnet. To obtain a large solid angle x area of acceptance the magnetic field must present a large area to the incident particles, and visual detectors capable of covering a considerable area are required. Neon flash tubes were used as visual detectors since they had previously been used successfully in large arrays (Hayman and Wolfendale, 1962, Earnshaw et al., 1967)

Nuclear-interacting particles were identified by the response of a neutron monitor to their interactions in the lead neutron-producing layer as used previously by Hughes et al., 1964. The neutron monitor (NM) was situated underneath the spectrograph and, to reduce the number of chance coincidences between charged particles and background neutrons, the sensitive time of the monitor was limited to within a few hundred μsecs after the passage of the charged particle. The multiplicity of neutrons detected in pairs of non-adjacent counters was recorded to assist in the identification of an NAP in shower events when more than one track was recorded in the spectrograph since the neutrons should be detected close to their point of production.

The equipment was operated initially for a period of 4 months in summer 1969 with the spectrograph triggered by small EAS which were detected by an array of 4 water Čerenkov detectors. From the results of this period of operation it was concluded that the rate of measurable NAPs in EAS was lower than expected due mainly to obscuration of the lower part of the spectrograph by the electromagnetic component of the EAS, and ambiguity in identification of the NAP. Hence it was decided to modify the equipment in an attempt to improve the rate of analysable NAP events, and, at the same time, to extend the measurements to the momentum spectra of unaccompanied NAPs.

In the attempt to improve the rate of measurable NAPs in EAS events the following modifications were installed:-

a) a wall of barytes-concrete bricks, of thickness > 4 radiation lengths, was placed around 3 sides of the lower part of the spectrograph, to reduce contamination by the electromagnetic component of the EAS,

b) the multiplicity of neutrons detected in each neutron counter was recorded separately, to reduce the ambiguity in NAP identification.

A diagram of the modified NAP spectrograph is given in figure 2.1.

To enable single particles in the instrument to be selected, trays of Geiger-Müller (GM) counters were installed at various positions

Fig. 2.1 The Modified Air Gap Spectrograph.

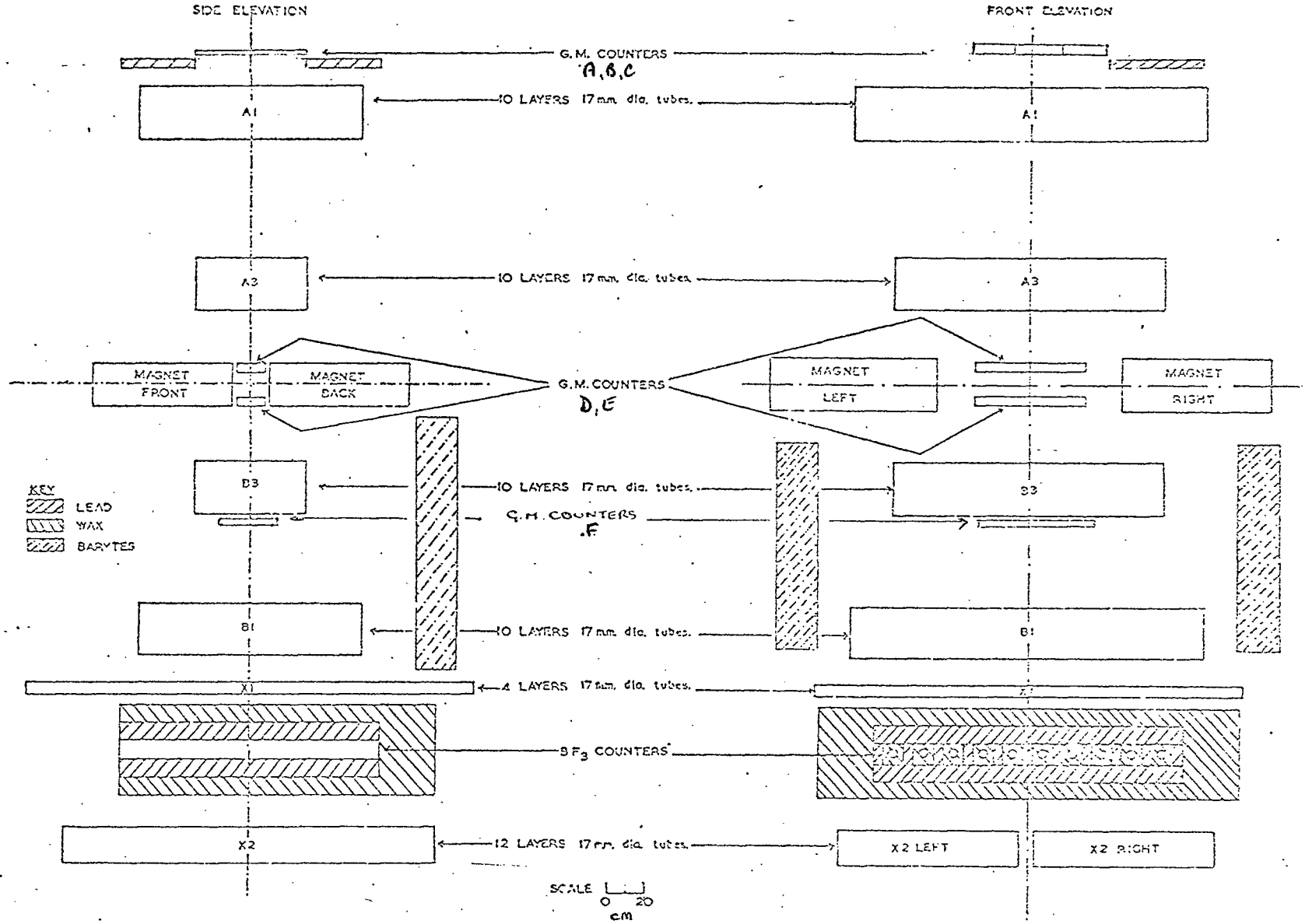

throughout the spectrograph. However, if all the coincidences between GM counters had been recorded, the percentage of useful NAP events would have been small since the ratio of unaccompanied NAPs to unaccompanied muons at sea level is approximately 1%.

It was necessary, therefore, to select, and then record, only those events which produced a response from the neutron monitor. Since the neutrons in the neutron monitor may be detected up to several hundred μsecs after the passage of the charged particle, it was essential that the particle tracks could be recorded after a similar delay. This was done by using the method developed by Brooke and Wolfendale, 1964, which utilised the "after-flashing" property of neon flash tubes. It had been observed by Coxell and Wolfendale, 1960, that, when a neon flash tube had flashed, there was a high probability of the tube flashing again if a further high voltage pulse was applied within a short time interval (~tens of millisecs). In this way a memory may be impressed on neon flash tubes by applying a high voltage pulse immediately a charged particle is detected, enabling the particle tracks to be recorded several msecs later. During the modifications, electromechanical shutters were placed in front of the cameras and, only when a particle with a response from the neutron monitor had been detected was the event recorded, by automatically opening the shutters and repeatedly pulsing the flash tubes. Equipment has been constructed to enable the water Čerenkov detector responses to be stored, and recorded digitally, if required, but has not been used during the work to be described in this thesis, which is confined to measurements of the momentum spectra of unaccompanied NAPs and attempts to obtain measurable fluxes of NAPs in showers.

The sequence of events was as follows for the spectrograph when operated to record single NAPs.

1) A single charged particle was selected, the neon flash tubes were pulsed and paralysis was applied to the system.

2) One or more neutrons were detected within 40 to 340μsecs of the passage of the charged particle and the multiplicities of neutrons detected by each counter were stored.

3) The camera shutters were opened and the flash tubes repeatedly pulsed.

4) The neutron multiplicities were recorded, fiducial lights on the flash tube trays were flashed and an identifying frame number was recorded on each film.

5) The films were advanced and the frame number was incremented by one.

6) The paralysis was removed.

If no neutron was detected operations 3-5 inclusive were not carried out.

2.2 The Magnet Spectrograph

2.2.1 The Air-Gap Magnet

a) Design and Construction

The form of construction of the air-gap magnet is shown in figure 2.2. This design was developed to incorporate materials available from earlier solid iron "picture-frame" type of magnets as used by O'Connor and Wolfendale, 1960, and Earnshaw et al., 1967. Pairs of iron plates from a "picture-frame" magnet were placed side by side and cut to the shape indicated in figure 2.2a. Twenty four of these pairs of plates were then placed on top of each other, and firmly bolted together, to form the main body of the magnet with a thickness of 30 cms. Coils of copper wire (C,D) were wound around the poles and, to increase the magnetic flux density in the air-gap, further coils of copper wire (A,B) were wound around the short arms of the main body of the magnet.

The magnet had a useful volume of $0.1 m^3$ with a maximum magnetic flux density of 0.45 tesla when a current of 30A was passed through the coils dissipating up to 12 kw of power, which was removed by forced-air cooling. To prevent overheating, and damage to the magnet, protective devices were installed which comprised:-

a) Plan

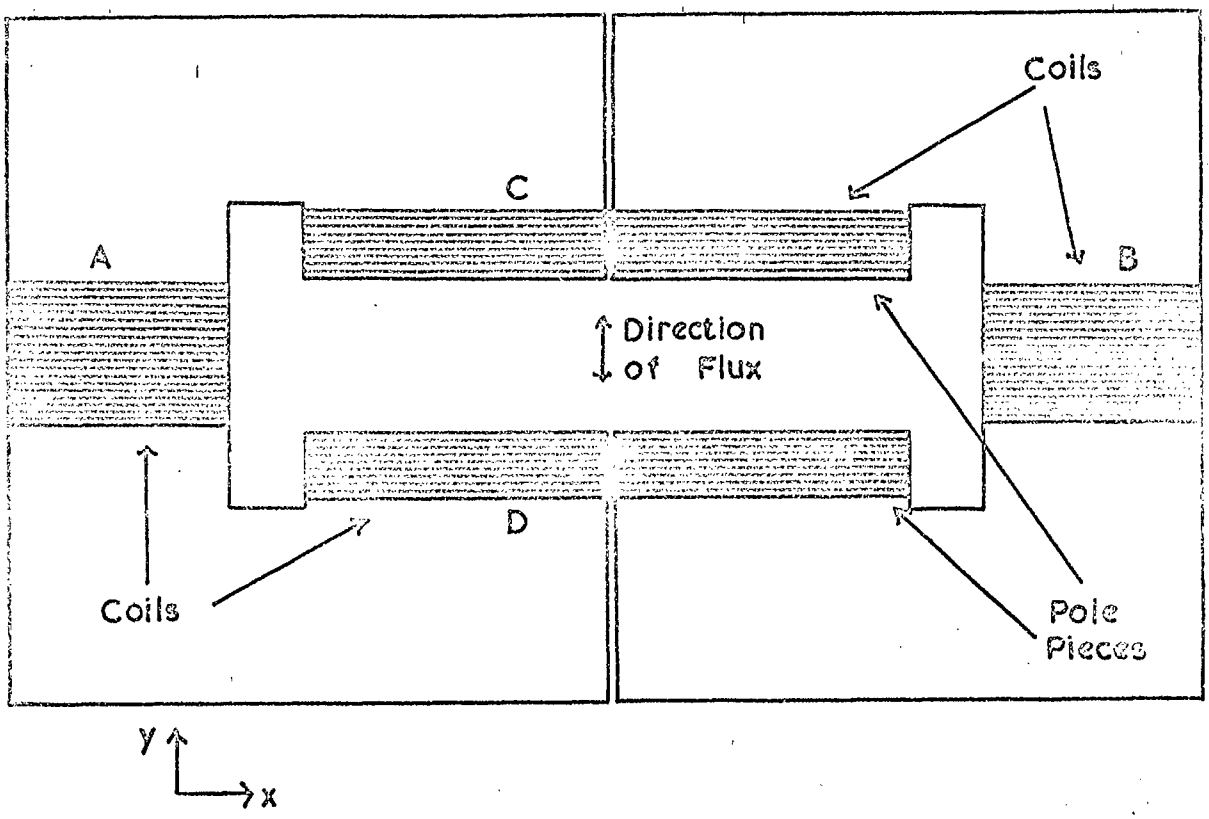

b) End Elevation

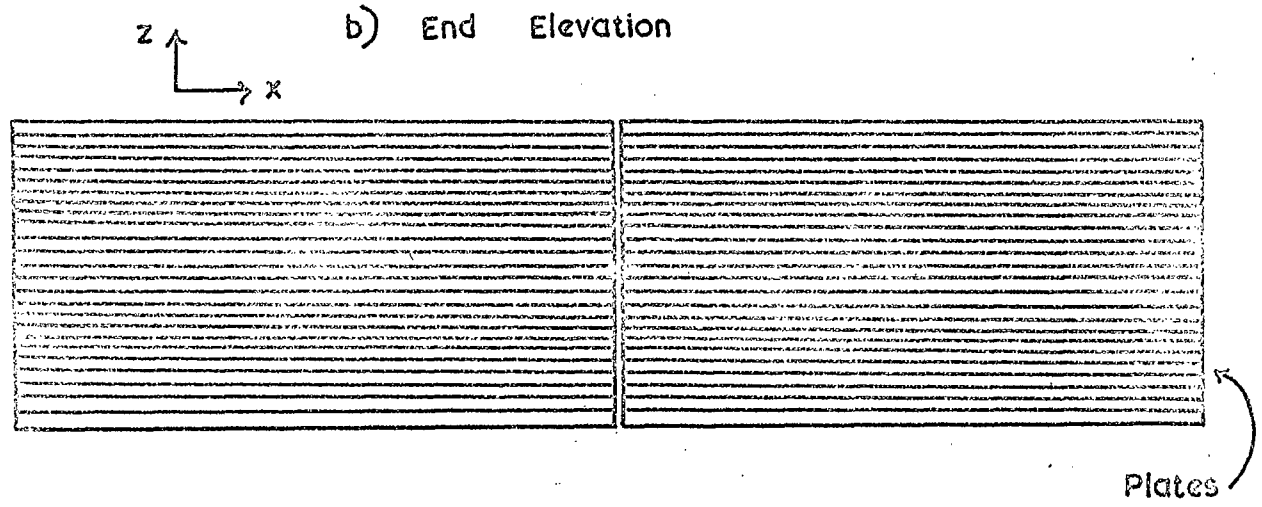

Fig 2.2 The Constructruction of the Air-Gap Magnet

(i) a pressure-operated switch placed in the outlet of the cooling ducts so that, if the cooling fan should fail, the current in the magnet would be reduced to zero,

(ii) thermal cut-out switches installed around the magnet coils, to switch off the magnet power supply should the coils overheat,

(iii) temperature-sensitive devices were placed in the input and output air-streams and the temperatures continuously monitored.

b) Operation of the Air-gap Magnet

Throughout the work described in this thesis the magnet was operated at a nominal current of 20A. The actual current was recorded continuously so that, if needed, the value of the precise current at any time was available. It was found that the current varied with the ambient temperature, but the maximum variation throughout the entire run was only $\pm$ 3% and has been ignored.

The polarity of the magnetic flux was changed daily to reduce any biasses which may arise if the acceptance of the spectrograph was not a symmetric function of the particle deflection.

c) Spatial Variation of the Magnetic Field

The magnetic flux density at each of a matrix of points in and around the air-gap of the magnet was measured with a calibrated Hall effect probe. The results are shown in figure 2.3 from which it can be seen that the flux density was uniform over a large proportion of the air-gap and that the variations over the regions of the air-gap which were used were negligble. Also marked on figure 2.3 are the positions of the lower and upper edges of the neon flash tube trays A3, B3 (see §2.2.2a). The magnetic field within these flash tube trays can be seen to be measurable, but it has been shown that the deflection of particles within the trays was negligble. From the measurements it was found that the value of $\int B d\ell$ was 250 kG cm for a current of 30A.

Fig 2.3 The Spatial Variation of the Magnetic Field.

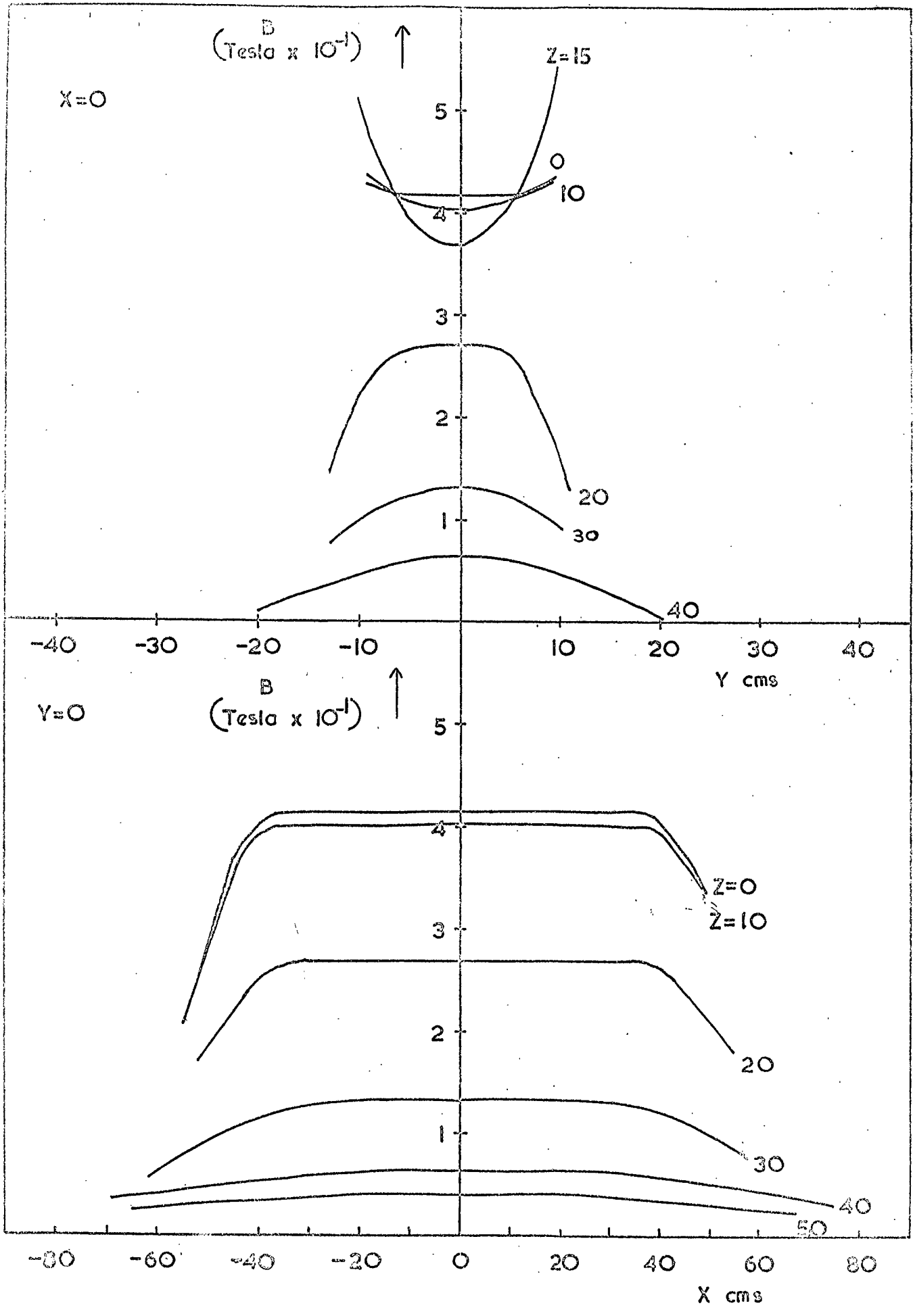

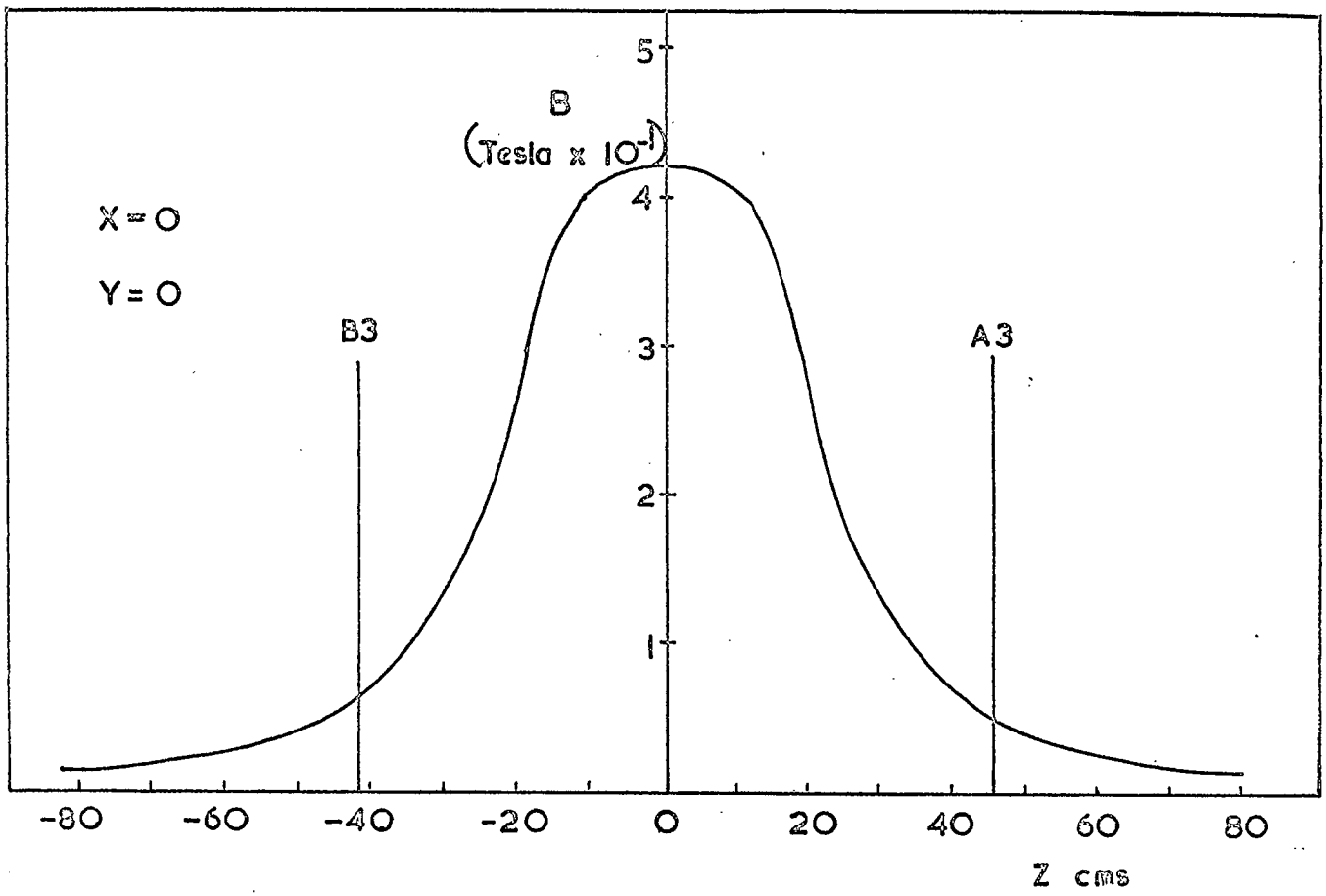
B
(Tesla x 10⁻⁴)
X = O
Y = O
B3
A3
5
4
3
2
1
-80
-60
-40
-20
0
20
40
60
80
Z cms

2.2.2 The Visual Detectors

Neon flash tubes, first developed by Conversi et al., 1955, and then by Gardner et al., 1957, had been used successfully in large spectrographs (Hayman and Wolfendale, 1962, Earnshaw et al., 1967) and have formed the large area visual detectors in this experiment. Unlike spark chambers they function in regions of high particle density without loss of efficiency due to preferential discharge of single tracks, and can readily be used in extensive arrays. The flash tubes used here were of mean internal diameter 1.6 cms, mean external diameter 1.8 cms, filled with neon gas to a pressure of 60 cms Hg and placed with their axes horizontal and parallel to the lines of magnetic flux.

a) The Momentum Measurement Flash Tube Trays

Four trays of accurately located neon flash tubes were used for the measurement of the deflection of the particle in the magnetic field; two trays above and two trays below the magnet (A1, A3 and B3, B1 respectively in figure 2.1). Reconstruction of the track in A1 and A3 led to the angle of incidence of the particle on the magnetic field, while the track in B3 and B1 gave the emergent angle. Each tray contained ten horizontal layers of neon flash tubes and eleven horizontal electrodes of aluminium sheet 0.5 mm thick positioned as shown in figure 2-4a. The vertical pitch of the flash tube layers within each tray was 3.2 cms and the centres of tubes in a layer were separated by 1.907 cms. The tubes in each layer were supported at their ends in slots accurately machined in rectangular duralumin tubing to ensure precisely known location. Trays A1 and B1 each contained 990 tubes of length 1.2m, while trays A3 and B3 each contained 760 tubes of length 0.6m. The layers were positioned horizontally so that the pattern of the flash tubes in each tray was approximately as shown in

figure 2-4a. This configuration led to a maximum layer efficiency of 84%; the layer efficiency being defined as the average number of flashed tubes per track expressed as a percentage of the maximum number. The maximum layer efficiency is the ratio of the internal diameter of the flash tubes to the horizontal pitch, i.e. 1.6/1.907, expressed as a percentage, and should be observed experimentally for flash tubes with an internal efficiency of 100%.

The measured capacitance of each of the flash tube trays was:-

A1	8000 pF
A3	2900 pF
B3	3550 pF
B1	11,000 pF

b) The "Neutron-Monitor-Screen" Flash Tube Tray

A tray containing 4 layers of close-packed neon flash tubes of length 2.5 m. (tray X1, figure 2-1) with aluminium electrodes after every second layer (see figure 2-4b) was placed immediately above the neutron monitor. This flash tube tray indicated the presence of charged particles which were incident on the neutron monitor, but which, not having passed through the spectrograph, could have led to incorrect identification of particles. Since no angular measurements were to be made with this flash tube tray, accuracy of location was not important and the simple close-packed configuration of tubes was acceptable.

c) The Sub-Monitor Flash Tube Tray

In order to observe the charged particles emerging from the neutron monitor, two trays of neon flash tubes were situated underneath the neutron monitor (X2, figure 2-1). Each tray consisted of 642 neon flash tubes (length 2.0m) in 12 close-packed layers with aluminium electrodes after every second layer (see figure 2-4b). These trays were used to measure the lateral position of a particle emerging from the neutron monitor, which, when compared with the expected position, allowing for scattering in the material of the neutron monitor assuming the particle to be a muon,

Fig. 2.4. The Disposition of Neon Flash Tubes

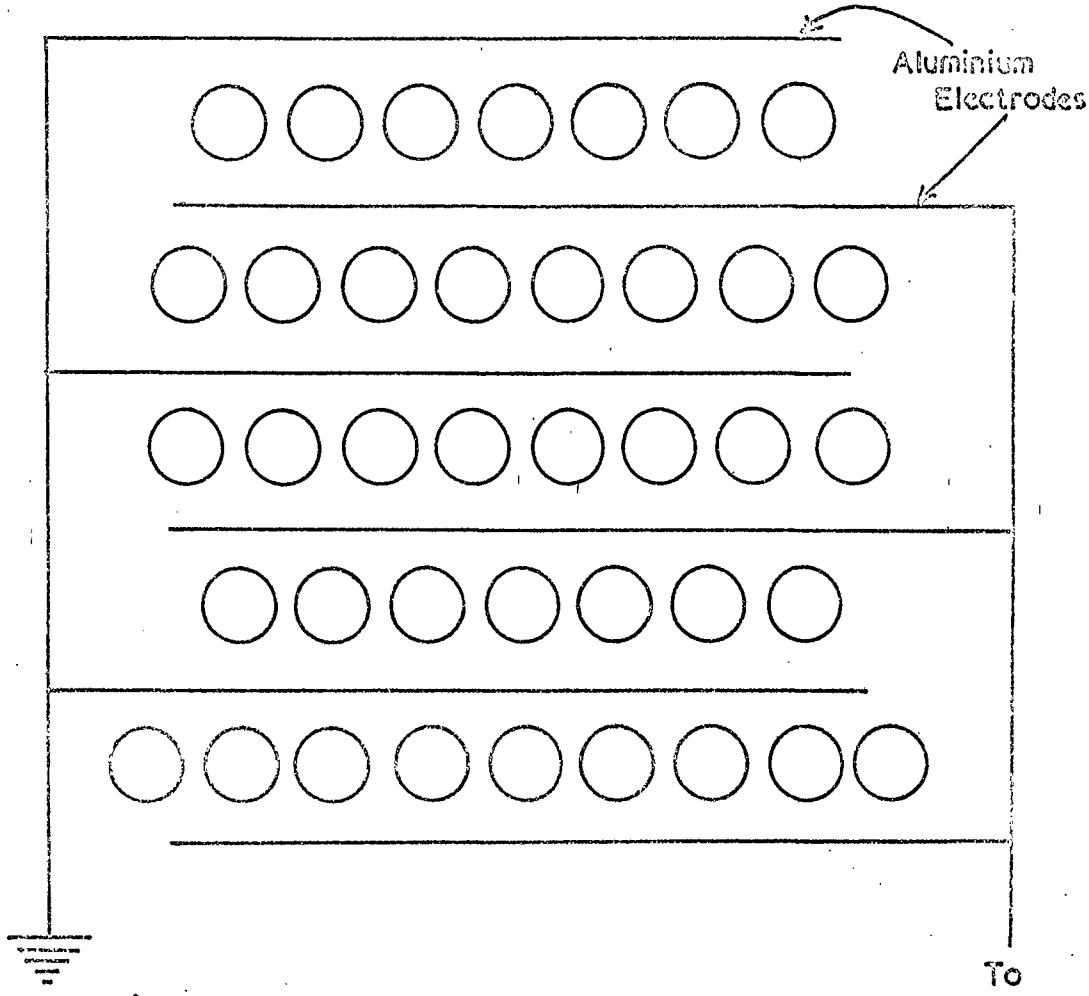

a) A Section of a Momentum Measurement Tray.

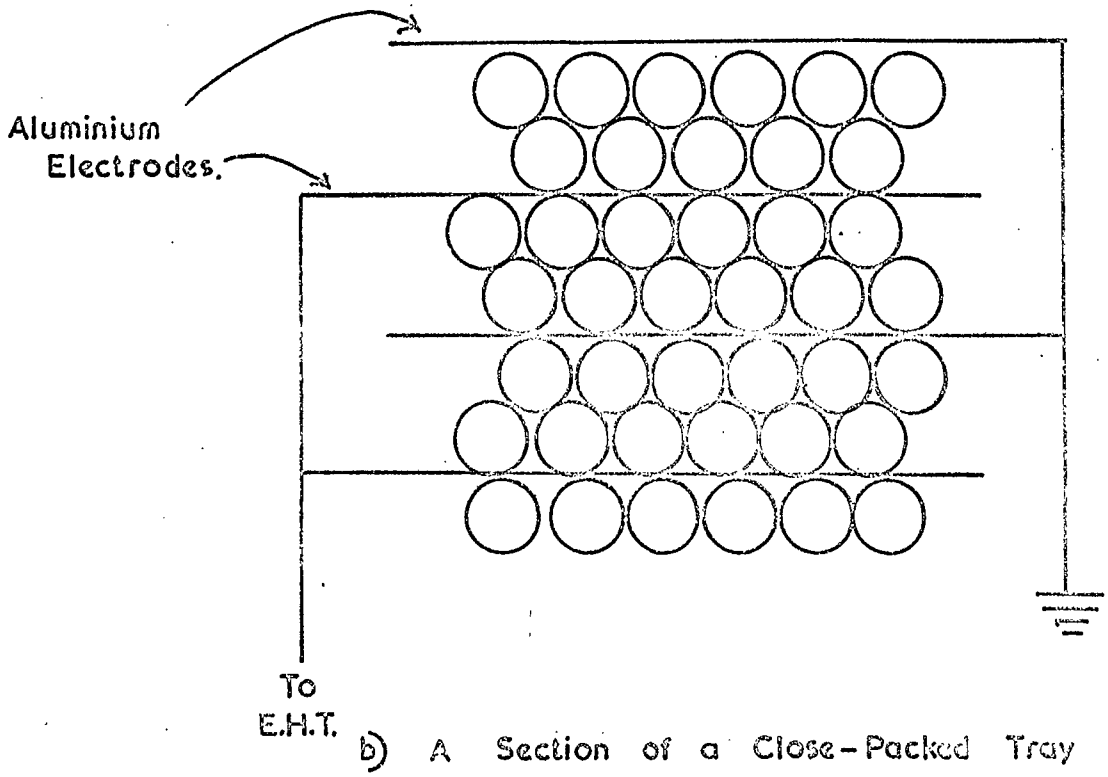

b) A Section of a Close-Packed Tray

enabled the incident particles to be identified (§3.4.3). Since the r.m.s. value of scatter expected at the level of the centre of tray X2 for a muon of momentum 3 GeV/c was ~10 mm, a location accuracy for the flash tubes of 1 mm, which could be achieved with the close-packed configuration, was satisfactory. The trays were positioned side by side, as close together as possible, although a gap about 10 cms wide remained between the tubes of the two trays. The effect of this gap on particle identification was allowed for in the analysis of the momentum spectra (§3.6.5)

d) The High Voltage Pulsing System

The high voltage pulse applied to the flash tube trays was generated by discharging a capacitor, C_p, through a thyratron and the primary winding of a high voltage pulse transformer, a technique used in the early applications of flash tubes. A diagram of the circuit used for pulsing the momentum-measurement trays (A1, A3, B3, B1, figure 2-1) is given in figure 2-5. The optimum values for the various resistors and capacitors in the circuit, and the advantages of including the mirror circuit, were determined empirically. A similar circuit (but without the mirror circuit) was used for the other flash tube trays.

The capacitor C_p was fully discharged each time the thyratron was triggered, and so, when multiple pulsing was required, a high voltage supply capable of recharging C_p with a time constant of ~10 msecs was needed. The use of an E.H.T. power supply capable of supplying the necessary average current of 0.32 amps was avoided by using a large storage capacitor, C_{ST}. The storage capacitor was continuously charged, to a potential of 8 kV, by the power supply through a 1MΩ resistor leading to a maximum charging current of 8 mA. When the thyratron was triggered C_p was discharged with a time constant of ~4 μsecs while C_{ST} was discharged with a time constant of 0.1 secs. So, when C_p was completely discharged and the thyratron had turned off, C_{ST} had lost a negligble amount of charge. Then C_{ST} transferred charge to C_p, with a time constant given by $R_1 C_{ST} C_p/(C_{ST} + C_p)$, (16 msecs for the values used) until the voltages of C_p and C_{ST} were equal. The final voltage reached, V_f, was $V_o C_{ST}/(C_{ST}+C_p)$, $(0.8V_o)$,

Fig. 2·5 The High Voltage Pulsing System.

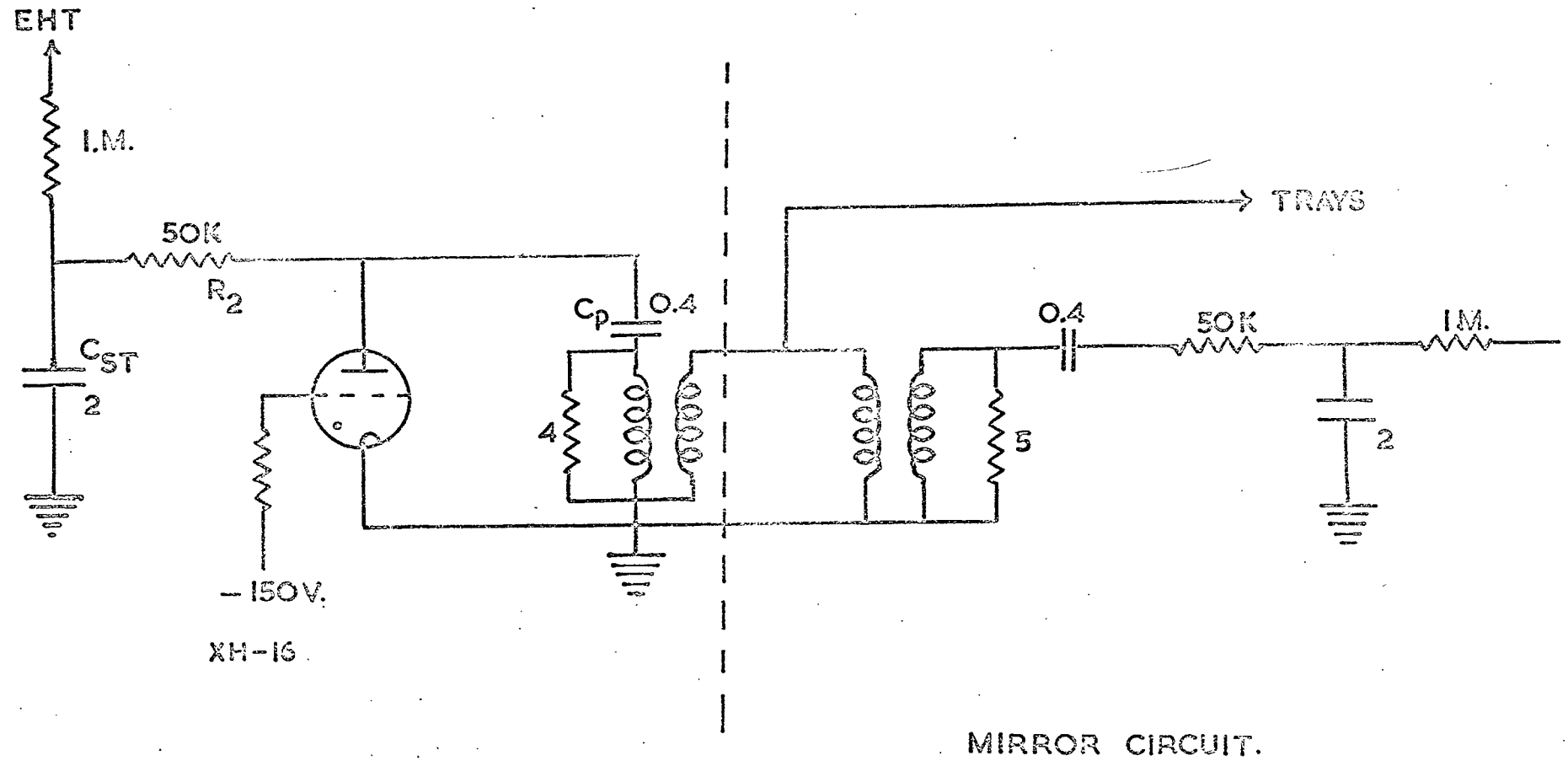

where V_o is the initial voltage of C_{ST}. Hence, V_f, is always less than V_o, although, if $C_{ST} >> C_p$, the reduction in voltage is small. This process was repeated after each pulse, leading to a decreasing E.H.T. for each successive pulse. The usual procedure was to pulse the equipment seven times, and on the completion of the seven pulses C_{ST} was left with ~26% of its initial charge and was recharged by the power supply with a time constant of 2 secs.

The low voltage (~4V) pulse from the control circuitry (§2.5) was amplified, sufficiently to trigger the thyratron, with the circuit shown in figure 2-6. A silicon controlled rectifier was triggered by the low voltage pulse, and the voltage pulse from the anode was inverted and matched to the grid of the thyratron by the pulse transformer.

e) Operational Characteristics of the Flash Tubes

The layer efficiency of the momentum-measurement trays was found to be 69% for protons which typically are minimum ionizing, when operated in the multiple pulse mode, with the shutters opening after the first pulse. When allowance was made for the geometry of the trays (see §2.2.2a), an internal efficiency of 82% was obtained. This figure is rather low, but there were additional losses of efficiency due to the finite time delay before application of the initial pulse to the flash tubes (~6μsecs), the non-unity probability of after-flashing, and the reduction in the effective aperture of the cameras by the shutters. An estimate of the latter two factors was made by triggering the system with cosmic ray beam muons and operating with the shutters, firstly, jammed open, and then removed. The first of these experiments removed the loss of efficiency due to the probability of after-flashing while the second allowed an estimate to be made of the effect of the shutters. From these experiments the probability of after-flashing was found to be ~0.95 per pulse while a reduction in layer efficiency of 5% was found to be caused by the shutters. Hence the true internal efficiency of the flash tubes was at least 91%

Fig. 2.6 The High Voltage Pulser Trigger Scheme.

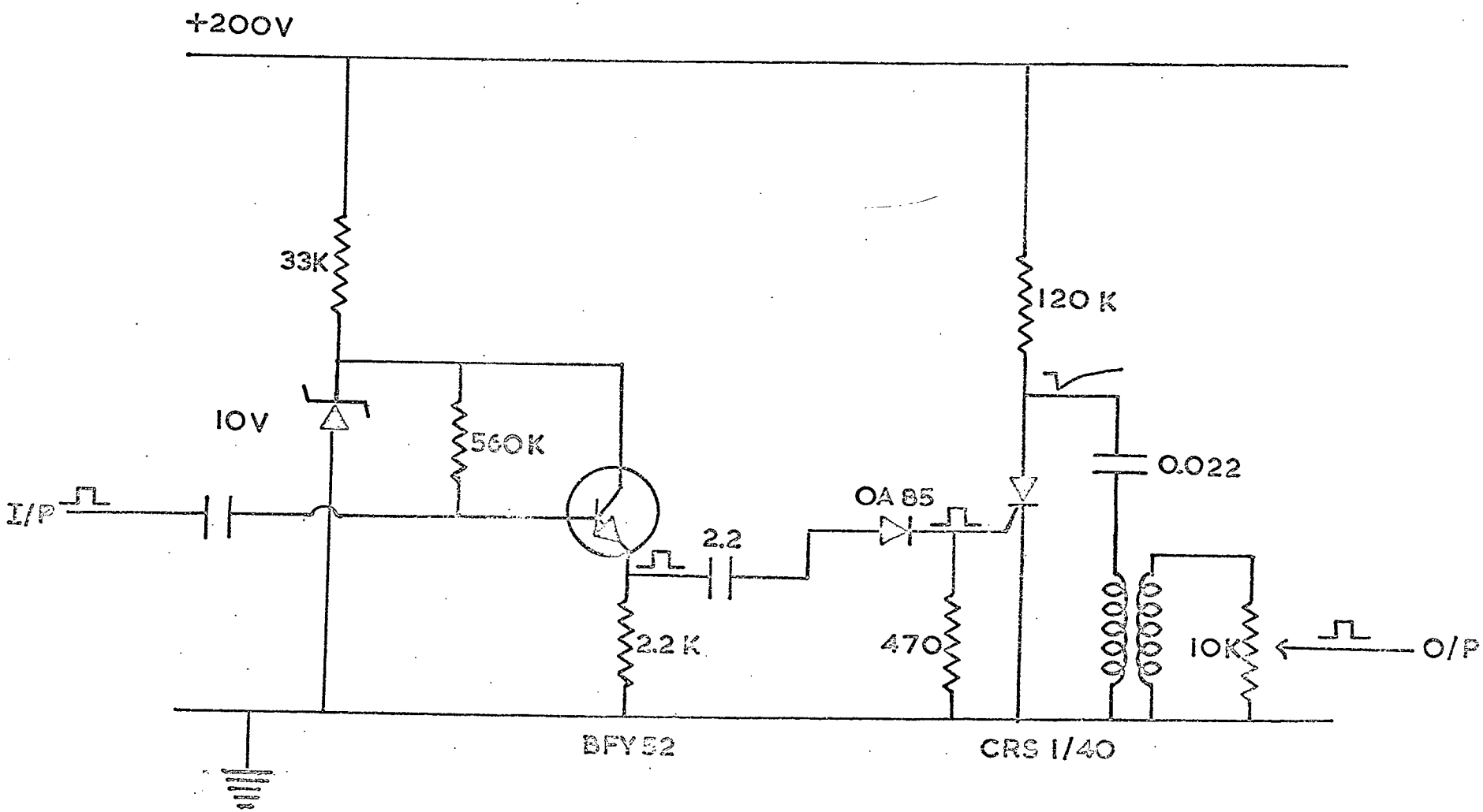

2.3. The Neutron Monitor

2.3.1 Introduction

The design of the standard neutron monitor adopted for studies of the low energy nucleon component of cosmic rays during the International Geophysical Year (I.G.Y.) was developed by Simpson, 1957, from the earlier arrangements of Tongiorgi, 1949, Simpson, 1949, Cocconi et al., 1950 Adams and Braddick, 1951, and Simpson, Fonger and Treiman, 1953. For a detailed discussion of neutron monitors, particularly their response to low energy nucleons (≤ 1 GeV) see Hatton, 1971.

In the standard monitor, evaporation neutrons, emitted from an excited nucleus produced in an interaction in a lead target, were detected through the reaction

$$^{10}B_5 + n \rightarrow {}^{7}Li_3 + {}^{4}He_2$$

using boron trifluoride (BF_3), enriched with the $^{10}B_5$ isotope, proportional counters of length 86.4 cms, diameter 3.8 cms and filled with BF_3 gas to a pressure of 45 cms Hg. The cross-section for this reaction follows a $1/v$ dependence (where v is the velocity of the neutron) and is $\sim$3820 barns for thermal neutrons. Since the mean energy of the evaporation neutrons is $\sim$2.5 MeV, the counters were surrounded by a moderating layer of paraffin wax to thermalise the neutrons and utilise the large cross-section. Neutrons produced in interactions in the atmosphere, and the surroundings of the NM, were excluded from the equipment by an outer layer of paraffin wax, which absorbed or reflected these neutrons. This layer also increased the counting rate of the NM by moderating, and reflecting back to the counters, some of the neutrons produced in the lead target. A lead target of thickness 13.5 cms (153 g cm^{-2} or 0.76 interaction lengths), an outer reflector of mean thickness 28 cms and an inner moderator of average thickness 3.7 cms were used in the standard I.G.Y. monitor. This neutron monitor responded to various components of the sea level cosmic rays, but predominantly ($\sim$80%) to interactions of low energy neutrons ($\sim$150 MeV). Evaporation neutrons are, however, also produced by protons, pions, extensive air showers, negatively

charged muons captured by Pb-nuclei and interactions of photons associated with muons of both charges.

In the present experiment an improved response to high energy charged particles was required in order to improve the detection efficiency of NAPs, especially those of typical energy ~10 GeV in EAS, and so a modified neutron monitor was used. It was also expected that the sensitivity of the multiplicity distribution of detected neutrons to the energy spectra of NAPs would be increased by the modifications and that measurements of the multiplicity distribution may be useful estimates of the energy spectra of NAPs in the range 1 - 150 GeV.

2.3.2. The Design of the Modified Monitor

Shown in figure 2-7 is the average number of evaporation neutrons, ν, produced per inelastic collision of an incident neutron of kinetic energy E_n, predicted from Monte Carlo simulations by Sheh, 1968, as a function of the thickness, t, of the lead target. It can be seen that ν increases with t and that the increase is greater for high energy than for low energy particles. Similar curves can be drawn for incident protons. Hence, to improve the response of the monitor to high energy particles, the average thickness of the lead target for vertical particles was increased from 13.5 cms to 23.3 cms (264 g cm^{-2} or 1.32 interaction lengths). Figure 2-8 shows the ratio of ν for this new thickness to that for the standard I.G.Y. monitor for incident neutrons and protons as a function of the kinetic energy of the incident particle. The increase in ν for low energy particles is smaller than that for high energy particles, and so the response to high energy particles should be enhanced.

It would be expected that the mean multiplicity of detected neutrons, defined as the mean number of neutrons, including the first neutron, detected within a given time of the detection of the first neutron, would be increased relative to a standard I.G.Y. neutron monitor, in the modified NM because of the increased ν. However, the thicker lead increases the number of negative muons which will be captured by Pb - nuclei and the number of neutron-

Fig. 2.7 The Average Number of Evaporation Neutrons produced per Inelastic Collision of an Incident Neutron of Kinetic Energy E_n as a Function of Lead Target Thickness (Shen (1968))

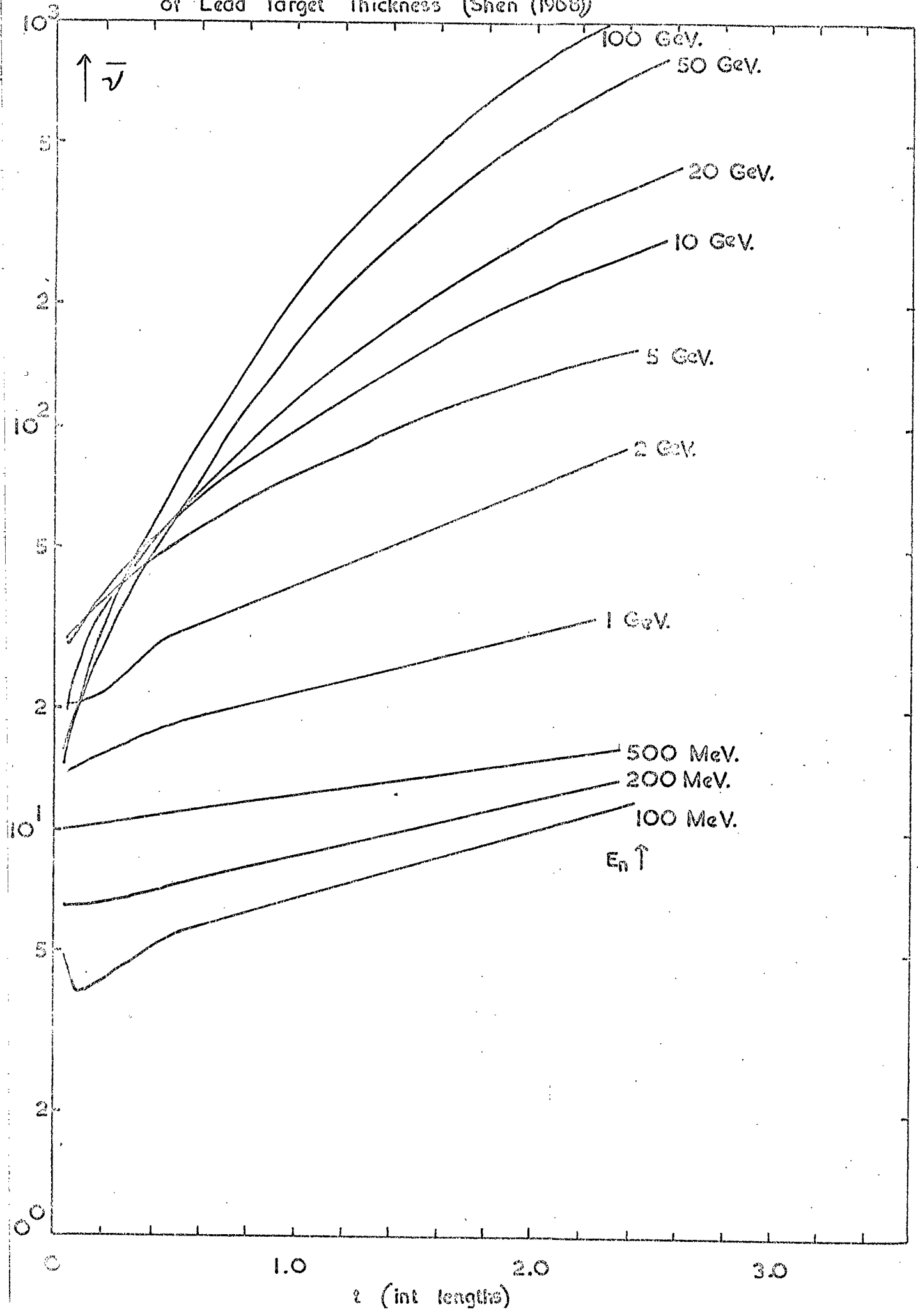

Fig. 2.8 Comparison of Average Number of Neutrons produced in a Standard I.G.Y. and the Modified Monitor.

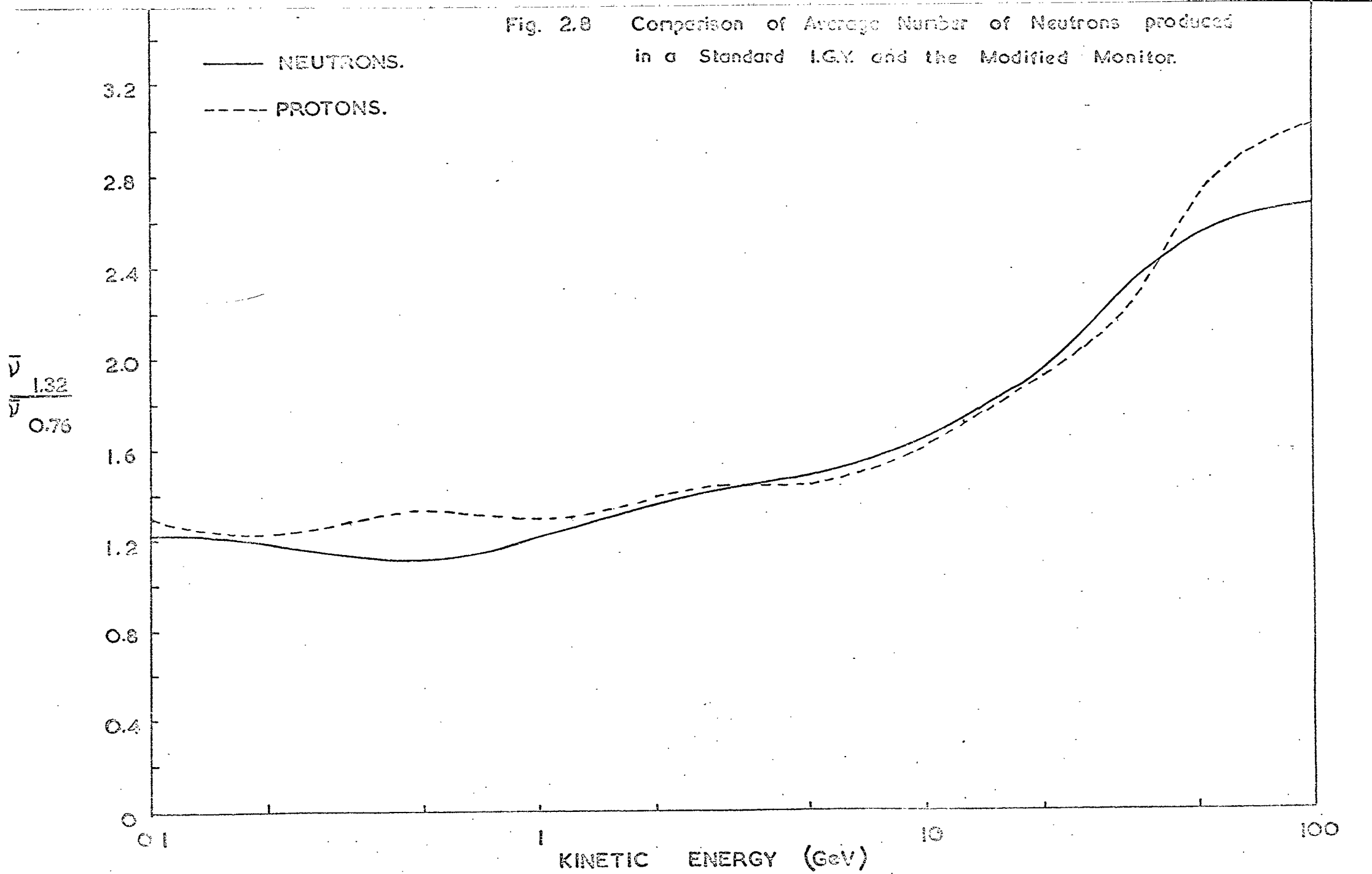

producing interactions of muons by a factor of ~2 compared with ~1.4 for the increased number of interactions from the other components. The mean multiplicity of evaporation neutrons produced in both these processes is very small (~2 for negative muon capture and ~9 for muon interactions) and will not be increased by the thicker lead. Hence, the increased contributions from these very low multiplicity processes will tend to reduce the mean multiplicity of detected neutrons. An approximate consideration of the expected performance of the present neutron monitor leads to a predicted mean multiplicity of 1.2. The mean multiplicity of the NM most similar in counter design, the Leeds, I.G.Y. neutron monitor was found to be 1.24 (Hatton, 1971) for a detection efficiency of 3%, which is reduced to 1.2 for a detection efficiency of 2%, this being more appropriate for comparison with the present NM since the sensitive times used were different. Thus it is expected that, although the rate of neutrons detected should be increased, the mean multiplicity of neutrons in the neutron monitor would not change much with respect to the Leeds I.G.Y. neutron monitor. The enhancement of the high energy response of the modified NM will only become apparent when the multiplicity distributions from interactions of high energy particles are considered.

In an attempt to increase the overall efficiency of the detection of thermal neutrons and the counting rate, the number, size and gas pressure of the thermal neutron detectors were increased. Ten cylindrical proportional counters (20th Century Electronics type 107 EB 70/50G) of diameter 5 cms and sensitive length 1.07m, filled with ^{10}B -enriched BF_3 gas, at a pressure of 70 cms Hg, were used. However, it should be noted that the anticipated increase in efficiency due to the increased diameter and gas pressure of the counters will be offset by the larger volume accessible to the evaporation neutrons due to the thicker producing layer. This reduces the density of the evaporation neutrons and hence the efficiency with which they are detected.

The thickness of the outer reflector of paraffin wax was reduced to 10 cms in the vertical direction, although a much greater thickness

was used at the sides and back. This reduced thickness was chosen so that the NM could be placed as close as possible underneath the flash tube trays of the spectrograph, in order to reduce the chance of background events caused by undetected charged particles. Adequate reflection of evaporation neutrons produced in the lead should be obtained with this thickness, but the attenuation of low energy neutrons produced in the atmosphere and the surroundings will not be complete. Neutrons with an energy of a few MeV should have an attenuation of ~5 and so will contribute more to the counting rate of this NM than to a standard I.G.Y. neutron monitor in which the attenuation is ~150. The multiplicity of evaporation neutrons produced by these low energy incident neutrons will be small, and their increased contribution to the counting rate will be another factor tending to decrease the mean multiplicity of detected neutrons discussed above.

In the normal mode of operation of a neutron monitor, the anodes of the proportional counters are electrically connected, and information concerning the location of detected neutrons, is lost. Since it was expected that the neutrons would be detected close to the point of production, a knowledge of the spatial location of a neutron, when detected, should aid the unambiguous identification of particles. The pulses from each counter were, therefore, recorded separately to provide such information.

2.3.3. The Proportional Counters

A block diagram of the electronic circuit used with each proportional counter is given in figure 2-9. A pulse transformer, with a centre-tapped secondary winding, was used to give two pulses, of opposite polarity, from the negative pulse of the counter. The turns-ratio of the transformer windings was chosen so that the effective resistance in the primary, when the pre-amplifier was connected, critically damped the circuit giving the optimum shape of pulse. The positive and negative pulses from the secondary of the transformer were fed into the inverting and non-inverting inputs, respectively, of a variable gain differential amplifier (S.G.S. type μA 702A). The amplified pulse, of negative polarity, was then discriminated

Fig. 2.9 The Proportional Counter Electronic System.

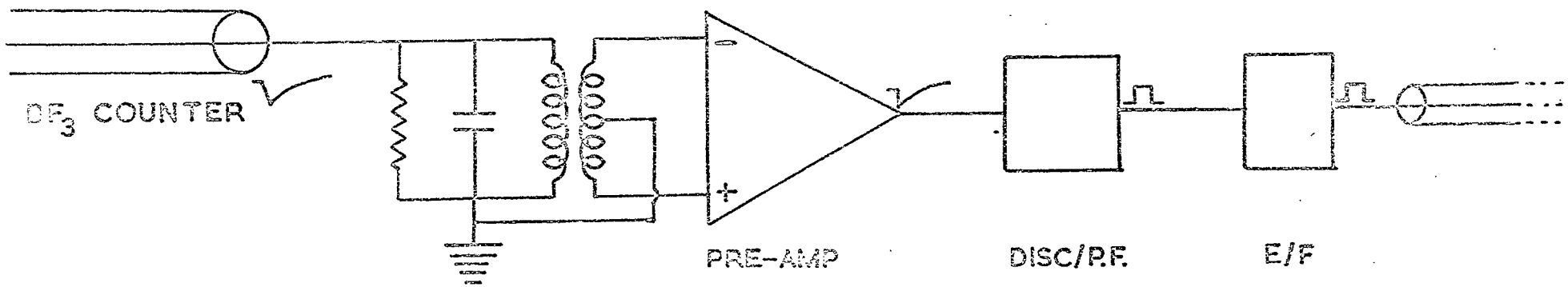

and shaped, in one operation, by an integrated circuit level detector (S.G.S. type μA 710A), connected as a pulse-former, which produced a positive square pulse of amplitude ~4V and duration~3 μsecs. This pulse was passed through an emitter-follower to a coaxial cable leading to the digital scaling circuits (§2.3.4). All the circuitry was enclosed in an earthed copper box to reduce the electronic pick-up from the high voltage pulse applied to the flash tubes.

All the proportional counters were operated from a common high voltage supply of -4.1 kV applied to the cathodes, and so the operating point of each counter was selected by varying the gain of the pre-amplifier. A pulse-height distribution from one counter, with the electronics disconnected, was measured (figure 2-10) and the rate of "genuine" neutrons deduced from these data. For each counter, the gain of the pre-amplifier was then adjusted until the rate of pulses from the discriminator/pulse-former unit equalled the rate of "genuine" neutrons. A similar technique was used to set up the edge counters where the counting rate was reduced relative to a counter in the centre of the monitor.

2.3.4 The Recording and Control Electronics.

When a neutron was detected by a proportional counter, a shaped pulse was transmitted along 68 Ω coaxial cable from the NM to the remote digital electronics. The digital electronics were required to provide a master pulse when one or more neutrons had been detected in coincidence with a charged particle and to record and display the number of neutrons detected in each counter. The pulses from each proportional counter were fed into individual identical circuits so that the neutrons detected by each counter were recorded separately.

Figure 2-11 is a diagram of the circuit used to provide the neutron coincidence signal. Each channel was gated by a long (~6 msec) pulse from an S.C.R. unit (figure 2-12), with the output normally grounded, to improve the rejection of pulses induced by the high voltage pulse applied to the flash tubes. This gate inverted the, initially positive, neutron

Fig. 2.10 The Pulse Height Distribution from a Proportional Counter.

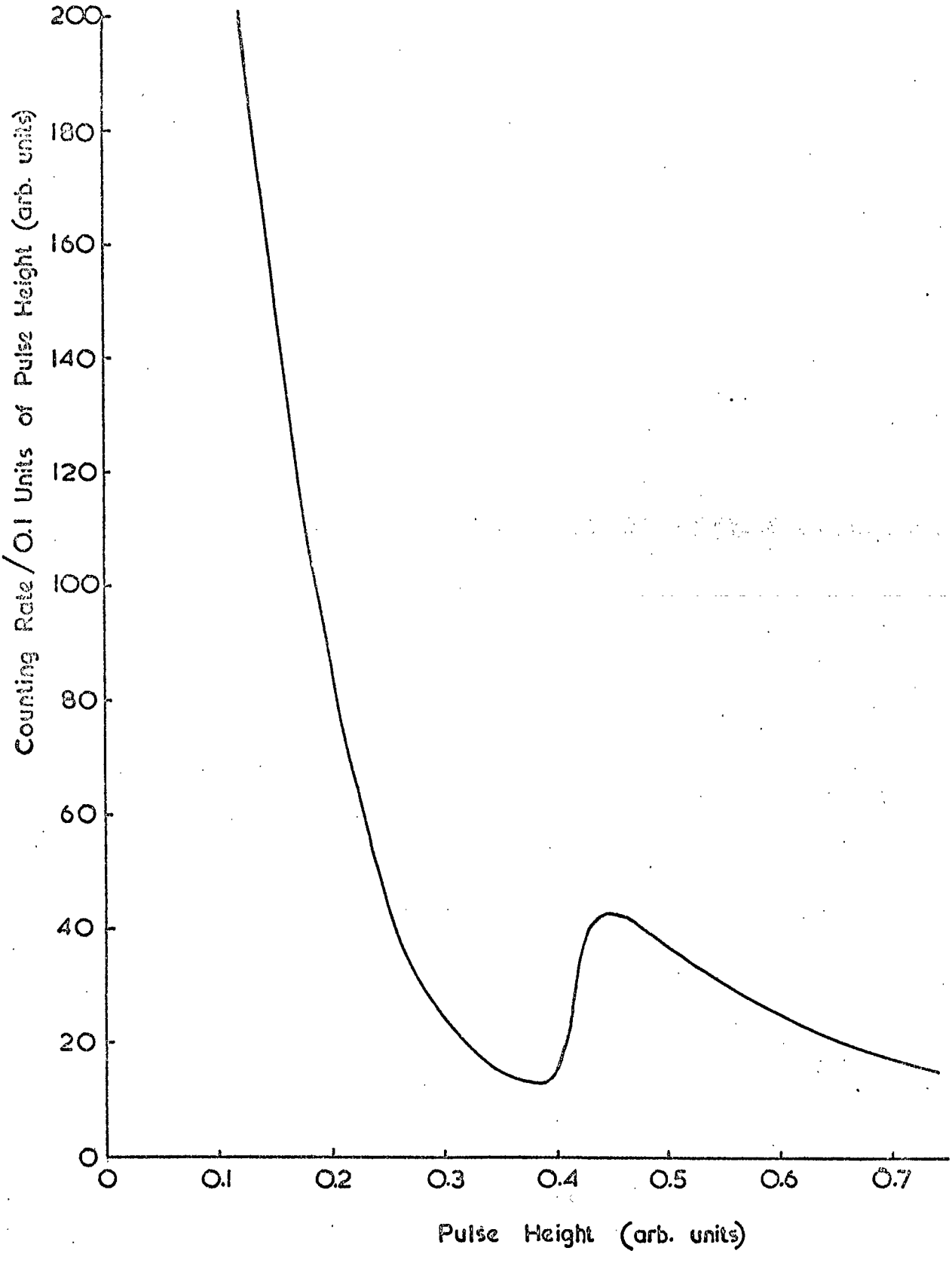

ig. 2.11. The Neutron Counter Event Selector.

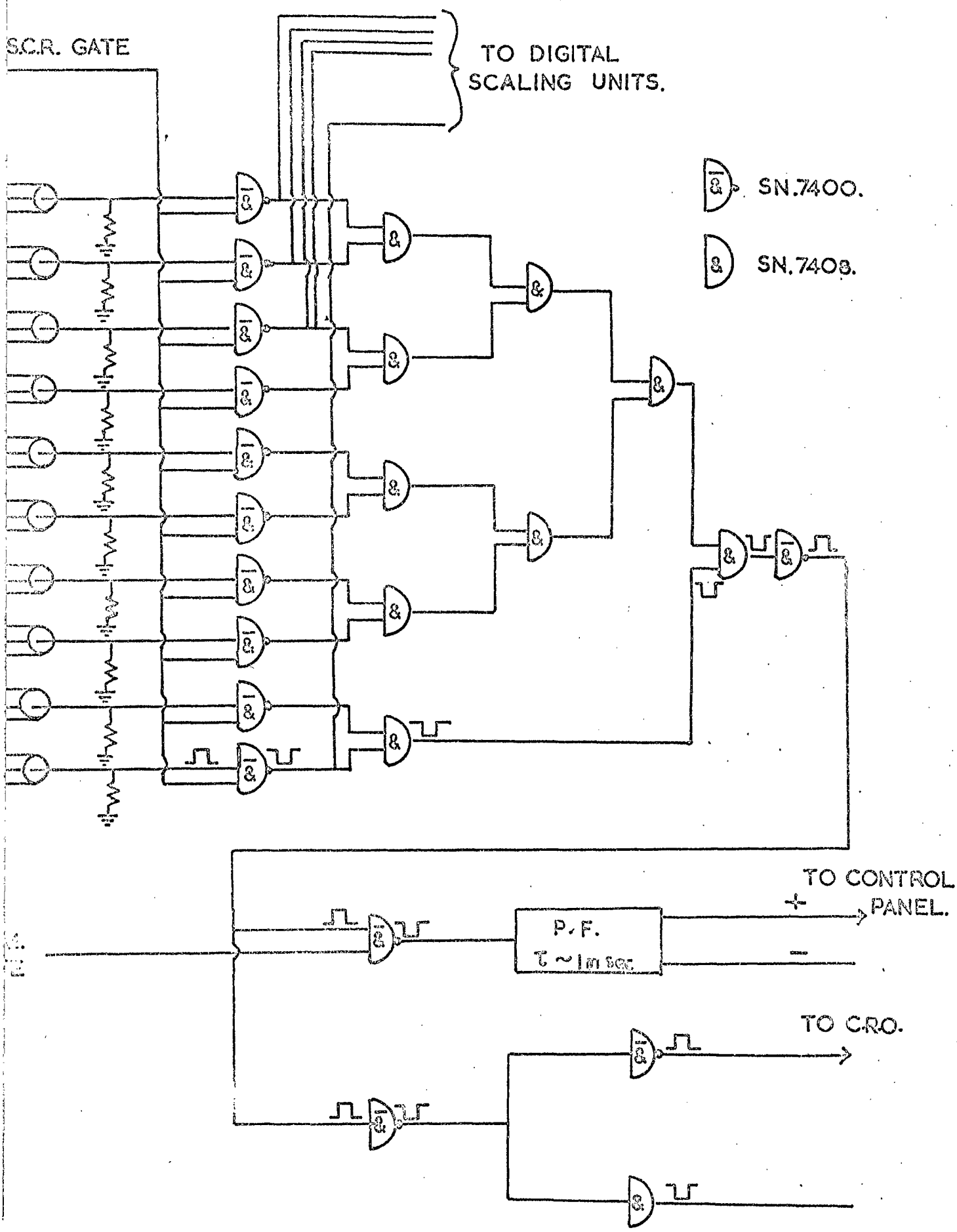

Fig. 2.12 The Neutron Detector S.C.R. Gating Unit.

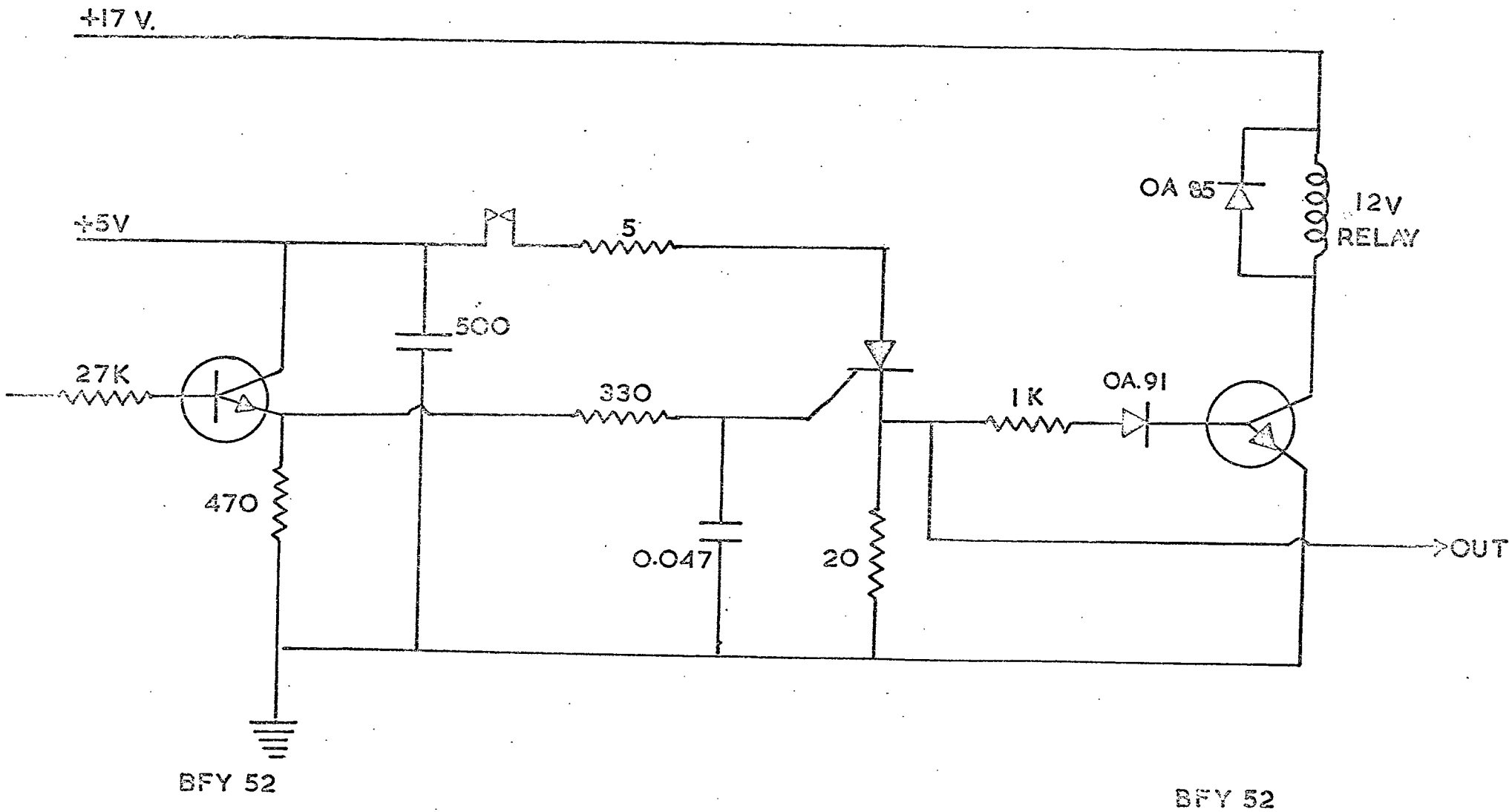

pulses and so "positive logic AND" gates were used to combine the pulses from all channels. This "added" signal was then gated by the "neutron monitor gate" (the NM gate) which was a positive pulse of accurately determined duration (300 μsecs) and delay (45μsecs) relative to the GM coincidence (see §2.4.4). If a neutron was detected within the duration of the NM gate, a pulse of length 1 msec was generated and sent to the control circuit (§2.5.1) to indicate a neutron coincidence. Also available from this circuit were positive and negative versions of the "added" signal ungated by the NM gate. The positive pulses were displayed on a cathode ray oscilloscope and photographed (see §2.7) as confirmation of the satisfactory performance of the NM.

Figure 2-13 is a diagram of the scaling unit of one channel. The pulses, after the S.C.R. gate, were inverted and then gated with the NM gate. Any pulses detected within the duration of the NM gate were counted by the 4-bit binary counter unambiguously up to a maximum of 15. Multiplicities M, greater than 15 were counted as M=15. The multiplicities in each of the channels were displayed in binary form using bulbs, situated on the spectrograph, which were photographed on the same frame as the flash tube information. Binary digit '0' was represented by an illuminated bulb, and so, since most binary digits were '0' most of the read-out system was tested every time an event was recorded.

The shaped pulses from each BF_3 counter were fed to ratemeters so that the counting rate of each of the counters in the NM could be continuously monitored and any significant change in the performance of any counter could easily be detected. The individual counter rates were checked at least twice daily, at the beginning and end of each film.

2.3.5 The Multiplicity Recorder

In order to check the performance of the neutron monitor, an instrument was designed and constructed to record the multiplicity distributions of detected neutrons under various conditions. The equipment could be triggered either by a detected neutron or by any desired pulse (e.g. a coincidence from the single particle selection system or an EAS signal). A block diagram of the system is given in figure 2-14. The trigger pulse initiated

Fig 2.13 The Neutron Multiplicity Recording System

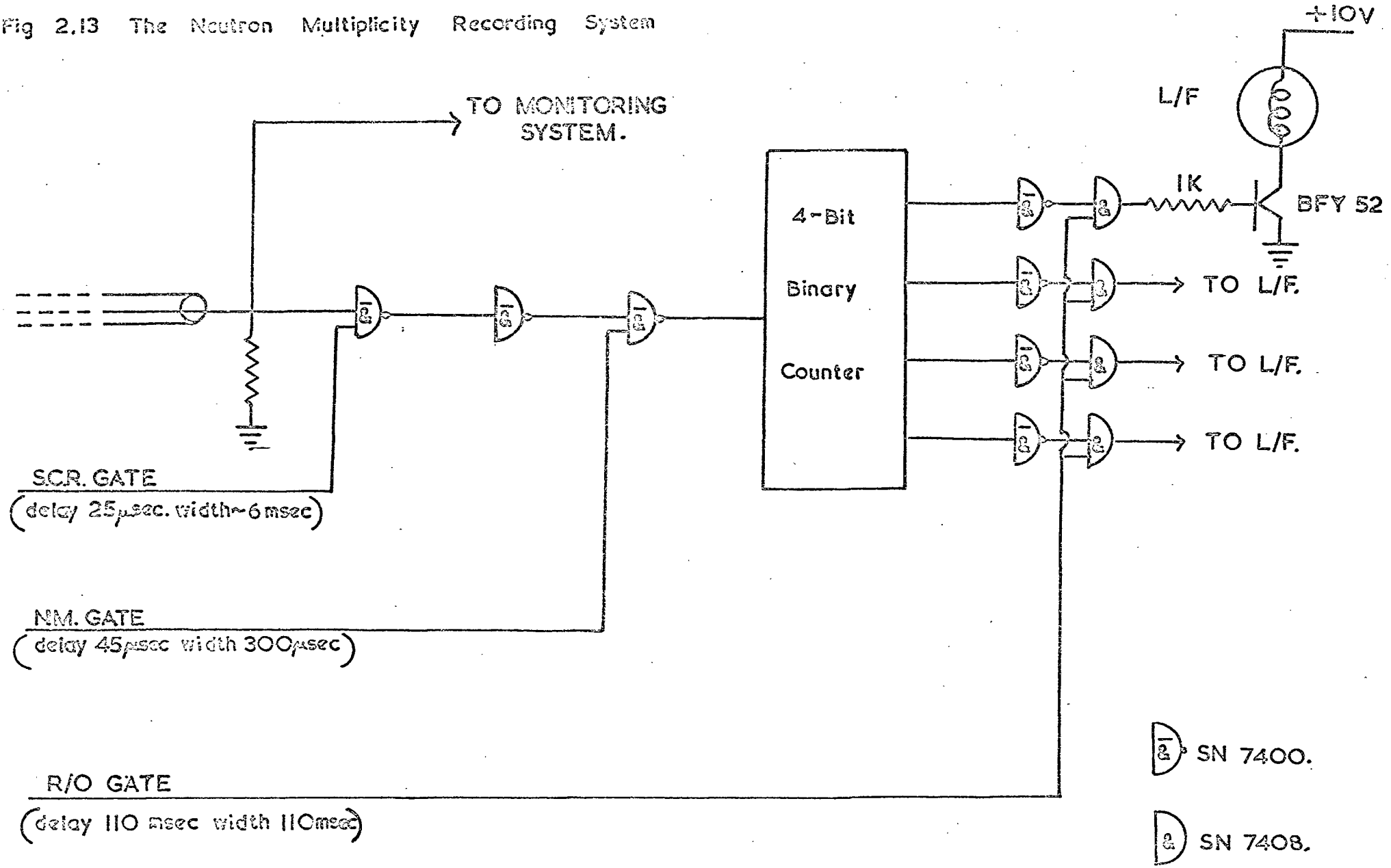

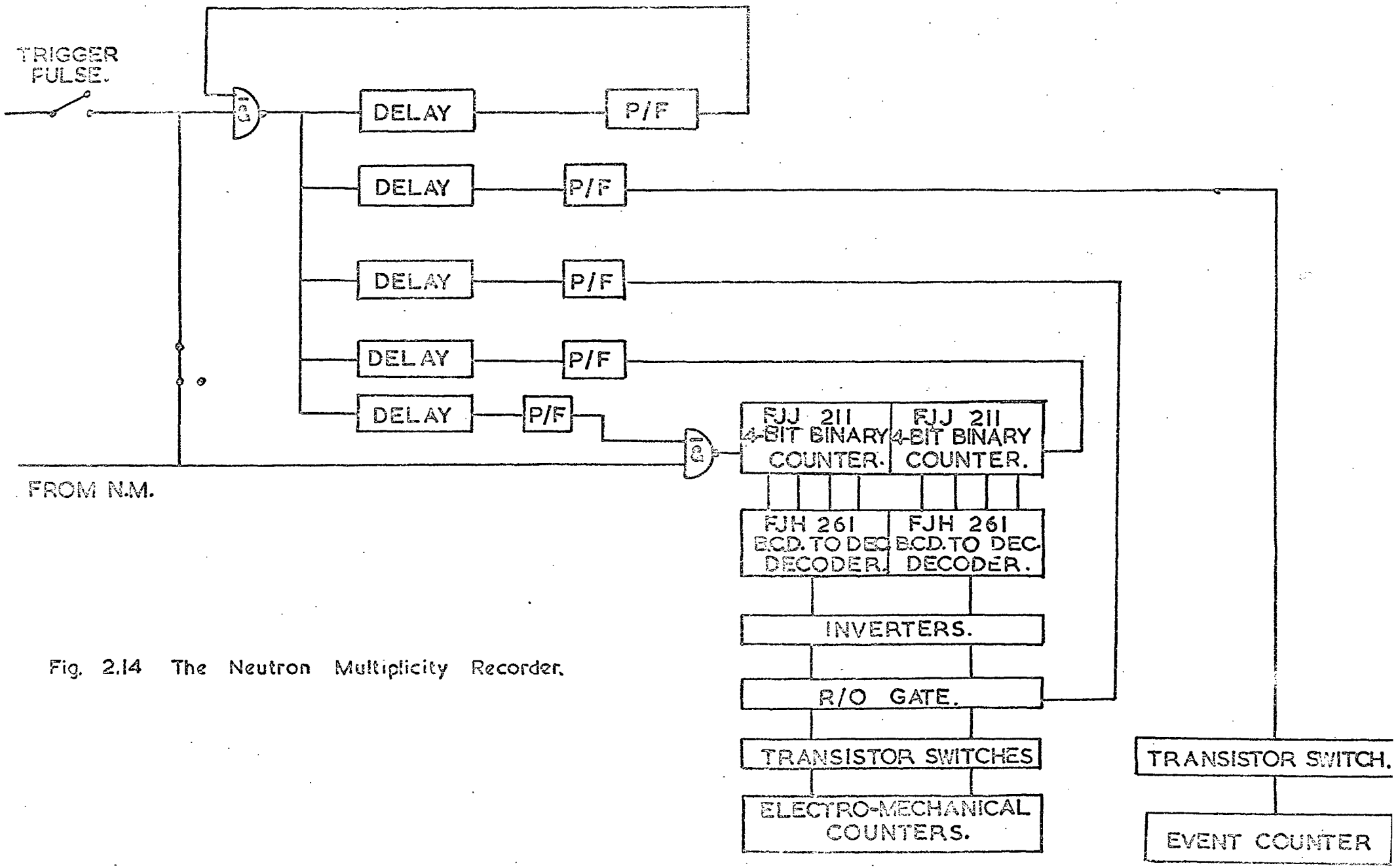

Fig. 2.14 The Neutron Multiplicity Recorder.

a series of monostable multivibrators which provided, in a suitable sequence.

a) a paralysis to the system,

b) a gate pulse which enabled neutrons to be counted,

c) a read-out pulse which caused the multiplicity of neutrons, detected in coincidence with the trigger pulse to be recorded,

d) a reset pulse which returned the neutron counters to zero,

and e) a pulse which advanced an event counter.

Neutrons detected within the duration of the gate were counted by two 4-bit binary counters, the outputs of which were decoded to give multiplicities of 0 to 15 and greater than 15. The decoded outputs were read-out on electromechanical counters. The counter gate was delayed by 45 μsecs and of duration 300 μsecs so as to simulate the normal operation of the spectrograph scaling units. This led to an underestimate of the true multiplicity since any neutrons which were detected within 45 μsecs of the trigger pulse would not have been counted.

2.3.6 Performance Checks

Various tests were carried out to measure the characteristics of the neutron monitor in order to confirm that it was operating satisfactorily and to obtain an understanding of its response.

a) Dependence of total counting rate on atmospheric pressure

The total number of neutrons detected during periods of approximately one hour (typically $\sim 3 \times 10^4$) was recorded for various values of the atmospheric pressure. Figure 2-15 shows the counting rate of the neutron monitor as a function of the atmospheric pressure. The attenuation, or barometric, coefficient of the counting rate, α, defined by

$$dN = -\alpha N \, dp$$

where N is the counting rate and P is the atmospheric pressure, was found to be 1.08% $(\text{mm Hg})^{-1}$ at 760 mm Hg, in reasonable agreement with the precise value of (0.991 ± 0.007) % $(\text{mm Hg})^{-1}$ found by Griffiths et al., 1966, for the Leeds I.G.Y. monitor.

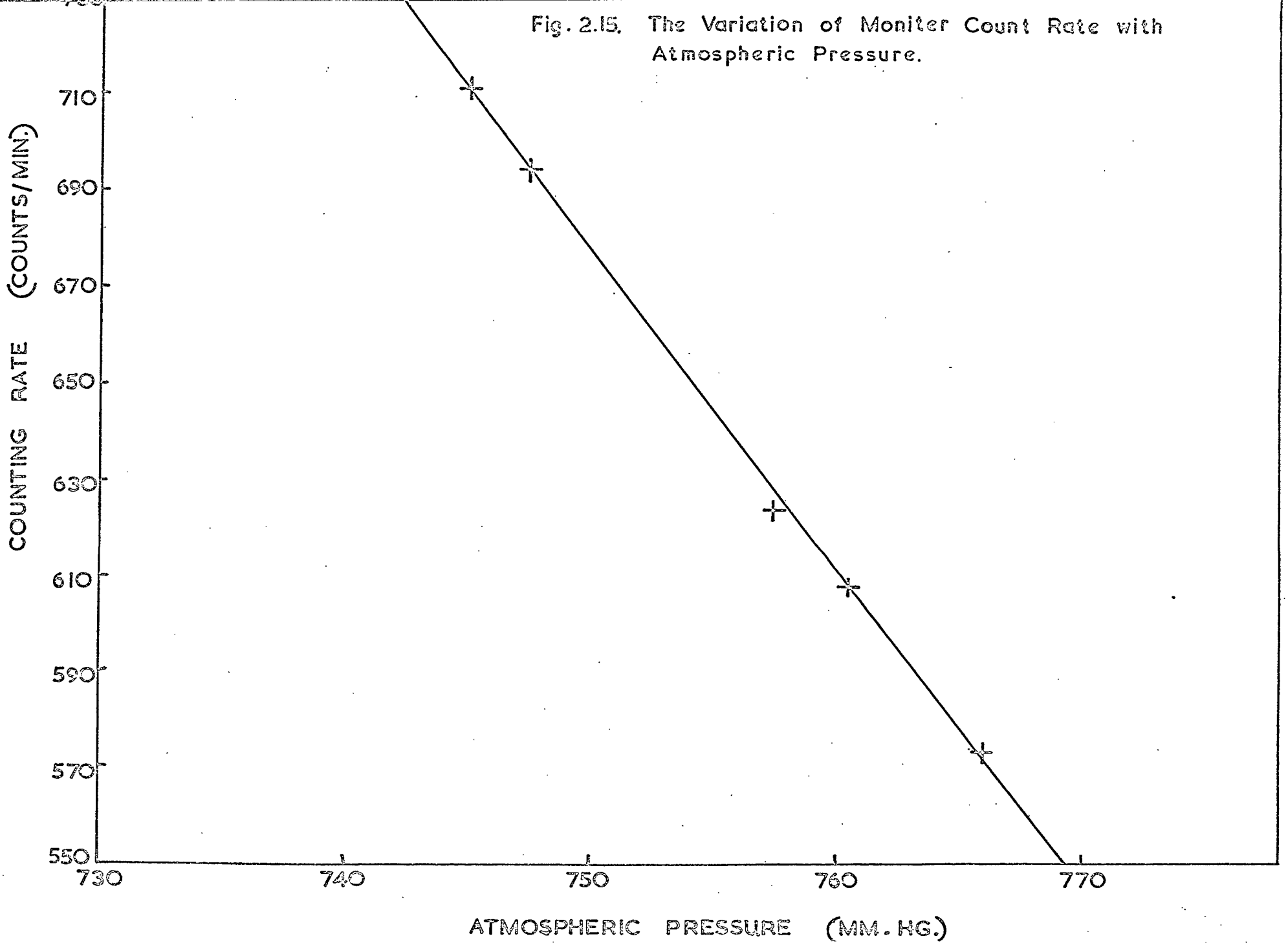

Fig. 2.15. The Variation of Moniter Count Rate with Atmospheric Pressure.

b) Arrival Time Distributions

Arrival time distributions were measured by displaying the shaped pulses, after mixing, on an oscilloscope and photographing the trace.

Two time distributions, which differed only in the definition of time zero, were measured. In one, time zero was defined as the time of the interaction which produced the evaporation neutrons, which in turn was defined as the time of detection of the charged particle which interacted, and hence can be measured only for charged particle interactions. This is the "real" time distribution. The other distribution is the "apparent" time distribution in which the arrival times were measured relative to the time of detection of a neutron.

Figures 2-16 and 2-17 show the measured real and apparent time distributions for this neutron monitor compared with the equivalent distributions for the Leeds I.G.Y. neutron monitor (Hatton and Tomlinson, 1968). The real time distributions are in good agreement over the range of times measured (40 to 340μ secs) and follow an exponential law. The main features of the apparent time distributions are also in good agreement, consisting of two sections. However, in the region of the section characterised by the longer time constant, the distribution for the present monitor falls significantly below that for the Leeds monitor, although the time constants are the same. Hatton and Tomlinson have suggested that the two sections of this distribution can be attributed to thermalisation of neutrons in the inner moderator (the short time constant section) and the outer reflector (the long time constant section); the reduction in the contribution from reflected neutrons in the present monitor is probably due to the reduced thickness of the outer reflector.

c) Multiplicity Distributions

Multiplicity distributions for each BF_3 counter were measured using the neutron multiplicity recorder triggered by a detected neutron. This gave the multiplicity distribution and counting rate of each counter and so the uniformity of the monitor could be checked. The counting rate of each of the counters across the monitor is shown in figure 2-18. This shows that

Fig. 2.16 The Distribution of Real Detection Time of Recorded Neutrons.

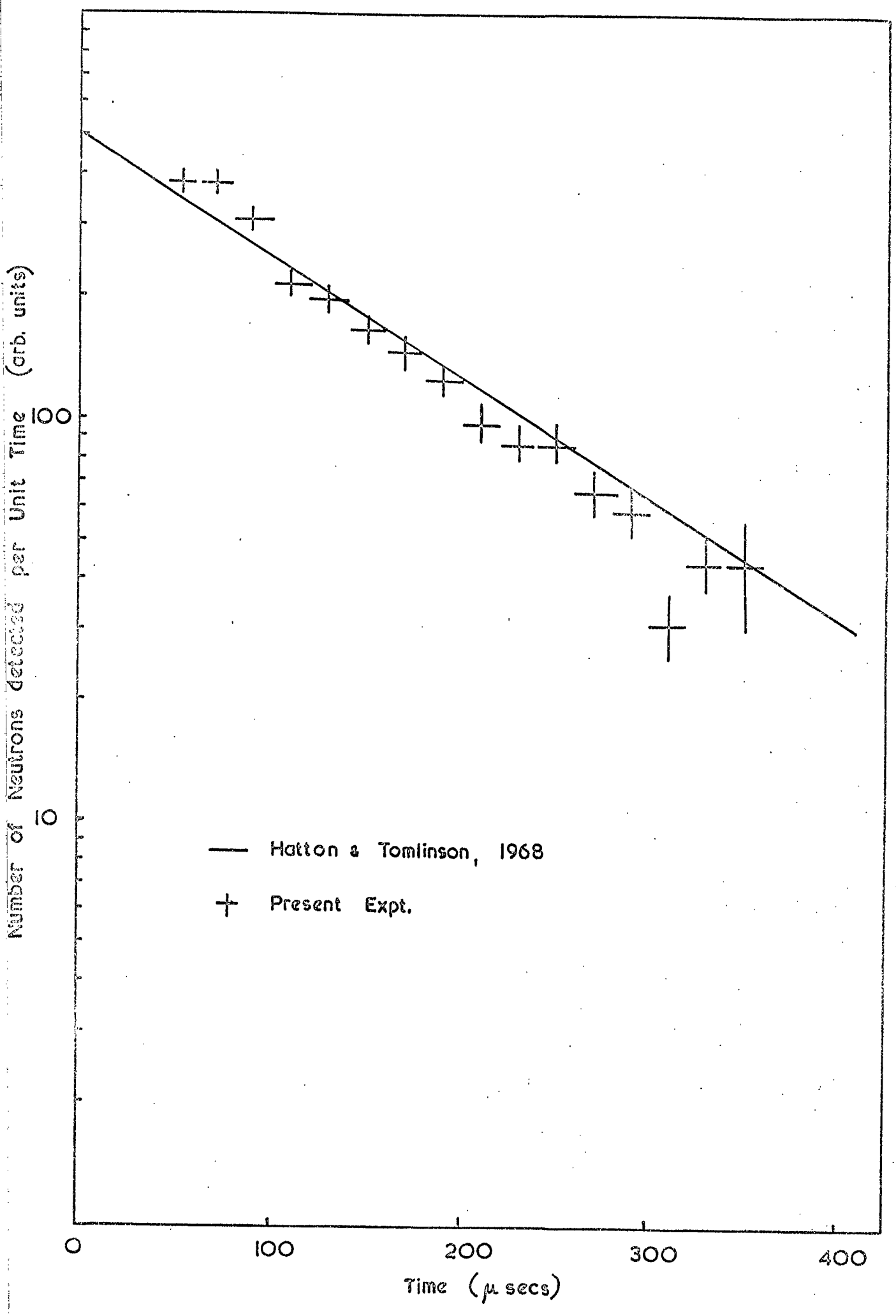

Fig. 2.17 The Distribution of Apparent Detection Time of Recorded Neutrons.

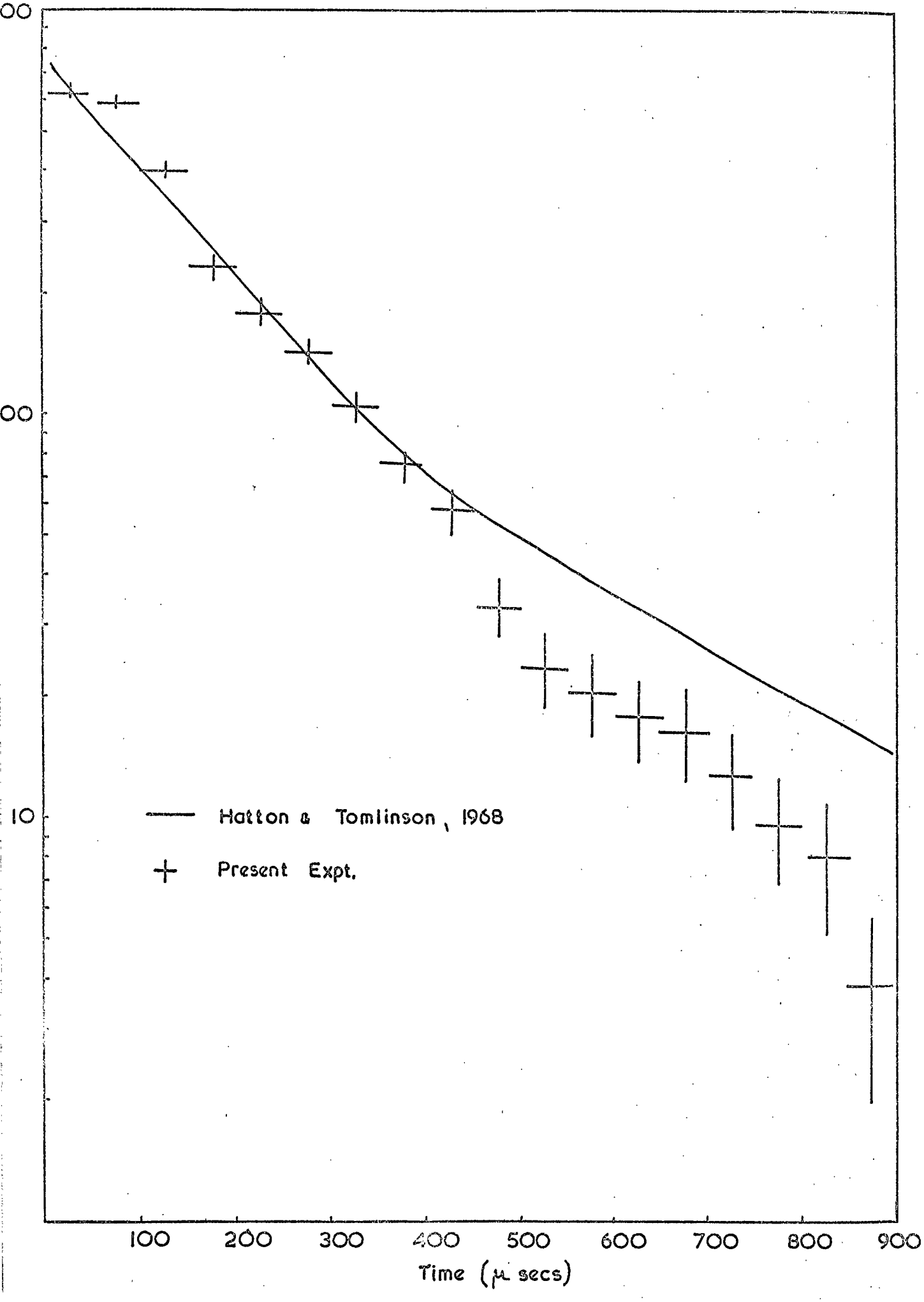

Fig 2.18 The Counting Rate of the BF_3 Counters of the Neutron Monitor.

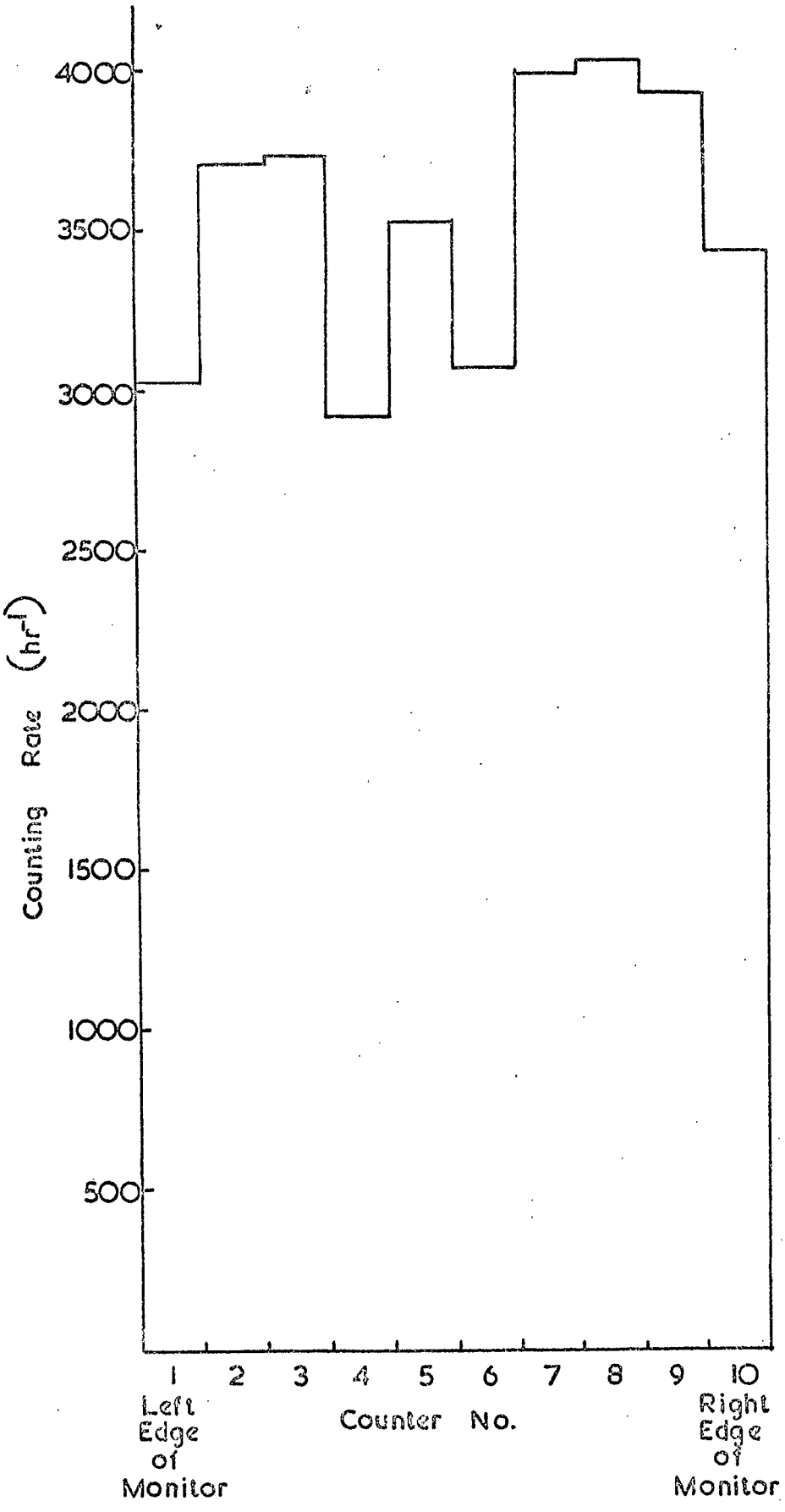

counters 4,6 were counting at a significantly lower rate than the other counters, although there was no detectable difference between the multiplicity distributions of the counters; the mean multiplicity from a single counter was 1.08.

As a further check on the uniformity of the monitor the events used in the measurement of the momentum spectra of unaccompanied NAPs were analysed to give distributions of:-

(i) the point of impact of the particle track on the neutron monitor, and

(ii) the proportional counter which detected the neutrons.

These distributions are shown in figure 2-19. In neither of these distributions does the apparent inefficiency of counters 4,6 appear. The dip at counter number 5 in the distribution of impact points is caused by the rejection of genuine NAPs because the particle track could have passed through the gap between the two trays of flash tubes which constitute the X2 tray and has been allowed for as described in §3.6.5.. Since these distributions were derived from the data used in the measurements of the momentum spectra, it is concluded that the monitor must have been operating uniformly during the collection of the experimental data.

A multiplicity distribution for the complete monitor was measured, triggering the multiplicity recorder by the first detected neutron. This distribution is shown in figure 2-20, where it is compared with the distribution found for the Leeds I.G.Y. monitor (Hatton, 1971). The distributions are seen to be similar and, as expected, there is no statistically significant difference between the mean multiplicities found for the two monitors.

On the basis of these results it was concluded that the neutron monitor was operating satisfactorily during the collection of the experimental data which formed the basis for the measurement of the momentum spectra.

Fig. 2.19. The Uniformity of the Response of the Neutron Monitor.

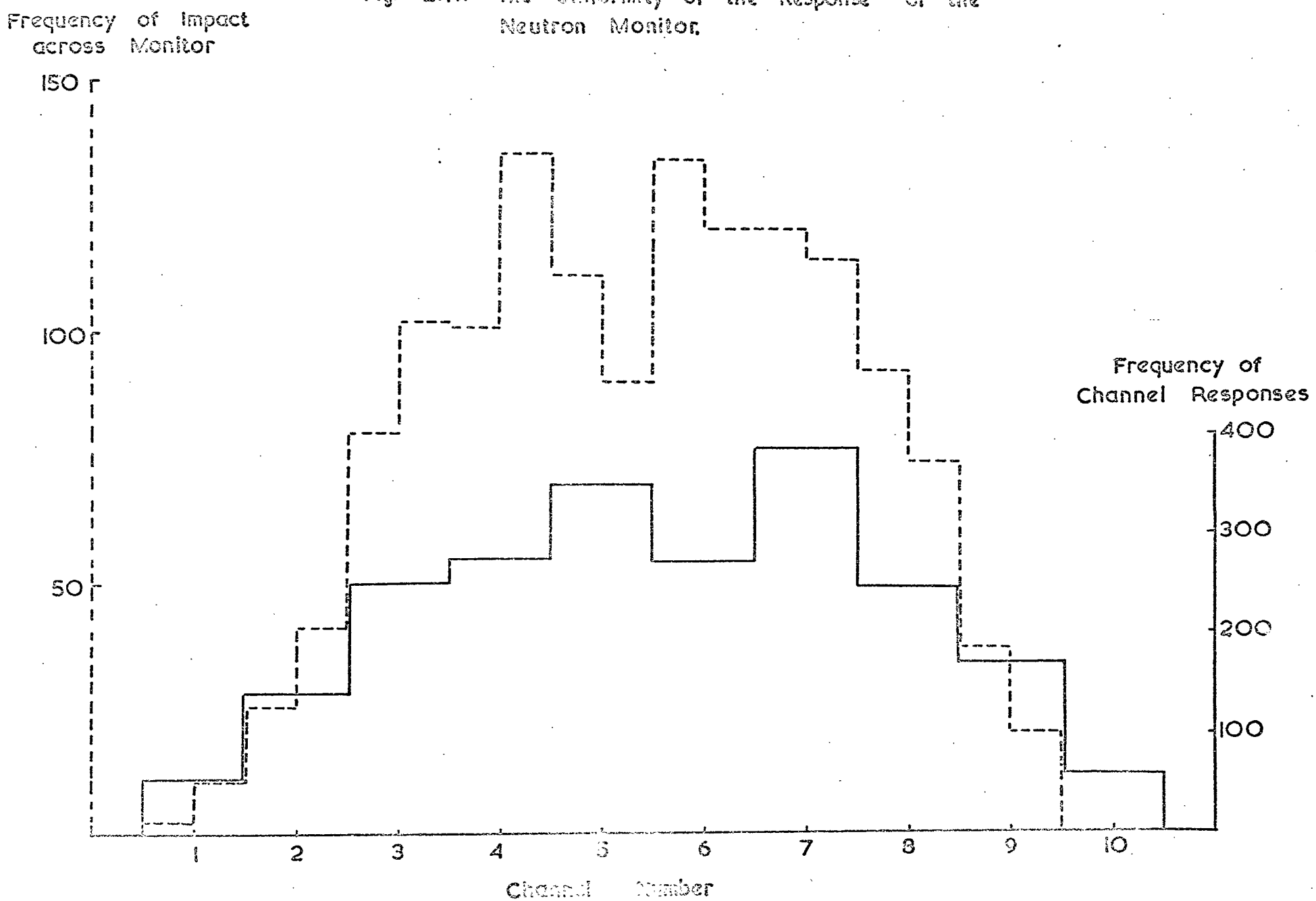

Fig. 2.20 The Multiplicity Distribution of Neutrons recorded in the Neutron Monitor in the Cosmic Ray Beam compared with that for a Leeds I.G.Y. Monitor.

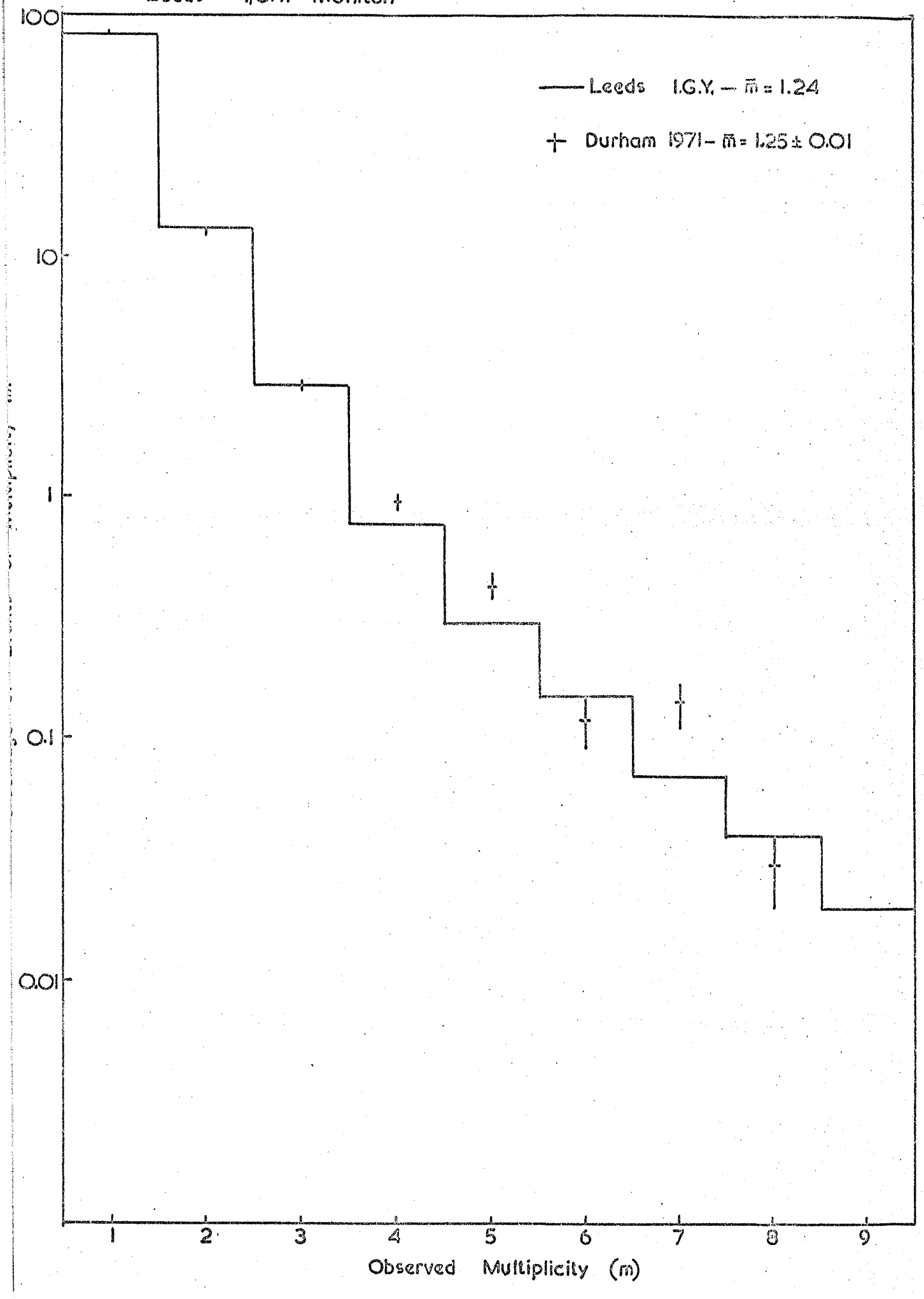

2.4 The Single Particle Selection System

Charged particles passing through the spectrograph were detected by four trays of Geiger-Muller (GM) counters (figure 2-1).

2.4.1 The Upper Detectors

On top of the spectrograph were three trays (A,B,C) each containing ten GM counters (20th Century Electronics Ltd. type G60) of length 0.6m and diameter 3 cms, arranged in a horizontal plane with their axes parallel to the neon flash tubes (§2.2.2). In each tray the counters were selected to have similar plateau voltages, so that only a single value of high voltage need be supplied, and the counters were connected in parallel enabling a single output cable to be used. The pulses from the trays were fed to a mixing unit, the output of which was shaped to produce a pulse of fixed amplitude and duration whenever any one of the GM counters was discharged.

2.4.2 The Magnet Air-gap Detectors

In the air-gap of the magnet were two trays (D,E figure 2-1), each containing 11 G60 GM counters arranged in two close-packed layers. The axes of the counters were horizontal but perpendicular to the axes of the neon flash tubes. Because of their inaccessibility and the high magnetic field in which these counters operated, all the electronic circuitry was remote and the voltage applied to each counter could be individually varied. The pulses from each counter were fed into an electronic selection system such that an output pulse, of fixed amplitude and duration, was produced when there was a coincidence between any counter in tray D and any counter in tray E.

2.4.3 The Sub-B3 Detector

A tray (F, figure 2-1) of 10 G60 GM counters was installed underneath the neon flash tube tray B3 with the counters placed parallel to the air-gap detectors, D,E. The counters in tray F were operated in the same manner as the detectors A,B,C (see §2.4.1).

2.4.4 The Selection System.

The shaped pulses from the three sets of detectors were fed into a coincidence unit, and, by suitable selection of plugs and switches, any combination of:-

a) any one of the 3 trays A, B and C, (A+B+C)

b) the 2-fold coincidence of the air-gap detectors, (D.E),

and c) the sub-B3 detector (F)

could be selected. However, throughout the unaccompanied NAP studies described in this thesis the following combination was used

$$(A + B + C).\ (D.E).\ F$$

but no provision was made for the electronic rejection of events with more than one particle incident upon the spectrograph.

2.4.5 The Monitoring System

As a check on the operation of the GM trays the rates of pulses from each of the units could be monitored on a ratemeter. The rates were observed at the beginning and end of each film and compared with the normal rates, due allowance being made for atmospheric pressure variations.

2.5. The Control System

2.5.1 The Electronic Circuits

Events accompanied by a neutron monitor response were selected by the electronic circuit shown, in block diagram form, in figure 2-21. All the delay and pulse-forming units and logic gates were made using SN7400 transistor-transistor logic integrated circuits. The circuit could be triggered by the pulse from the "single-particle" selection system (§2.4.4) either alone or in coincidence with another pulse (e.g. from the EAS array, see §2.6). A paralysis of 2.1 secs was applied, immediately after triggering, to the whole circuit so that the equipment could not be retriggered until the recording cycle had been completed. Pulses were transmitted, after suitable delays, to trigger the flash tube pulsing system (no delay), to open the gate which allowed neutrons to be recorded (45 μsecs delay), to reset to zero the neutron multiplicity

Fig. 2.21 Block Diagram of the Control Circuit.

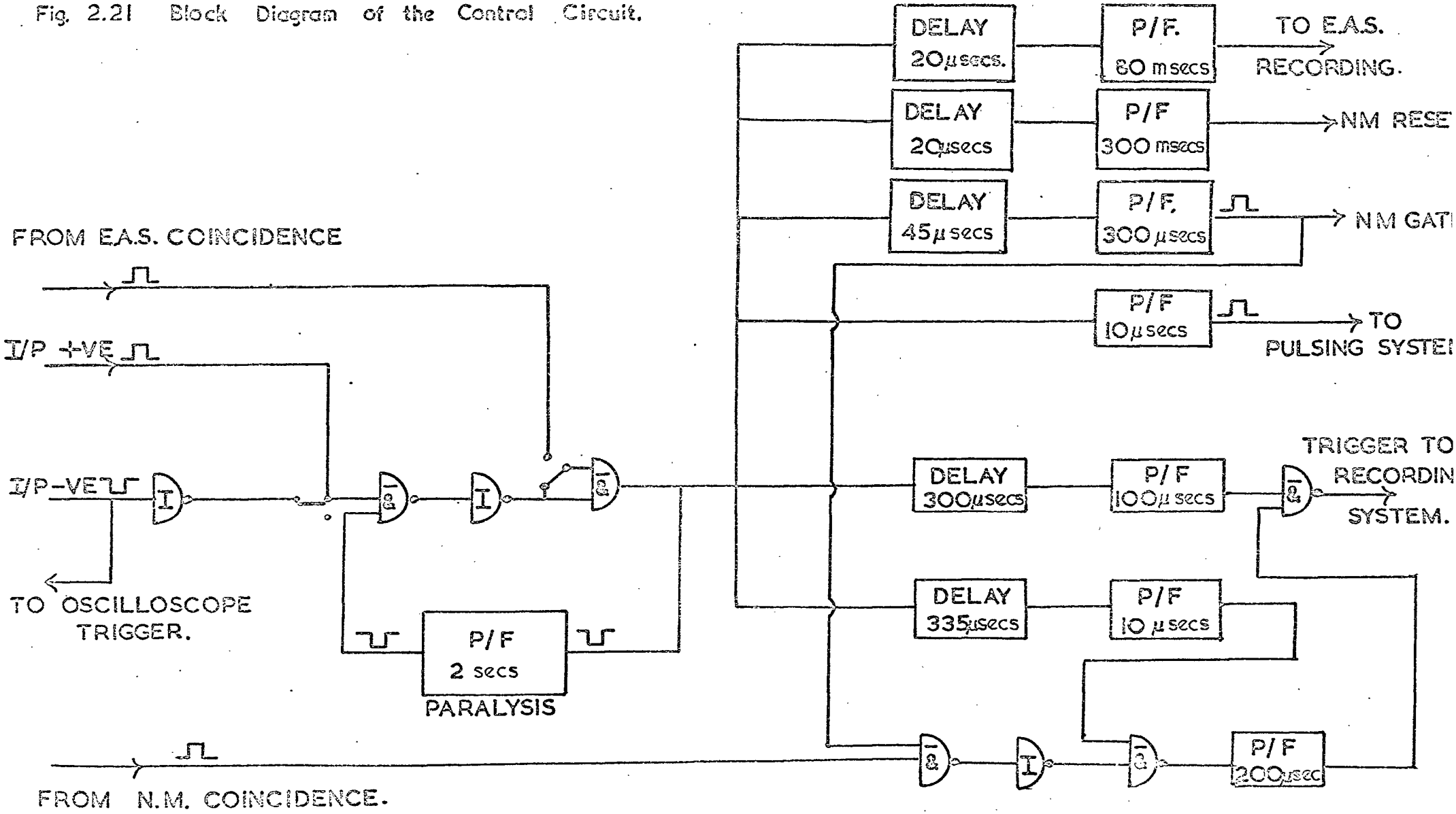

scalers (delay 240 msecs) and to the EAS recording system. The "single-particle" selection system pulse also triggered the time-base of the oscilloscope used to record the detection times of the neutrons.

If a neutron was detected within the sensitive time of the neutron gate, a pulse, after a fixed time (340 μsecs) relative to the initial triggering of the system, was sent to the circuit controlling the information-recording. This circuit produced pulses of various lengths, after appropriate delays, which operated the equipment required to record all the information. A diagram of the time-sequence of operations is given in figure 2.22.

2.5.2 Tests of the Control System

When the control system was first installed it was found that spurious triggers were induced when the flash tube high voltage pulse was applied. This was traced to direct radiated pick-up on the integrated circuit inputs, and was eliminated by filtering the high frequency components. Since the pick-up contained components of a higher frequency than the signals, the filtering did not affect the normal operation of the system.

However, it was found that there was still a low, but significant, rate of spurious events. These were caused by the flash tube high voltage pulse producing spurious neutron counts, within the sensitive time of the neutron gate, through pick-up on the anodes of the BF_3 proportional counters. The rate of these events was reduced to zero by delaying the opening of the neutron gate and modifying the take-off circuits of the proportional counters, to that shown in figure 2-9, to reduce the amount of pick-up.

The operation of the control system was tested by operating the equipment without applying any high voltage to the proportional counters in the neutron monitor. Under these conditions there should be no neutron pulses from the neutron monitor, and any events recorded will be spurious. The rate of spurious events was regarded as acceptable when the equipment had been operated in this way for 48 hours without any events being recorded.

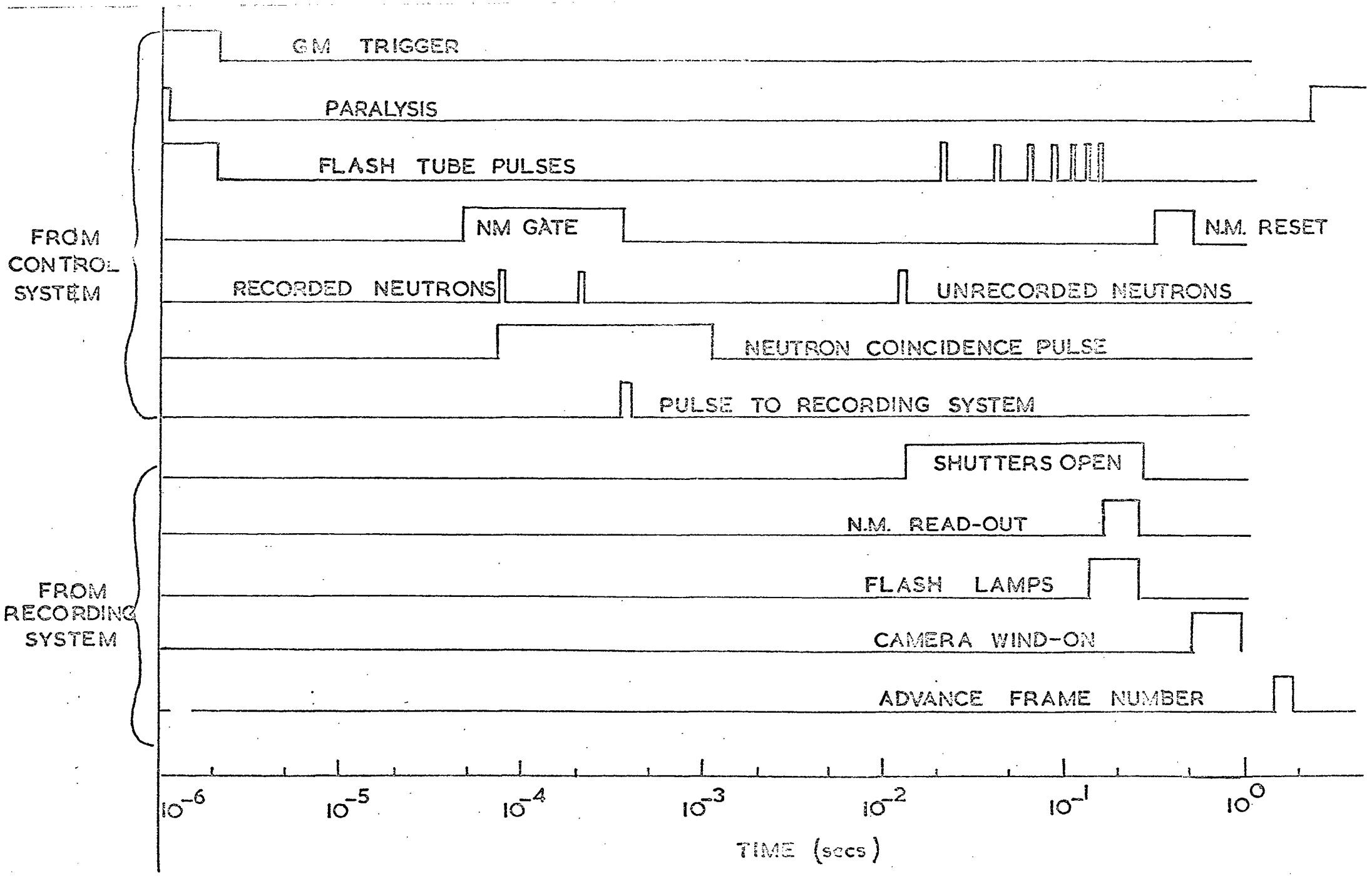

Fig. 2.22 The Time Sequencing of the Control System.

2.6. The Extensive Air Shower Array

A plan of the extensive air shower (EAS) array, including the location of the spectrograph, is shown in figure 2-23. Water Čerenkov detectors, similar in type to those used in the British Universities Joint Air Shower Array at Haverah Park were used as particle detectors (Wilson et al., 1963). Four detectors, each of area 1.5 m^2 and depth 0.6m, were used for the initial detection and analysis of the EAS. Eight smaller detectors, each 0.2 m^2 in area and 0.6m deep, were available for refinement of the accuracy of the location of the core of the EAS.

Because no electronic rejection of dense events was applied, any NAPs in EAS will be detected by the "single-particle" trigger used for the work on unaccompanied NAPs, and so, in order to reduce the work load, the EAS array was not operated during most of the work described in this thesis.

2.7 Recording of Information

The particle tracks in the spectrograph were recorded on 35 mm Ilford HP4 film using 2 Shackman automatic recording cameras. Trays A1 and A3 were recorded on one camera and B3, B1, X1 and X2 on the other. Since the light from a flash tube is emitted only into a small solid angle, the flash tube trays must be viewed by the cameras from a long distance. This was achieved by using a mirror system as shown in figure 2.24. The path length for light from each of the trays is given in table 2.1.

TABLE 2.1 OPTICAL PATH LENGTHS (FROM FLASH TUBE TRAYS

TRAY	PATH LENGTH (FT)
A1	24
A3	25
B3	23
B1	22
X1	24
X2	26

The path-lengths are all rather similar and hence the images of all the trays were in focus when a lens with an aperture of f1.9 was used.

Fig. 2.23 The E.A.S. Array.

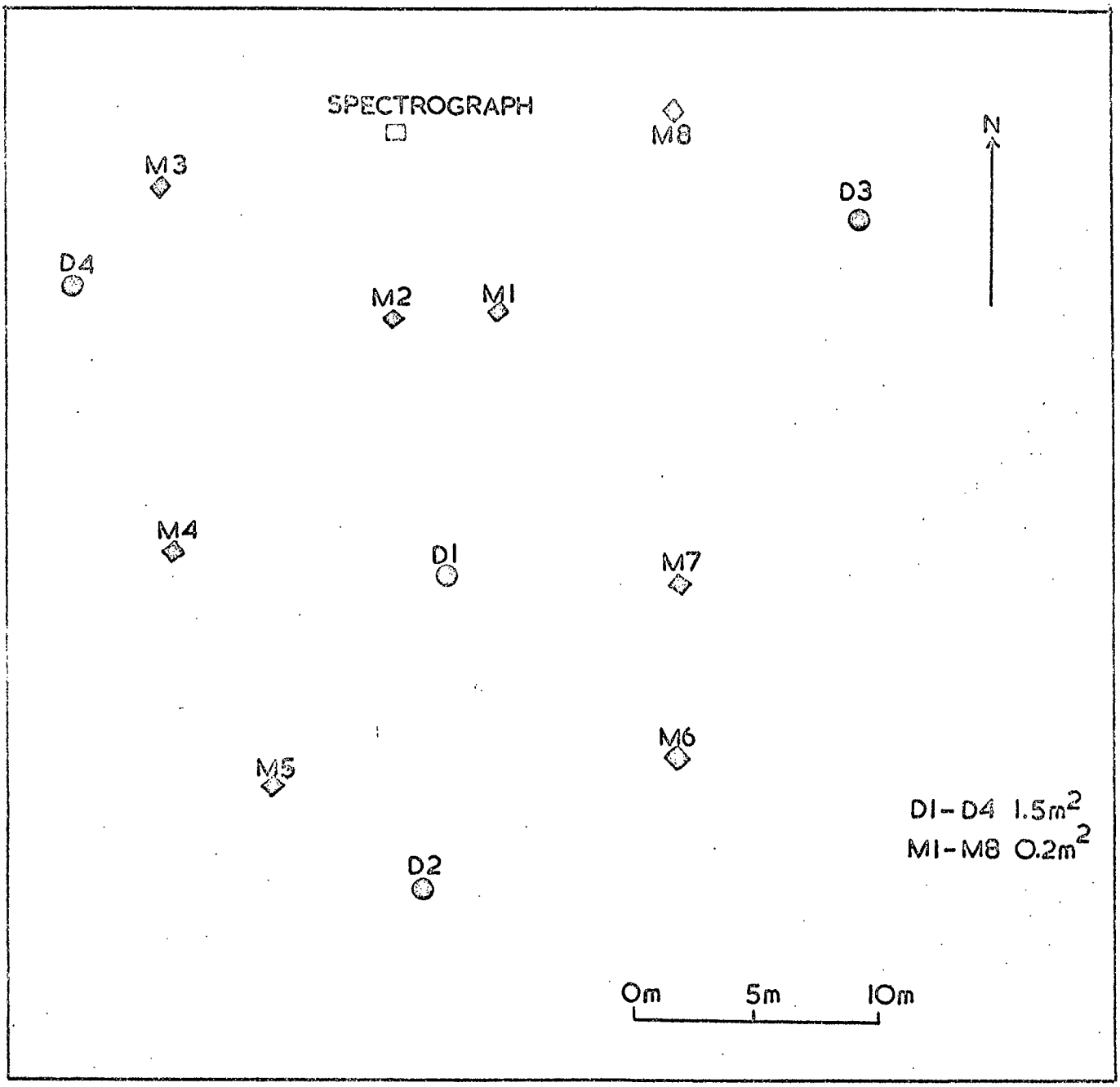

Fig. 2.24 The Optical System used in Photographic Recording.

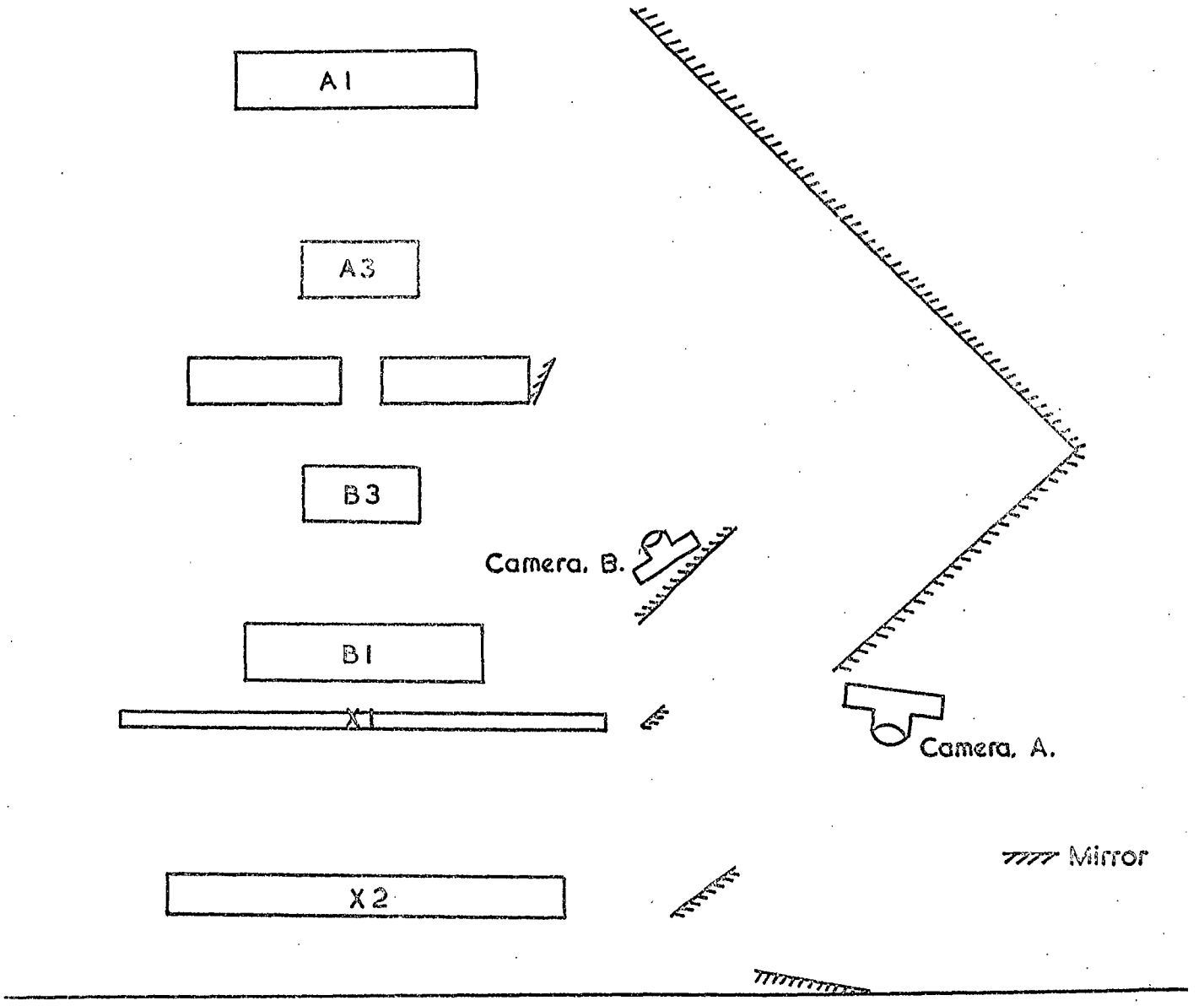

The shutters used were of the venetian blind type, mounted in front of the lens, operated by a solenoid and were fully open 13 msecs after the detection of a neutron coincidence.

In addition to the flash tube information, the multiplicity of neutrons detected in each counter was recorded by each camera and British Standard Time was recorded by camera A (figure 2-24).

The detection times of the neutrons were also recorded photographically by a third camera (camera C)

Also recorded on each frame was an event number used to assist in correlation of frames during analysis.

2.8 Run Statistics

For the measurements of the momentum spectra of unaccompanied protons and pions and the study of the production of neutrons by muons, events were recorded when the following conditions had been satisfied:-

a) a GM counter coincidence of the form

$$(A + B + C) \cdot (D.E) \cdot F$$

b) a neutron detected in the neutron monitor within 45 to 345 μsecs of the GM coincidence.

This method of operation is called the "single particle" mode.

The average rate of "single particle" events was $\sim 10\ hr^{-1}$ and the film was changed daily, the equipment being serviced at the same time. At the beginning and end of each film the frame number, British Standard Time and the current in the magnet coils were noted. In addition, at the end of each film period, the number of GM counter coincidences which had occurred during that period was noted. At the same time the counting rates of each of the proportional counters in the neutron monitor, and the GM counter coincidences (A + B + C), (D.E) and F were checked, and corrected if found to be abnormal. To correct for any asymmetries in the acceptance of the spectrograph as a function of the deflection of the particle, the magnetic field was reversed after each film, so that the on-time with each polarity was approximately equal.

The spectrograph was operated in this way during January and February 1971 for a total period of 986.8 hours. However, allowance must be made for the dead time of the equipment, equal to 2.1 secs per GM counter coincidence, and losses of sensitive time due to instrumental failure. The effective on-time of the equipment was 1.56×10^6 secs. During this period 867,617 GM counter coincidences were detected which gave 10,273 "single particle" triggers.

CHAPTER THREE

ANALYSIS OF DATA

3.1. Introduction

Using the apparatus and techniques described in Chapter 2, the following data were available for each event recorded by the spectrograph:-

a) British Standard Time,

b) the tracks of particles in the spectrograph,

c) the magnitude and polarity of the magnetic field,

d) the multiplicity of neutrons detected in each proportional counter in the neutron monitor and their detection times relative to the GM counter coincidence signal,

and, e) the tracks of any particles which emerge from the neutron monitor.

This information must be extracted from the films and converted to a form which can be analysed conveniently to provide angular deflection spectra of NAPs, from which momentum spectra can be derived.

The deflection of a particle is measured by reconstructing its track through the spectrograph to give its arrival direction projected on the measurement plane of the spectrograph and its angle of emergence from the magnetic field. Having thus determined the angular deflection, a knowledge of the lateral position of the particle track in the neutron monitor, the point of detection of the neutrons and the scattering of secondaries, if any, emerging from the neutron monitor leads to identification of the type of particle. Deflection spectra of NAPs can thus be obtained. Then, assuming there are no antiprotons in cosmic rays near sea level, and that the momentum spectra of positive and negative pions are identical, the momentum spectra of protons and pions can be derived, allowing for Coulomb scattering in the material of the spectrograph and errors of track location. These spectra must then be corrected for losses due to interactions in the material of the spectrograph and inefficiencies in the neutron monitor. Such procedures indicate the shapes of the momentum spectra and the relative intensities of protons and pions, but do not give their absolute intensities.

3.2. Extraction of Data

3.2.1 Initial Scanning of Films

The three films used to record the data were inspected, and the available information from each event was noted so that it was easily accessible for further analysis. The data noted were:-

a) the frame number and film number,

b) British Standard Time,

c) the multiplicity of neutrons detected in each counter,

d) the number of tracks observed in each flash tube tray,

e) whether there had been an interaction in a momentum measurement flash tube tray,

and ,f) the arrival times of recorded neutrons.

If there had been an interaction in a flash tube tray, the event was rejected since the track of the particle could not be accurately reconstructed. The remaining events were assigned to one of four categories, based upon the number of tracks in the momentum measurement trays, which were:-

(i) Dense events - events with many tracks in the spectrograph such that no track could be reliably reconstructed and which were rejected for the present analysis,

(ii)"B" events - events with one complete track, in the spectrograph,

(iii)"F" events - events with one complete track, suitable for analysis, together with partial tracks in one or two adjacent momentum measurement trays,

(iv)"EAS" events - events with more than one complete track, some or all of which could be reconstructed. These were designated "EAS" events to distinguish them from the single particle events in categories B and F.

3.2.2. Enumeration of Tracks

After initial classification as in §3.2.1 the particle tracks were reconstructed. In order to do so, it was necessary to determine which of the neon flash tubes had flashed to delineate the particle track. Each

flash tube in each layer was identified by numbering and so any flashed tube could be identified.

Those events which had only one track in each flash tube tray could be enumerated immediately. Thus, B and F events which had no more than one track in flash tube tray X2 were enumerated directly from the film. However, 'EAS' events and B and F events with more than one track in X2 were more complex, and had to be considered further before enumeration and so photographic prints were made of the events for detailed examination.

Direct Enumeration

The straightforward events were projected by a photographic enlarger onto an underlay on which the positions of the flash tubes in the spectrograph together with their numbers were marked. The track was enumerated by aligning the underlay with fiducial marks so that the flashed tube numbers could be encoded on punched cards ready for analysis by a digital computer.

Enumeration from Prints

The prints of the complex events were examined and the tracks which could be enumerated were selected. These were then enumerated from the prints using a transparent overlay on which were marked the fiducials and the positions of the tubes of the spectrograph.

3.3 Track Fitting

3.3.1 Introduction

Previously used methods of track reconstruction have involved the adjustment of a cursor over a scale model of the flash tube array (Hayman and Wolfendale, 1962), or the use of a computer technique, e.g. Bull et al., 1962. The former method suffers from the disadvantages of being subjective and limited in accuracy by the precision with which the scale model is constructed. An even greater drawback in the present experiment, involving the analysis of 10,000 tracks is that it is slow and laborious. Hence a computer method was devised and used for the reconstruction of the particle tracks.

Most methods of computer analysis of tracks have utilised a probability function $P(z)$ which is the probability that a tube will flash when a particle traverses it a distance z from the centre. A line was set up and the total

probability of the observed pattern of flashed tubes occurring was calculated. Various possible lines were then tried and that line which gave the highest probability was regarded as the 'best estimate' of the actual trajectory of the particle. However, it was found that the 'best estimate' track was sensitive to the form of the probability function used in the analysis (Orford 1968), and this probability function was not well known. In view of these disadvantages a computer track-fitting method was devised which, it was considered, would give the best simulation of the hand analysis method. For each line tried a 3-stage criterion was applied:-

a) Does the line miss fewer flashed tubes than the previous 'best estimate'.

b) If the number of missed flashed tubes is the same as for the previous 'best estimate', then, is the path-length in non-flashed tubes less than for the previous 'best estimate'.

c) If the path-length in non-flashed tubes equals that for the previous 'best estimate', is the path length in flashed tubes greater than in the previous 'best estimate'.

3.3.2 Computer Track Fitting Programme

A simplified flow chart for the computer programme used for the analysis of the particle tracks is given in figure 3-1.

An initial estimate of the particle trajectory must be made to use as a starting point for the lines which are to be tried in the analysis part of the programme. A least-squares fit is performed on the co-ordinates of the centres of the flashed tubes. The line which this gives is then used to find the gap between tubes in those layers with no flashed tubes which is nearest to the proposed trajectory. A line is then fitted to the centres of the flashed tubes and the gaps using the method of Gauss. This analysis gives the inclination of the line to the vertical (ψ_{GF}) and the lateral point (R_{GP}) at which it intersects a horizontal plane midway between the two trays of flash tubes. The number of ignored flashed tubes (IIG), the path-length in non-flashed tubes (BMIN) and the path-length in flashed tubes (BMAX) are then evaluated for a set of lines with a matrix of angles,

Fig. 3.1 Flow Diagram of Computer Track Fitting Programme.

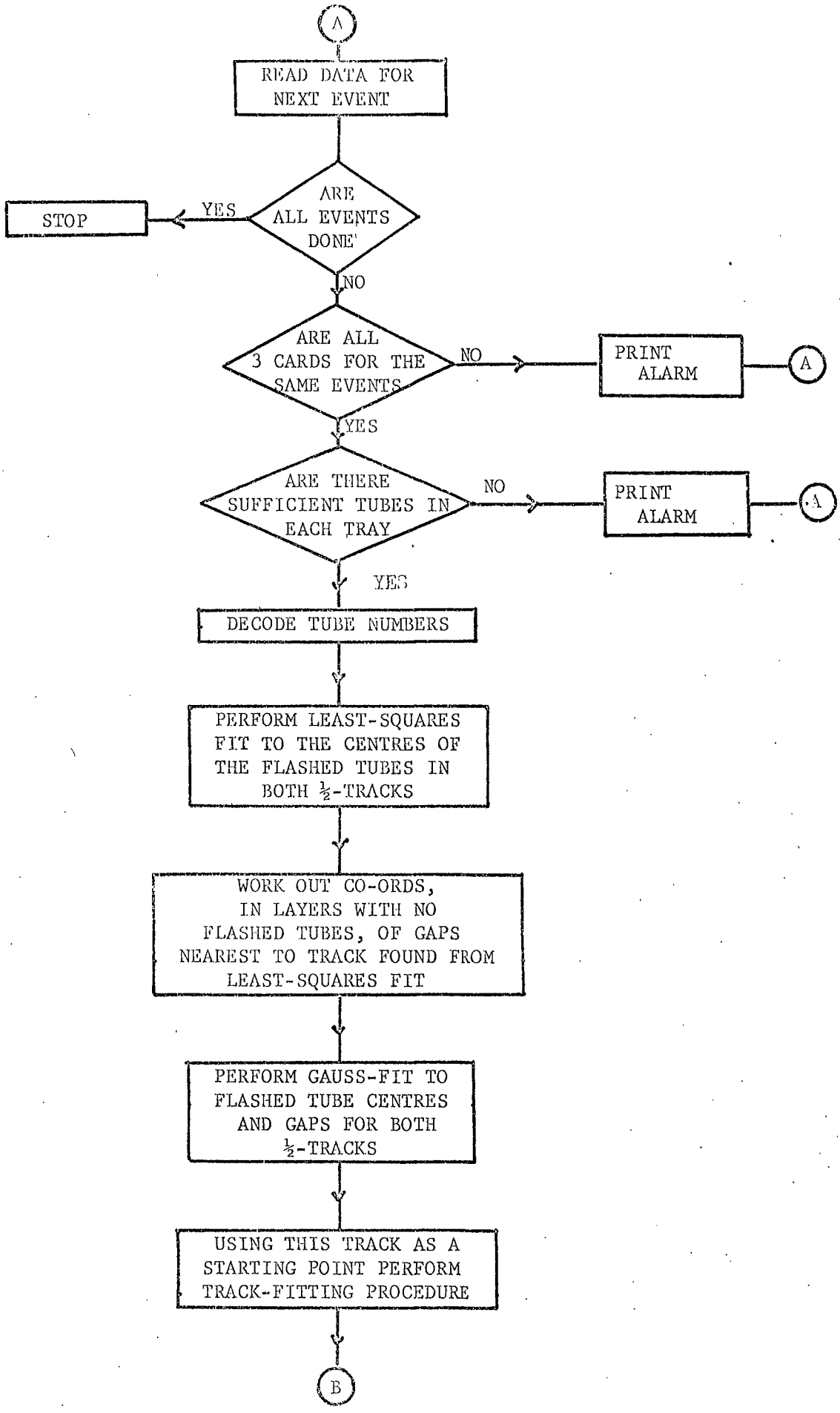

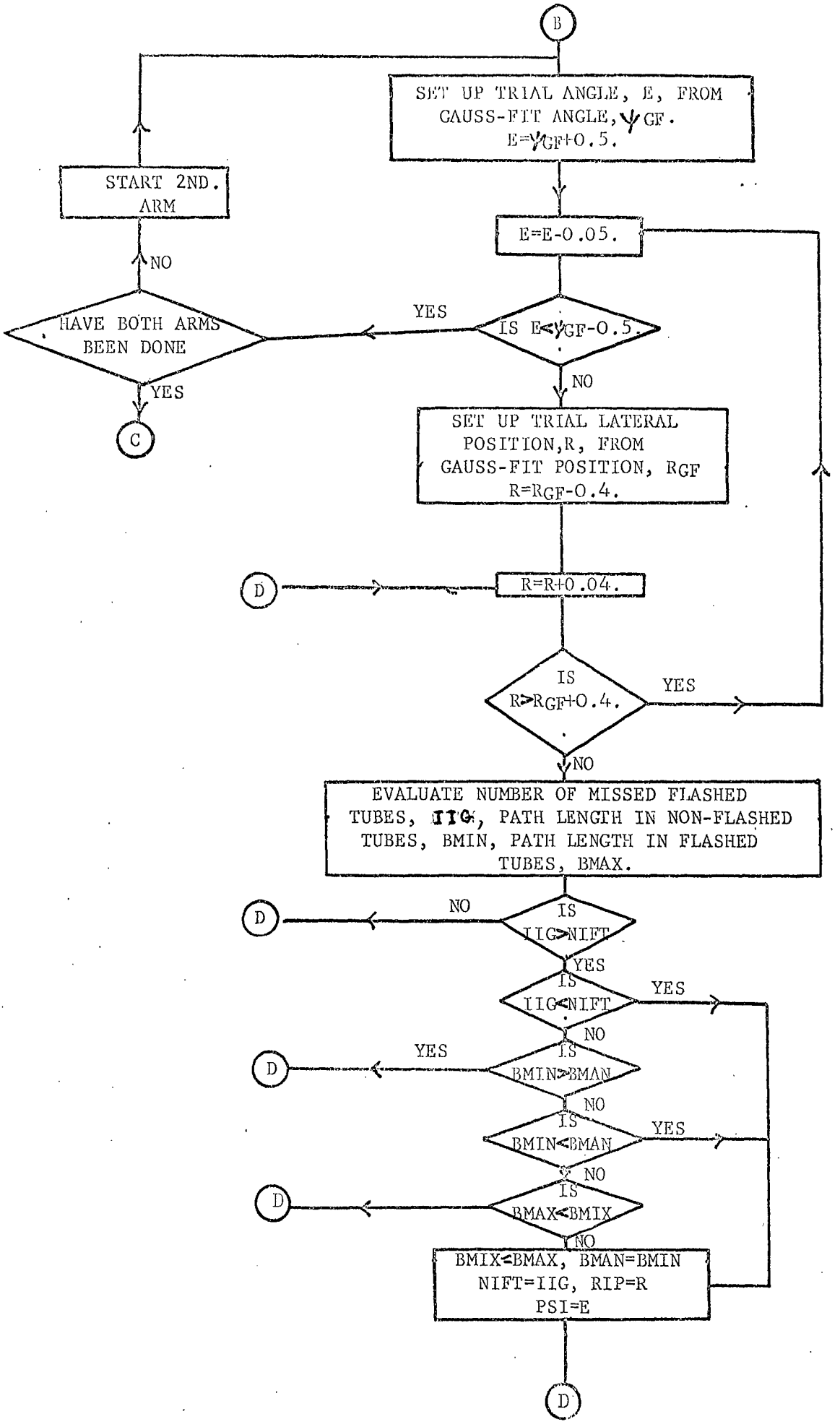
B
SET UP TRIAL ANGLE, E, FROM GAUSS-FIT ANGLE, ψGF. E=ψGF+0.5.
E=E-0.05.
IS E<ψGF-0.5.
YES
NO
HAVE BOTH ARMS BEEN DONE
NO
YES
START 2ND. ARM
C
SET UP TRIAL LATERAL POSITION, R, FROM GAUSS-FIT POSITION, RGF R=RGF-0.4.
D
R=R+0.04.
IS R>RGF+0.4.
YES
NO
EVALUATE NUMBER OF MISSED FLASHED TUBES, IIG, PATH LENGTH IN NON-FLASHED TUBES, BMIN, PATH LENGTH IN FLASHED TUBES, BMAX.
IS IIG>NIFT
NO
D
YES
IS IIG<NIFT
YES
NO
IS BMIN>BMAN
YES
D
NO
IS BMIN<BMAN
YES
NO
IS BMAX<BMIX
D
NO
BMIX=BMAX, BMAN=BMIN NIFT=IIG, RIP=R PSI=E
D

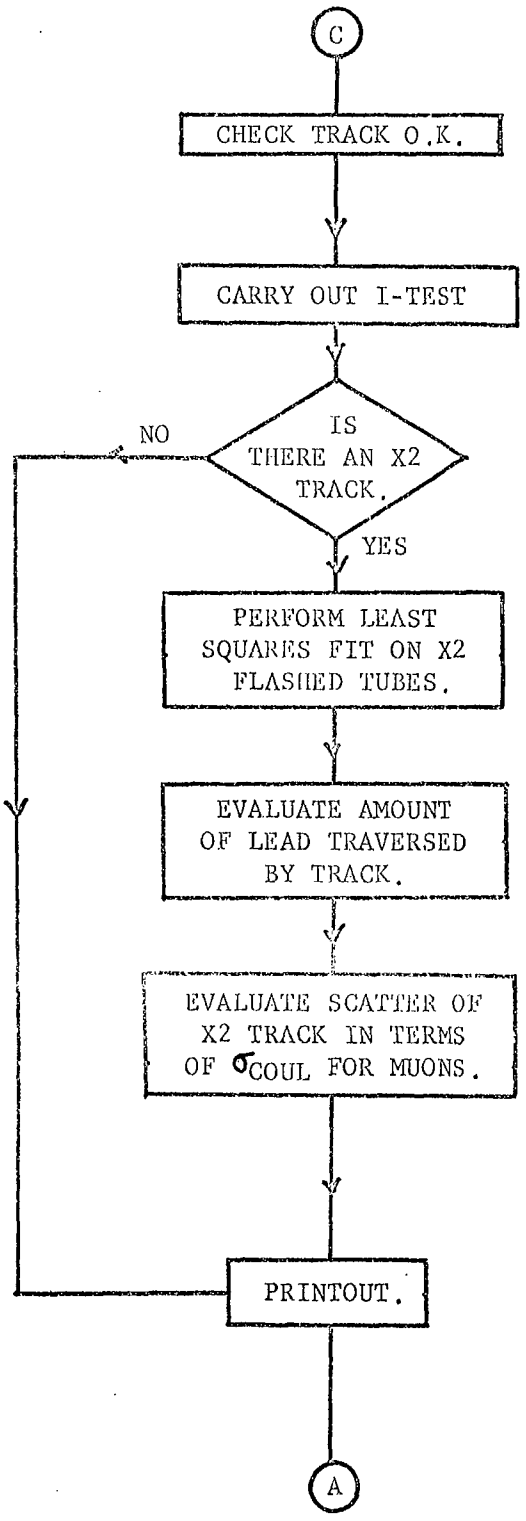
C
CHECK TRACK O.K.
CARRY OUT I-TEST
IS THERE AN X2 TRACK.
NO
YES
PERFORM LEAST SQUARES FIT ON X2 FLASHED TUBES.
EVALUATE AMOUNT OF LEAD TRAVERSED BY TRACK.
EVALUATE SCATTER OF X2 TRACK IN TERMS OF σ_{COUL} FOR MUONS.
PRINTOUT.
A

Fig. 3.3 A Histogram of the Angular Difference between Hand Analysis and Computer Track Fitting of Particle Trajectories.

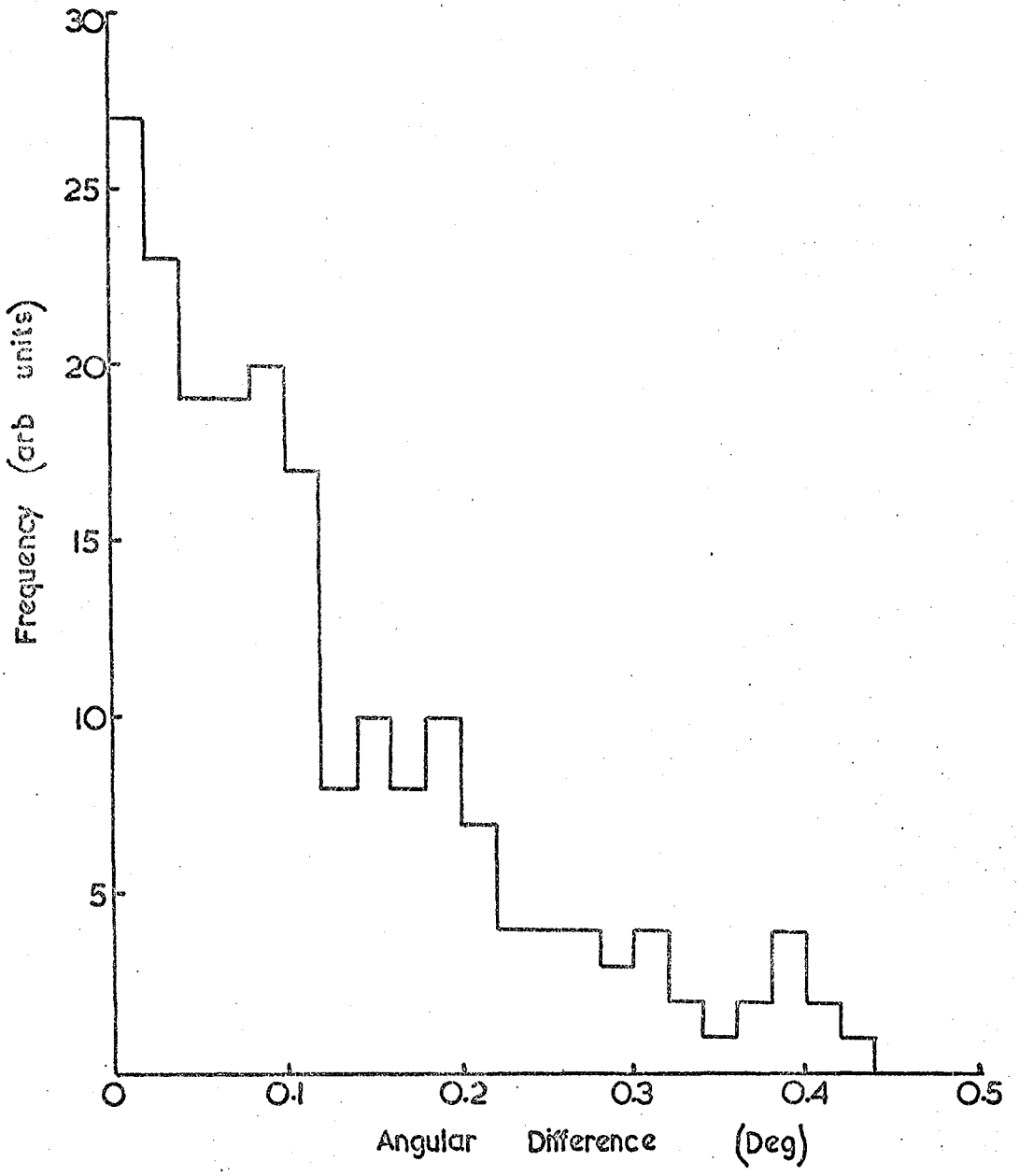

E, and lateral positions, R, symmetrically arranged around ψ_{GF} and R_{GF}. Lines up to $\psi_{GF} \pm 0.5^{o}$ and $R_{GF} \pm 0.4$ cms. were tried using angular steps of 0.05^{o} and lateral steps of 0.04 cms. Using the criteria outlined in §3.3.1, the "best track" is selected and its angle, ψ_{BF}, and lateral position, R_{BF}, are stored. This process is carried out on the track in both arms of the spectrograph.

This flow chart assumes only one flash tube has flashed in each layer, but the programme can handle a limited number of layers with more than one flashed tube. Tracks using all possible combinations of tubes are tried in turn and the 'best track' for each combination is selected. The 'best tracks' are then compared and the 'best track' is chosen. A maximum of 9 combinations can be so evaluated.

Having estimated the 'best track' for each half of the spectrograph independently, various parameters, some of which indicate the acceptability of the 'best track' (see §3.3.4) and others which are needed for the later derivation of the momentum spectra (§3.6) can be calculated. The latter are:-

a) the angular deflection, $\Delta\psi$,

b) the approximate impact point of the 'best track' on the neutron monitor. For the purposes of this measurement the neutron monitor is split up, at the level of the top of the inner moderators, into 80 cells and the cell in which the 'best track' impacts is calculated.

c) the momentum, p, corresponding to a deflection, $\Delta\psi$, in the magnetic field (no allowance being made for Coulomb scattering or errors of track location),

d) the apparent charge of the particle.

On completion of the analysis of the track in the spectrograph, any track in tray X2 (see §2.2.2c) is analysed. Since the accuracy required from this flash tube tray is not as great as for the spectrograph, the analysis carried out is confined to a least-squares fit to the flashed tubes, leading to estimates of the co-ordinates of the centre-of-gravity of the flashed tubes and the angle of inclination of the track

to the vertical.

3.3.3 Tests of Validity of Procedure

The reliability of the computer track-fitting programme was checked in the following ways:-

a) computer fitted events were compared with the results of hand analysis of the same events - 200 comparisons in all being made,

b) artificial tracks with known angles and lateral positions were generated and the results of fitting by the computer prggramme compared with the known parameters,

c) a momentum spectrum of comsic ray muons was measured and compared with the previous measurements.

a) Comparison with Hand Analysis

Scale drawings (2/3 actual size) of each half of the spectrograph were constructed and used to give estimates of the trajectory of a particle (the "hand analysis" method). Figure 3-2 shows a plot of ψ_C (ψ_{BF} from the computer analysis) against ψ_H (ψ_{BF} from the hand analysis) and figure 3-3 is a histogram of $|\psi_C - \psi_H|$. It can be seen that there is good agreement between the trajectories selected by the computer programme and the hand analysis. Hence, if hand analysis gives a good estimate of the trajectory, then so will the computer analysis.

b) Artificial Events

Events were generated by positioning a line randomly on the two trays of flash tubes in an arm of the spectrograph and then determining through which flash tubes the line passed. For each tube the probability of flashing was then determined using a probability function, and a random number between 0 and 1 was generated. If the random number was less than the probability of flashing then the tube was considered to have flashed. The events generated in this way were then analysed by the computer programme and the resulting "best tracks" compared with the known trajectories. It has been shown that the precise form of the probability function is not important when generating tracks in this way and 3 different forms of the function were considered. In

Fig 3.2 Comparison of Hand Analysis and Computer Fitting of Particle Trajectories

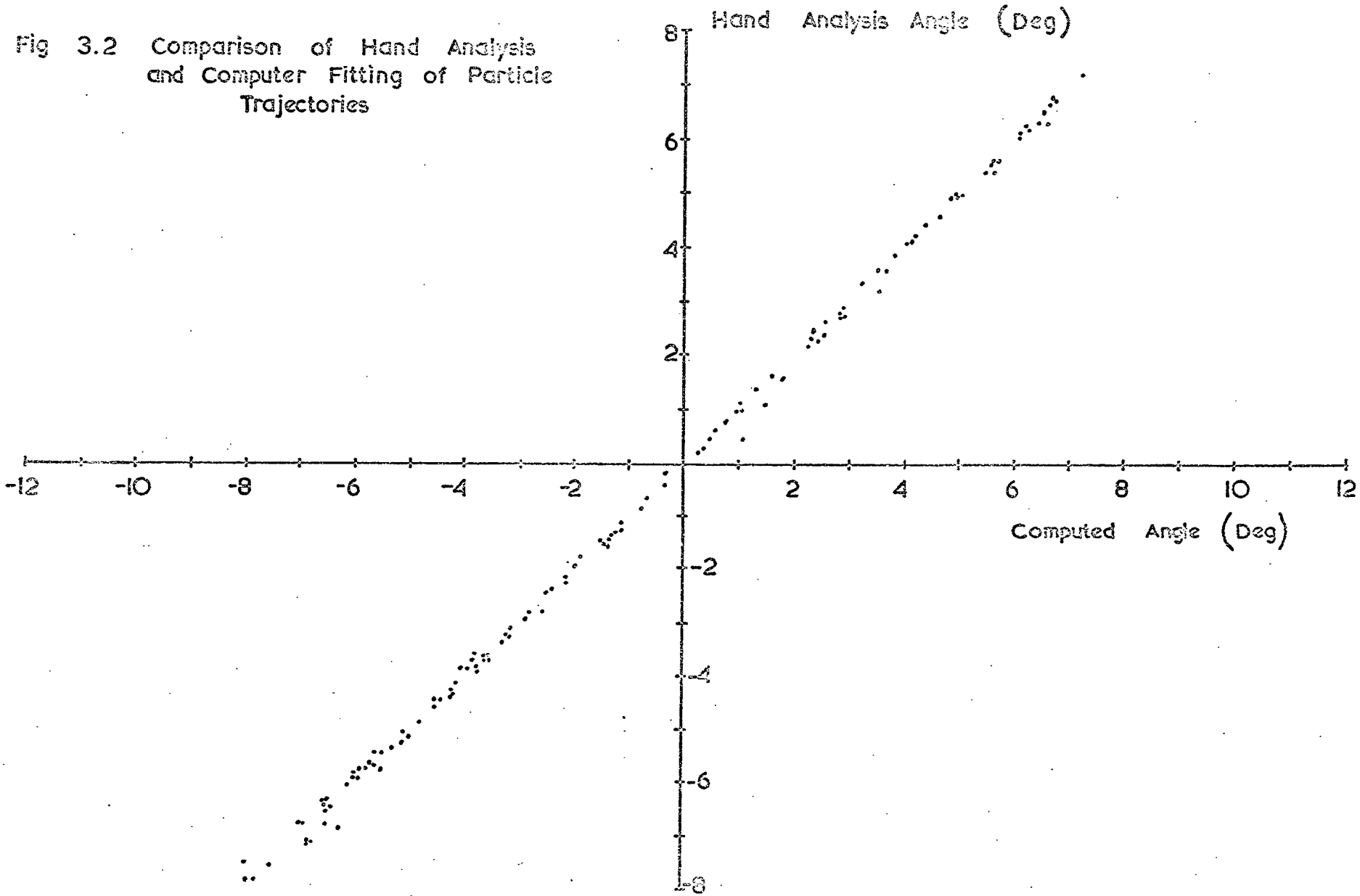

each case the r.m.s. angular difference between the actual artificial track and the best track selected by the computer was $< 0.1^{\circ}$.

c) The Measured Muon Momentum Spectrum

About 1000 events were recorded by the spectrograph when triggered solely by a GM counter coincidence (A+B+C). (D.E). F (see Chapter 2). These events were predominantly unassociated muons which were analysed in the same way as the "single particles". A value of apparent momentum was determined for each event and the resulting integral momentum spectrum is shown in figure 3.4, where it is compared with the muon spectrum of Allkofer et al., 1971. The two spectra are arbitrarily normalised at a momentum of 1 GeV/c, and no corrections for scattering and instrumental errors have been applied to the present spectrum. It can be seen that the agreement is good up to ~30 GeV/c, indicating that the present instrument and analysis techniques may be reliably used up to this value without any correction, and to higher momenta if the appropriate allowance is made for scattering effects.

3.3.4 Checks of the Validity of Computed Particle Tracks

When an event had been analysed by the computer, various tests were applied to the track to check whether a satisfactory "best estimate" of the trajectory had been obtained. Poor results can be produced through errors in the enumeration of the track, or through problems in the subsequent analysis. The human errors were usually incorrect enumeration of flashed tubes or the failure to note a flashed tube from the film record.

The following parameters of the track were computed and used in checks of its acceptability:-

a) the number of ignored flashed tubes (IIG),

b) the "efficiency" of the track, defined as the path-length in flashed tubes as a percentage of the total path-length in the neon gas of flash tubes, BMAX/(BMAX + |BMIN|),

c) the lateral positions, y_o and y_1, of the intersection point of the upper and lower tracks, respectively, with the horizontal plane through the centre of the magnet air-gap and their

Fig. 3.4. The Integral Muon Momentum Spectrum recorded with the present instrument (no corrections for instrumental noise have been made.)

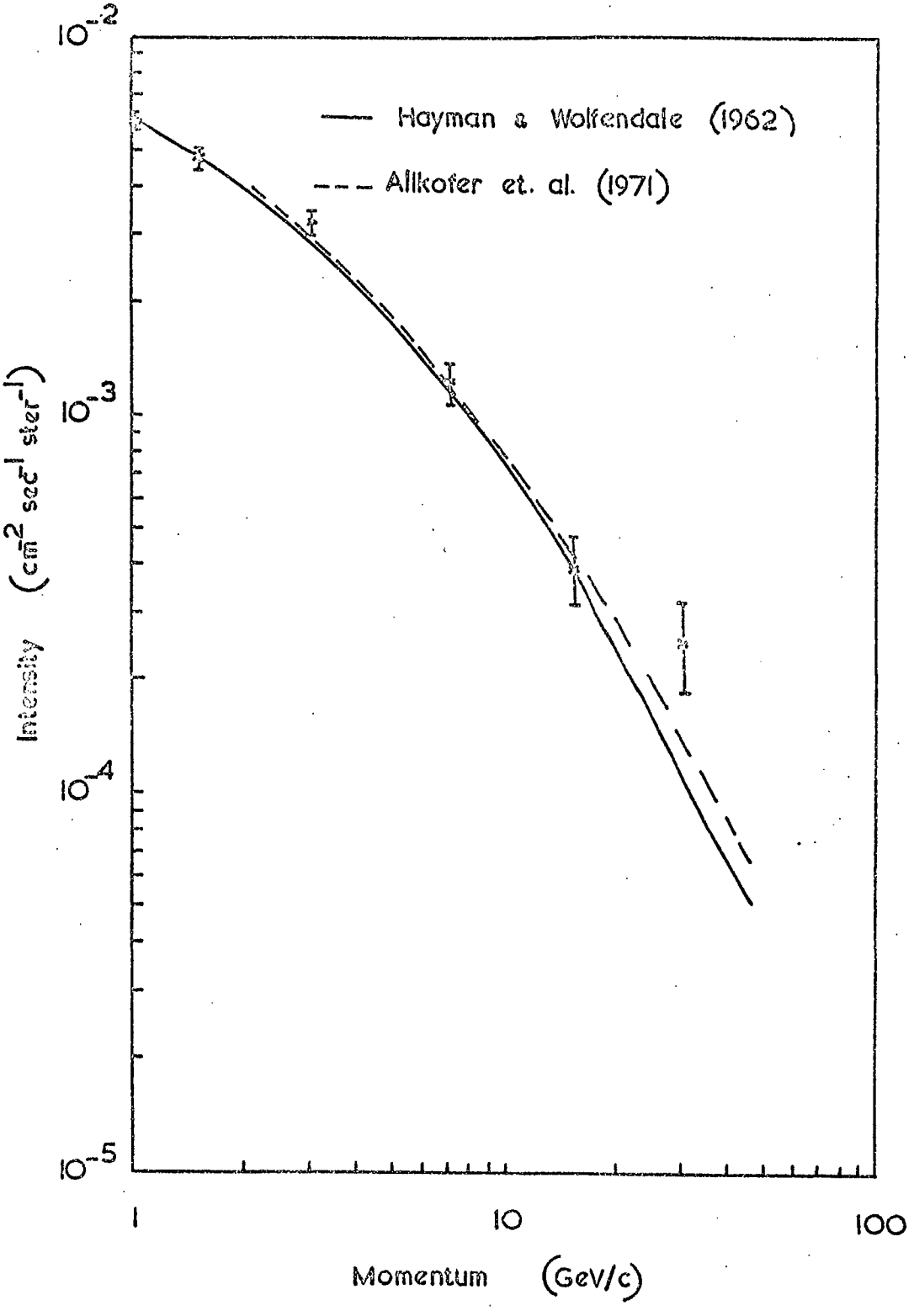

difference, Δ (= $y_1 - y_o$).

d) the intersection points of the appropriate tracks with the various GM counter trays.

If tubes were incorrectly enumerated, it was impossible to fit a straight line through all the flashed tubes and hence test a), together with test (b) would indicate such mistakes. Missed, and ignored, flashed tubes would be indicated by test (b) since the path-length in non-flashed tubes would be increased and the path-length in flashed tubes decreased with respect to their values for the correctly enumerated event and so the efficiency would be noticeably reduced. Figure 3-5 is a histogram of the efficiency obtained with good tracks, and on the basis of this information tracks having efficiency less than 70% were further scrutinised.

The remaining tests, (c) and (d), detect other poor track reconstructions.

The simple theory of the propagation of a charged particle through the magnetic field in the spectrograph indicates that the value of Δ obtained for all events should be zero. However, scattering in the material of the spectrograph and instrumental errors will mean that finite, but small, values of Δ will be obtained for most events and the actual distribution obtained is given in figure 3-6. Erroneous analysis will give rise to larger than normal values of Δ for tracks which can be detected and re-examined.

To have triggered the spectrograph the particle must have passed through all the GM counter trays, and so any track which, apparently, does not do so must be faulty and will be detected by test (d).

Any event which failed any of these tests was automatically re-enumerated. If the enumeration was found to be different the event was re-analysed by the computer and further checks made. For those events still faulty on one or more criteria, for which the enumeration was found to be correct, the tracks were examined closely to see if any reason for the poor fit could be found. Correctly enumerated tracks which were found to ignore one flashed tube were accepted since they may be expected to arise from knock-on electrons which cause tubes to flash which are near,

Fig 3.5 Distribution in Efficiency of Reconstructed Tracks

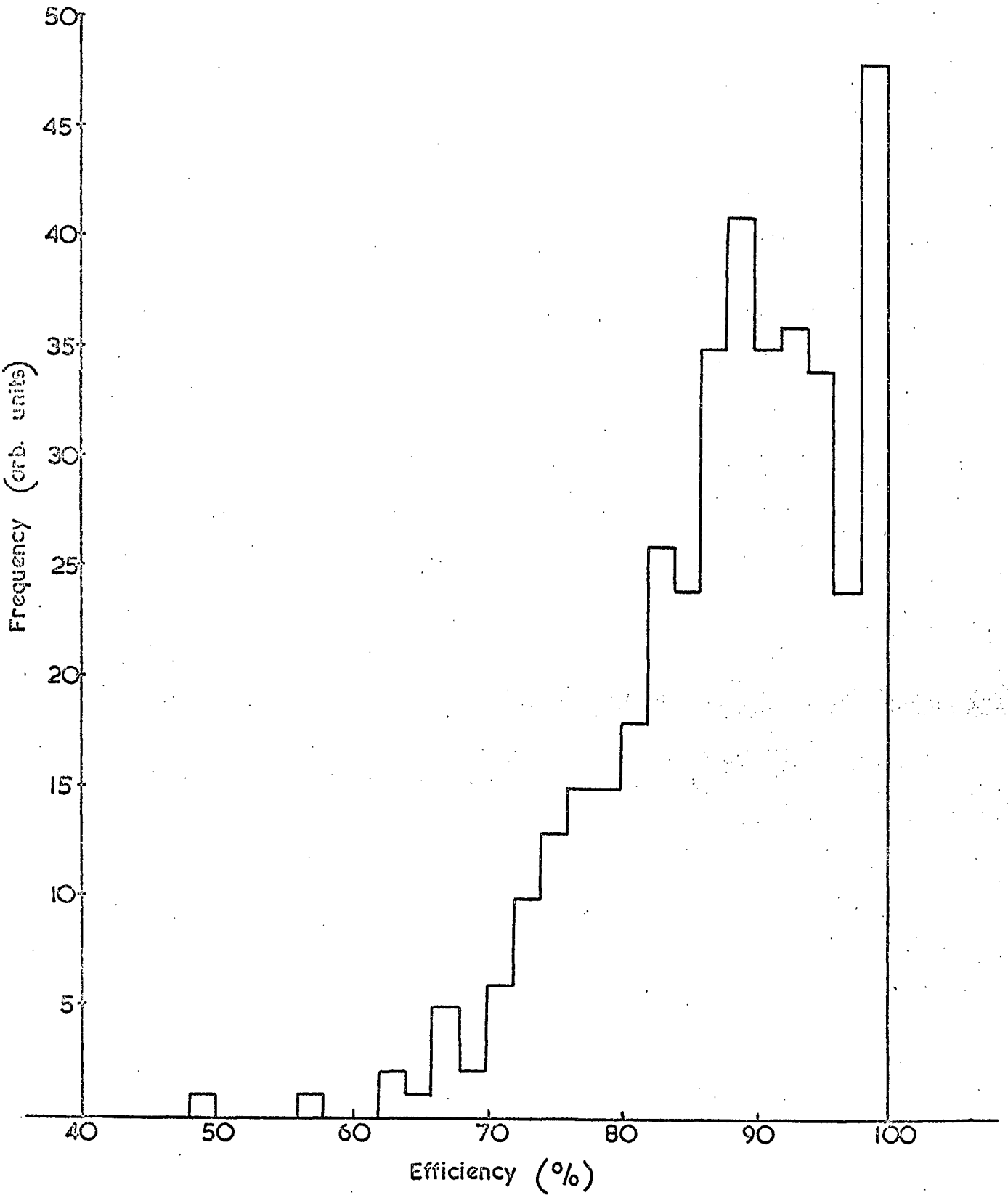

Fig 3.6 Distribution of the Lateral Separation in the Mid Plane of the Magnet of Incident and Emergent Particle Trajectories

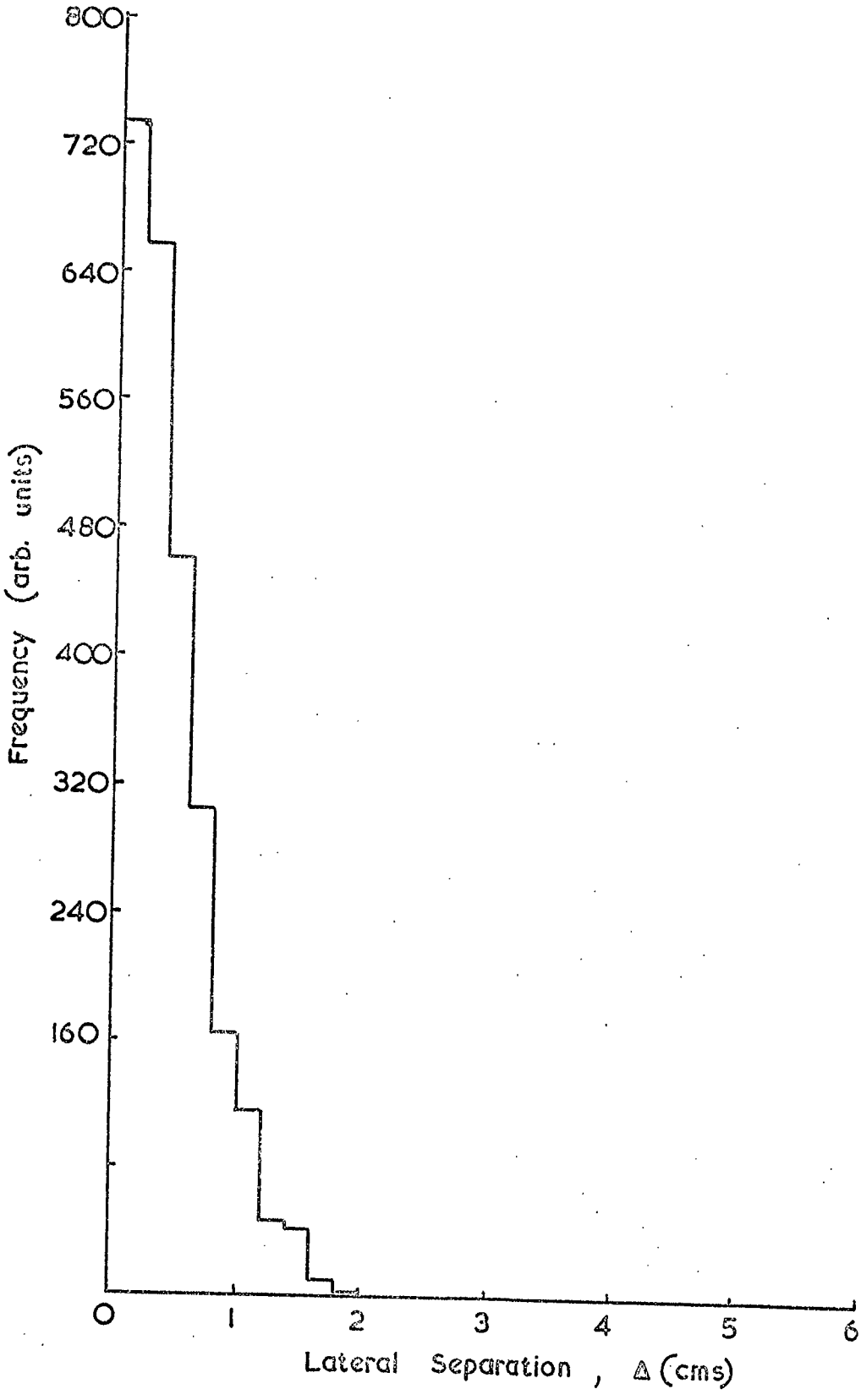

but not on, the particle trajectory. The only events which remained unexplained were a few with comparatively large values of Δ and these were taken to be the extreme tail of the distribution of Δ , and accepted in the analysis.

3.4. Identification of Particles

3.4.1. Introduction

Assuming there are no anti-protons in the cosmic radiation at sea level, there are four categories of particle which are expected to be recorded by the present equipment:-

a) nuclear-active particles consisting of protons and positive and negative pions,

b) low energy negative muons which stop in the neutron monitor and are captured by Pb-nuclei to produce a response,

c) muons which have produced a response in the neutron monitor through a photo-nuclear interaction,

d) cosmic ray particles (predominantly muons) in accidental coincidence with a neutron recorded by the neutron monitor.

Using the data obtained from the film records and that deduced from the particle track analysis, each event may be identified as belonging to one of these four categories.

The data available for use in identification are:-

(i) the impact point on the neutron monitor of the particle;

(ii) the magnetic deflection of the particle which leads to estimates of the momentum and charge;

(iii) the location of the neutrons detected in the neutron monitor;

and (iv) the number and location of any particles emerging from the neutron monitor.

The momentum of muons which would traverse the neutron monitor, average thickness 264 $g.cm^{-2}$, is 0.45 GeV/c (Joseph , 1969). Thus, if all events with a measured momentum $<$ 1GeV/c are rejected, the low energy negative muons will be much reduced. The limit of 1 GeV/c allows for errors in momentum measurement due to scattering in the spectrograph. Similarly,

any particle which has a measured momentum $\geq$ 1 GeV/c and is absorbed in the neutron monitor can be identified as an NAP.

As stated earlier, it was expected that the evaporation neutrons produced by an interaction would be detected close to the point of production, and that this property could be useful in identifying particle. The point of impact of the track on the neutron monitor at the level of the top of the inner moderator was calculated. The number of 2 cm. cells between this point and the centre of the nearest counter which had detected a neutron was then estimated. If the distance were $>$ 15 cells (see §3.4.2), and if there were a track emerging from the neutron monitor, the particle was said to be an accidental muon. If there were no track underneath the monitor the event was rejected and a correction for the events lost in this way was applied later. In this way the events with no track in flash tube tray X2 were identified and some of the accidental muons were eliminated.

There will, however, be muons which have impact distances $\leq$ 15 cells, and also NAPs which have tracks in X2. These were separated using the scattering of the particles in the neutron monitor. From the flash tube data in trays B3 and B1, the expected position of the particle in the X2 tray, in the absence of the material of the neutron monitor, can be predicted. Also the approximate thickness of lead traversed by the particle can be estimated and, using the estimated momentum of the particle, the r.m.s. Coulomb scattering, σ_y, can be predicted, assuming the particle to be a muon. The position of the particle in X2 is known and so the actual amount of scatter, S, can be compared with σ_y. If $s \geq 8\sigma_y$ (see §3.4.3 for the justification of this limit) then the particle was identified as an NAP, while, if $s < 8\sigma_y$ the particle was said to be a muon. Hence the NAPs were selected from the total events and distributions of the measured deflection for positive and negative particles were compiled.

Those events in which the predicted position of the particle in the X2 flash tube tray was close to the gap between the two trays which constitute X2, and there was no visible track in this tray, were

rejected and the necessary correction was applied to the data.

3.4.2. Impact Criterion

The evaporation neutrons emitted by an excited nucleus are characterised by an isotropic angular distribution and an energy spectrum which is peaked around a few MeV (Hatton, 1971). Neglecting scattering in the lead since the cross-section for elastic scattering of 2 MeV neutrons is ~1 barn and the angular scattering distribution is peaked in the forward direction, and assuming that neutrons are detected by the counter in the moderator on which they are incident, it can be seen that the majority of evaporation neutrons will be detected in the nearest counter, since this counter subtends the largest solid angle at the excited nucleus. Hence it is expected that the majority of the evaporation neutrons will be detected close to the point of production.

The neutron monitor was divided into 80 cells, of approximate width 2 cms, and the cell upon which the 'best track' impacts was calculated. Then the number of cells from this point to the centre of the nearest counter unit which had detected a neutron was estimated and called the impact distance. Figure 3-7 shows the distribution of impact distances obtained for all the analysed events. Superimposed on this distribution is the distribution which would be expected if all the events were muons in accidental coincidence with a background counting rate uniform across the neutron monitor. As suggested these distributions indicate that the evaporation neutrons are indeed detected close to their production point.

Figure 3-8 shows the distribution of impact distances for events which can be directly identified as NAPs. These are the events with measured momentum $\geq$ 1 GeV/c and no secondaries emerging from the neutron monitor. On the same figure the expected distribution of impact distances, calculated under the above assumptions, is drawn. The similarity of the distributions indicates that the assumptions are not unreasonable.

From these results an impact distance of $\leq$15 cells was considered necessary for the particle to be identified as an NAP, and for the necessary

Fig. 3.8 A Comparison between the Observed and Predicted Impact Distance Distributions for N.A.P.s

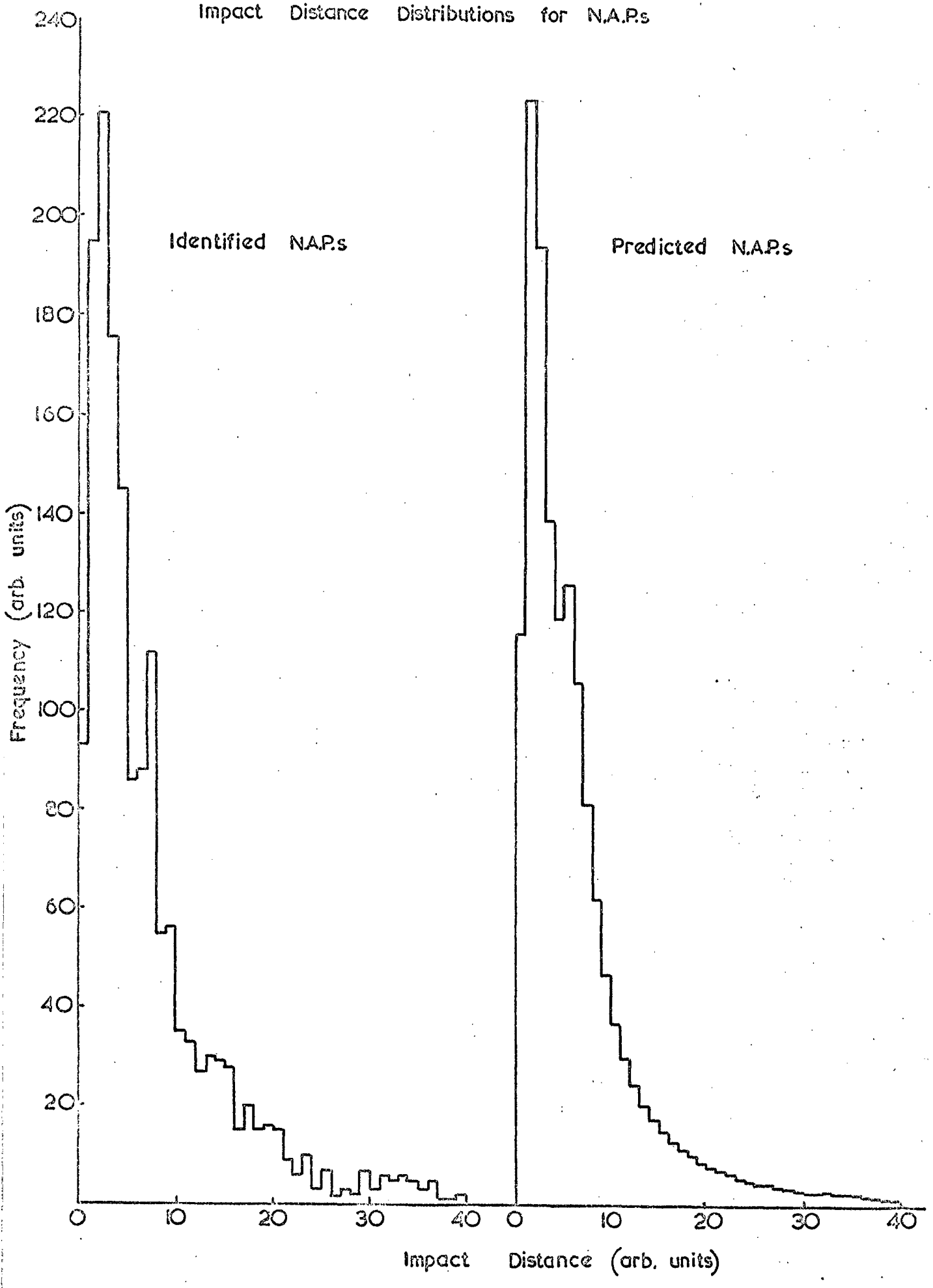

correction to be of limited effect.

3.4.3 Scattering of Particles in the Neutron Monitor

To identify those events which have one or more particles emerging from the neutron monitor, and which have impact distances ≤ 15 cells, the different scattering in the neutron monitor expected for NAPs and muons is used. The events which constitute this group may be accidental muons, interacting muons or NAPs.

In an inelastic proton-Pb nucleus interaction the surviving nucleon retains ~0.5 of the incident energy and so will be the most energetic emergent particle. Assuming the distribution of traverse momentum of all types of particle to be the same, the surviving nucleon will be scattered the least. So, in those events which had more than one track beneath the neutron monitor, the track which was closest to the predicted position was measured and used in identification procedures.

The method of calculation of the scattering is indicated in figure 3-9. The "actual position" of the particle is taken to be the centre-of-gravity of the flashed tubes in the X2 flash tube tray, and the perpendicular distance from this point to the "best track" found for the lower half of the spectrograph is considered to be the scatter, S. Knowing the angle and lateral position of the spectrograph track the amount of lead traversed by the particle can be approximately calculated and hence, using the measured value of momentum, p, in GeV/c, the r.m.s. projected angle of Coulomb scatter can be calculated from

$$\sigma_c = 15.\times 10^{-3} \frac{x}{p\beta(p\beta - \epsilon x)}$$

where ϵ is the energy loss per radiation length for muons (taken as 0.008 GeV/radn. length), β is the velocity of the particle in terms of the velocity of light, assuming the particle to be a muon, and x is the thickness of lead traversed in radiation lengths. The measured value of momentum is that found by applying the simple theory of the motion of a charged particle in a magnetic field, neglecting scattering and instrumental noise, and is given by

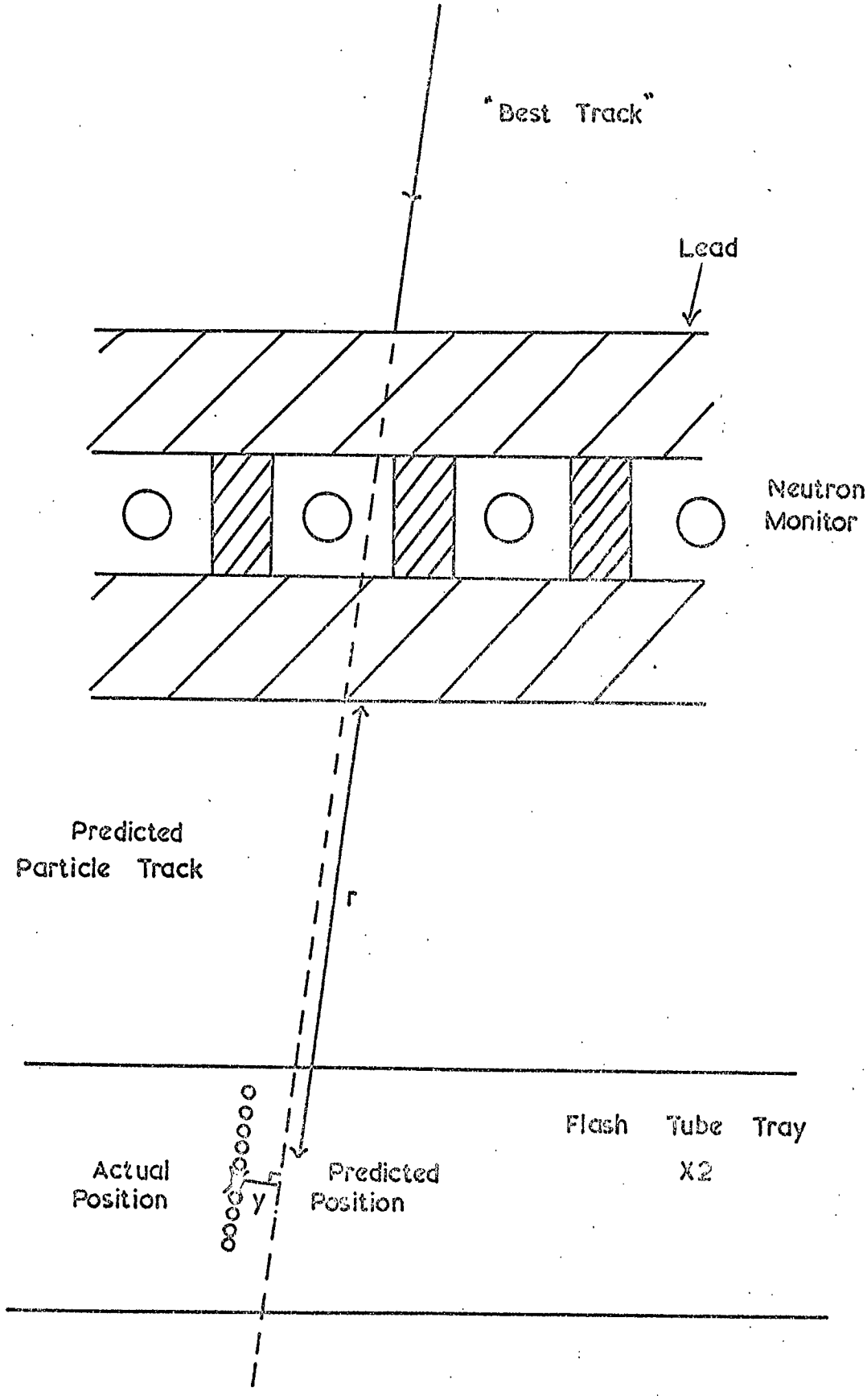

Fig. 3.9. The Scattering of Particles in the Neutron Monitor.

$$p = \frac{K}{\Delta\psi} \quad \text{GeV/c}$$

where K = 2.95 for this spectrograph.

Having found σ_c, the distance r along the predicted particle track to the predicted position in X2 is found and then the r.m.s value of scatter, σ_y, is found from

$$\sigma_y = r\sigma_c \quad \text{cms.}$$

The accidental muons will have undergone only Coulomb scattering in the material of the neutron monitor and so 94% of them should have the emergent track within $2\sigma_y$ of the expected position. Since the cross-section for nuclear interactions of muons falls rapidly with increasing four-momentum transfer squared, the angular scattering of interacting muons will be small also. The observed distribution of the scattering, expressed in terms of σ_y is shown in figure 3-10. It appears that the data in this figure are drawn from two poulations and, in view of the expected small scatter of muons, those events with large scatter were considered to be NAPs. The limiting value of scatter was arbitrarily chosen, from the distribution, to be $8\sigma_y$. Thus particles with values of scatter $\geq 8\sigma_y$ were identified as NAPs.

Since the measurement of the scatter is made in a plane, there will be errors introduced due to the projected scattering of an NAP being less than the $8\sigma_y$ limit. However, from figure 3-10, the number of NAPs which will be incorrectly identified will be small and can be estimated, and thus a correction may be applied.

It should be noted that in inelastic pion- Pb nucleus interactions the incident particle is not known to survive and so the analysis of the least scattered track is not justified. However, the technique will lead to the rejection of some genuine pion events rather than the acceptance of muon events so that the pion momentum spectrum will be underestimated in the high momentum region. Since the number of such events may be expected to be small, the error in the spectrum due to this cause will be small also and has been neglected in the present work.

Fig. 3.10 The Distribution of Scattering in the Lead of the Neutron Monitor.

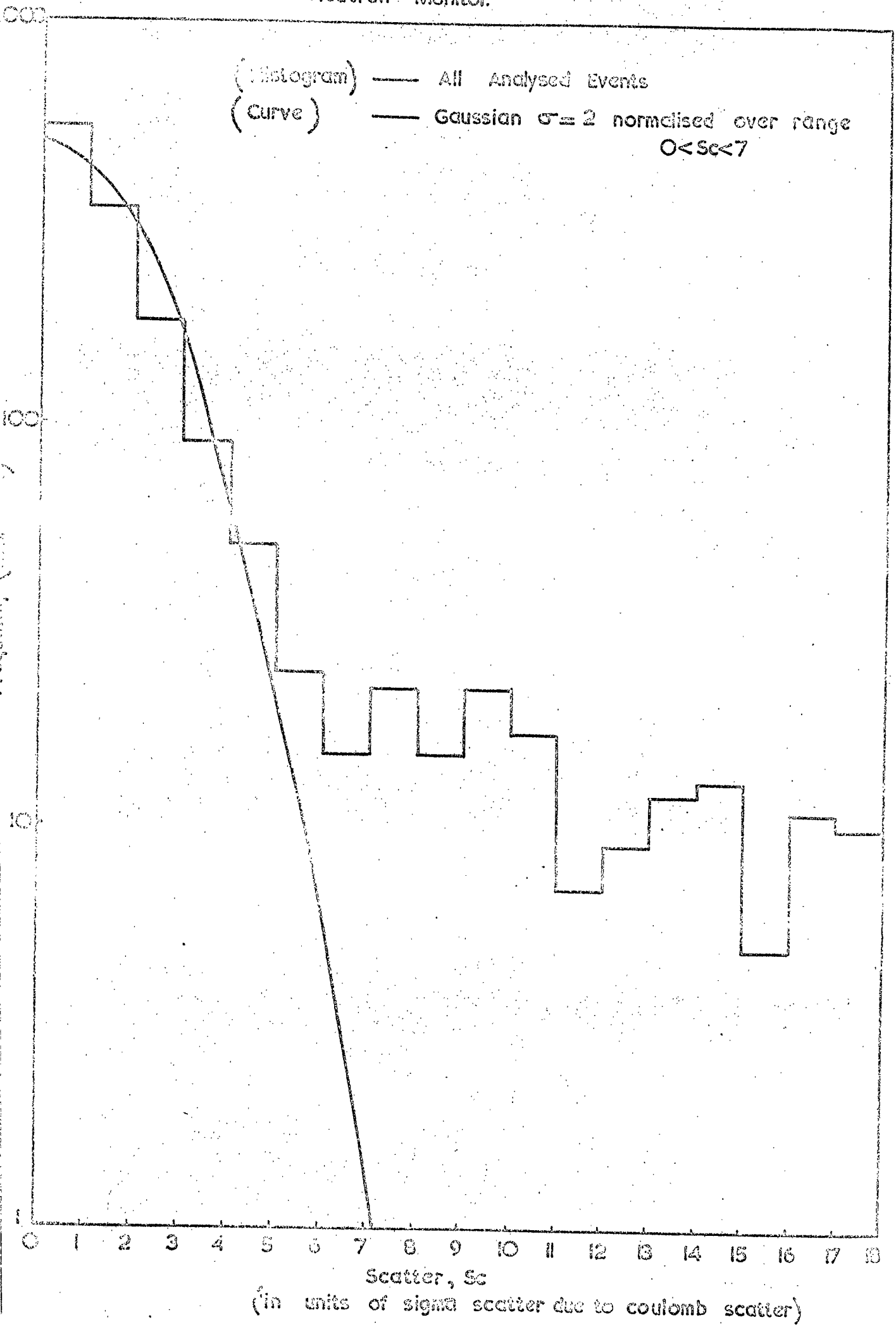

3.4.4 Summary

A flow diagram of the procedure used to identify the events is given in figure 3-11.

Table 3-1 gives a summary of the proportions of each type of event which was collected by the 'single particle' mode of spectrograph triggering.

Table 3-1

TYPE	%
Dense	15
'EAS'	<1
Momentum <1 GeV/c	22
NAP	22
Reject	6
Muon	15
Interaction in Flash Tube Tray	19

3.5. Estimation of Measurement Noise

3.5.1. Introduction

When a vertical particle, of momentum p, passes through the spectrograph it is deflected through an angle $\Delta\psi_m$ by the magnetic field, where

$$\Delta\psi_m = \frac{K}{p}$$

However, on traversing the material of the spectrograph, the particle is scattered by collisions with nuclei and, when the track is reconstructed, a random error is made in estimating the angle of the 'best fit', assumed to be normally distributed about the actual trajectory. Thus, in general, the actual measured deflection, $\Delta\psi$, will not equal $\Delta\psi_m$ but a beam of

Fig. 3.11. Flow Diagram of Procedure Used for Identification of Particles.

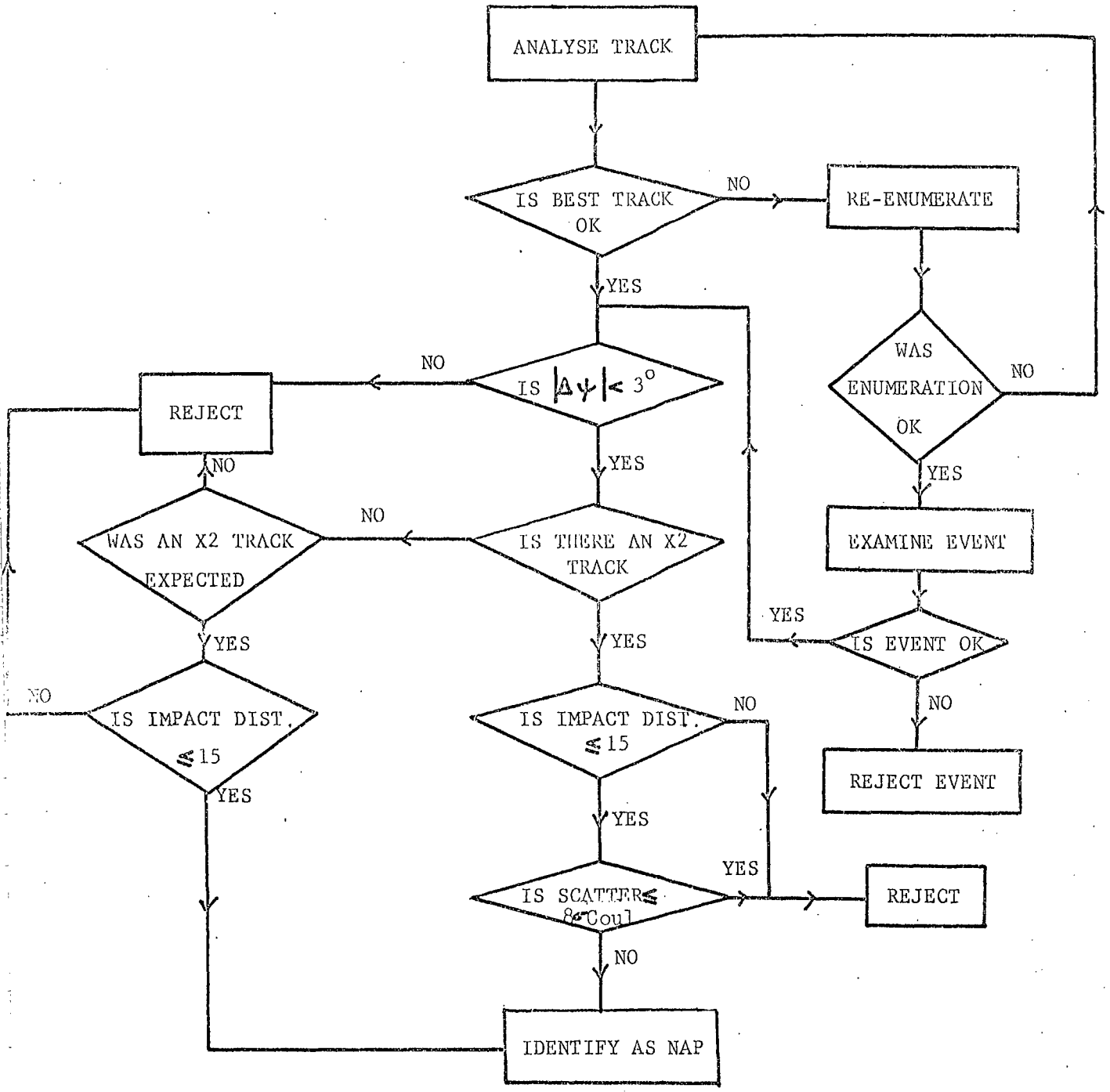

vertical particles, of momentum p, will give a distribution of measured deflections such that

$$P(\Delta\psi)\, d\Delta\psi = \frac{1}{\sigma\sqrt{2\pi}}\, e^{-\frac{(\Delta\psi - \Delta\psi_m)^2}{2\sigma^2}}\, d\Delta\psi$$

where $P(\Delta\psi)d\Delta\psi$ is the probability of observing a deflection $\Delta\psi$ to $\Delta\psi + d\Delta\psi$. The standard deviation, σ, of this distribution is given by

$$\sigma^2 = \sigma_c^2 + \sigma_T^2.$$

σ_c is the r.m.s. value of scattering due to collisions with nuclei, given by $\sigma_c = 0.148\sqrt{x}/p\beta$ where x is the thickness of material traversed in radiation lengths and β is the velocity of the particle in terms of the velocity of light, and σ_T is the r.m.s. value of the error due to track reconstruction and is a constant. It can be seen that, as p increases, $\Delta\psi_m$ and σ_c decrease so that the distribution of deflections becomes effectively independent of p and the accuracy of the momentum measurement decreases. The effect of the distribution of deflections can be allowed for in the analysis procedure (see §3.6) but, in order to do so correctly, and to extend the measurements to as large a value of momentum as possible, the value of σ_T must be small and accurately known.

In order to reduce σ_T to a low value the neon flash tubes were accurately located and σ_T was measured in three independent ways:-

(a) The distribution of the lateral separation of the intersection of the two halves of a track with the horizontal plane through the centre of the magnet was measured,

(b) The distribution of deflections of particles passing through the spectrograph with zero magnetic field was measured;

(c) The momentum spectrum of unaccompanied cosmic ray muons was measured.

3.5.2. The Location of the Flash Tubes

The flash tubes in each layer of the four momentum measurement trays were supported at their ends in accurately machined duralumin supports. A sample of the supports was measured accurately using a travelling microscope and the horizontal pitch of the flash tubes was found to 1.907 ± 0.008 cms.

With the flash tube trays in position the distance from a key point on each support to an arbitrarily defined plane parallel to the lines of magnetic flux was measured using a telescope mounted on a travelling microscope stand. From estimates of the accuracy of these measurements the value of σ_T was expected to be $\sim 0.1^{\circ}$.

3.5.3. The Distribution in Leteral Separation of Tracks in the Mid-plane of the Spectrograph

It is shown in the appendix that a graph of σ_Δ^2, the mean square value of the lateral separation of the upper and lower tracks in the mid-plane of the spectrograph, against $|\Delta\psi|^2$ where $\Delta\psi$ is the magnetic deflection of the particle, should be a straight line with an intercept on the σ_Δ^2- axis proportional to σ_T^2 where σ_T^2 is the instrumental noise. But σ_Δ^2 was evaluated for a small range of values of $\Delta\psi$ and so $\overline{|\Delta\psi|}^2$ was plotted and the graph is given in figure 3-12. Figure 3-13 is the distribution in Δ for $|\Delta\psi| < 0.5^{\circ}$ when the instrumental noise should be dominant, and it can be seen that the distribution is closely gaussian. From figure 3-12 σ_n was found to be $0.17^{\circ} \pm 0.02^{\circ}$ which gives an error on $\Delta\psi$ due to instrumental noise σ_T, of $0.24^{\circ} \pm 0.03^{\circ}$.

3.5.4. The Zero-field Run.

If the spectrograph is operated without a magnetic field and is used to detect unassociated muons in the cosmic ray beam, all the tracks should have zero deflection. However, due to scattering in the material of the spectrograph and errors due to instrumental noise, an event will not, in general, have zero deflection, and the distribution of deflection, $\Delta\psi$, will be given by

Fig. 3.12 A Graph of σ_Δ^2 against $\overline{|\Delta\psi|}^2$ for Cosmic Ray Muons.

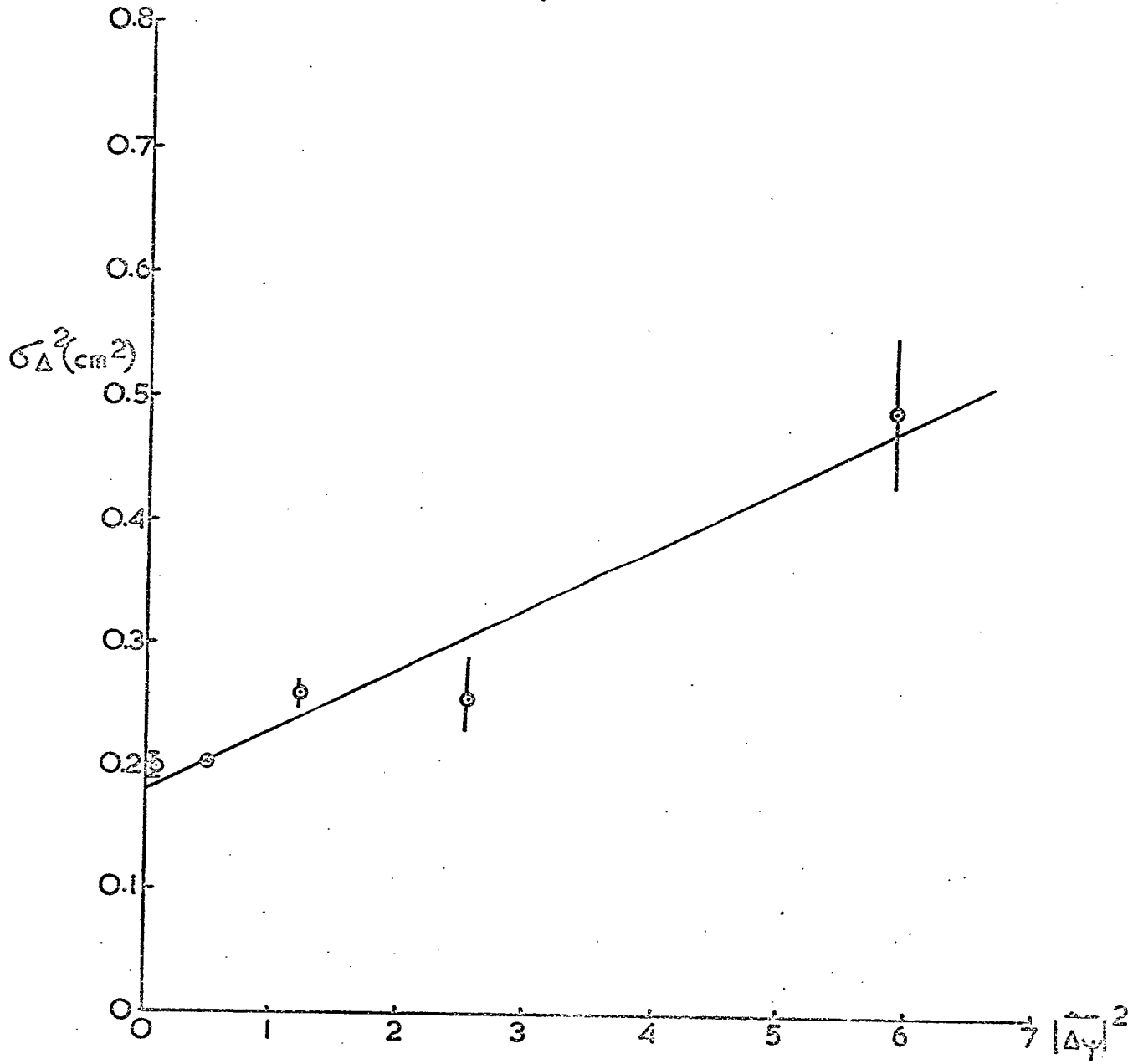

Fig. 3.13 The Distribution in Lateral Separation of Tracks in the Mid Plane of the Spectrograph for $|\Delta y| < 0.5^{\circ}$.

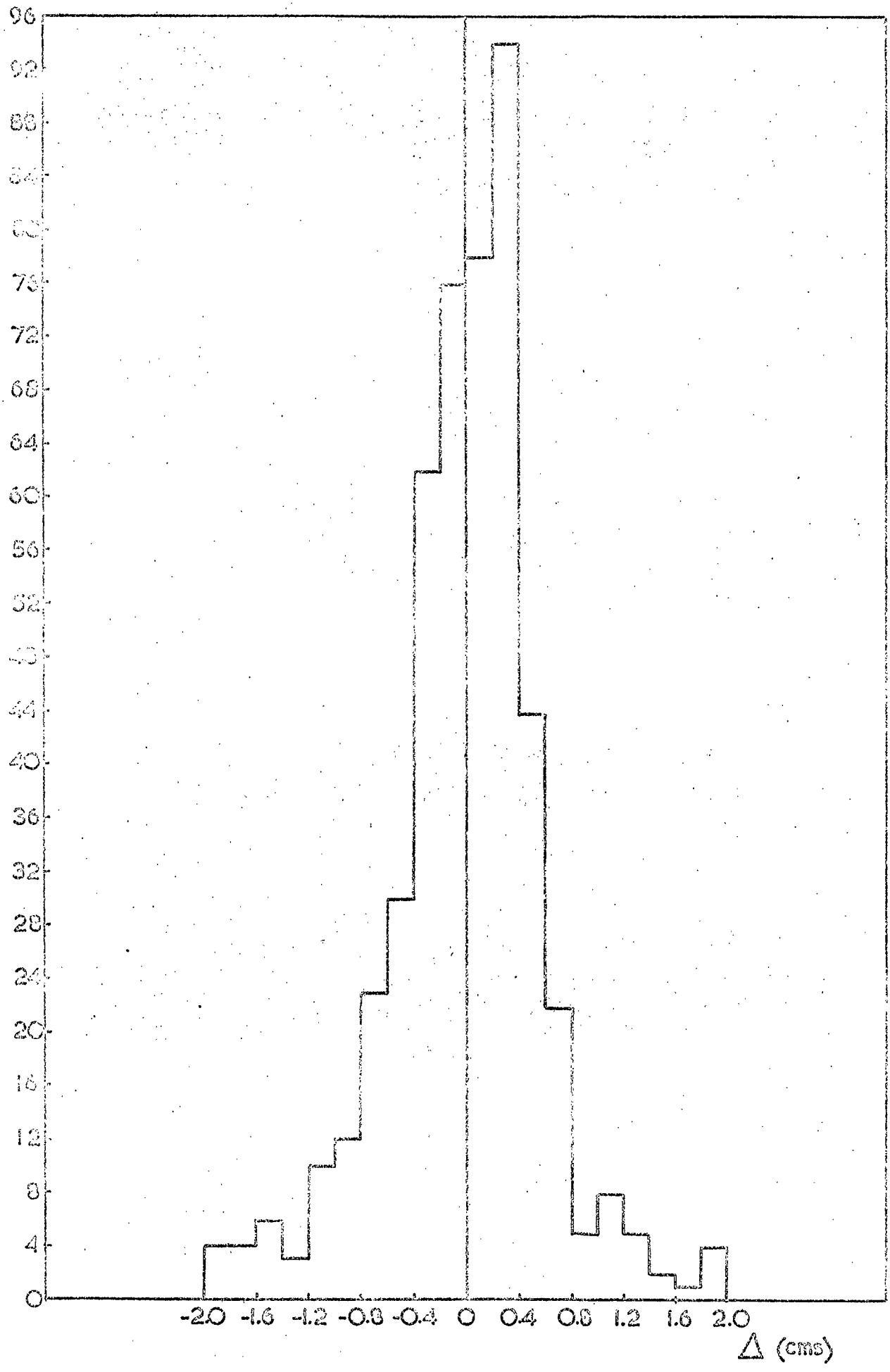

$$f(\Delta\psi)\, d\Delta\psi = \frac{\int_{p_o}^{\infty} S(p)\, P(p,\Delta\psi)\, d\Delta\psi \; dp}{\int_{p_o}^{\infty} S(p) \; dp}$$

where $S(p)\, dp$ is the momentum spectrum of unassociated cosmic ray muons and $P(p,\Delta\psi)d\Delta\psi$ is the probability of a muon, of momentum p, being observed to have a deflection $\Delta\psi$, and

$$P(p,\Delta\psi)\, d\Delta\psi = \frac{1}{\sigma(p)\sqrt{2\pi}}\, e^{\frac{-\Delta\psi^2}{2\sigma^2(p)}}\, d\Delta\psi$$

$\sigma(p)$ is given by

$$\sigma^2(p) = \frac{K}{p^2} + \sigma_T^2$$

where K/p^2 is due to scattering in the material of the spectrograph and σ_T is the standard deviation of the distribution due to measurement noise, assumed to be normal.

Thus $f(\Delta\psi)\, d\Delta\psi$ should be a normal distribution with a standard deviation, $\sigma_{\Delta\psi}$, given by

$$\sigma_{\Delta\psi}^2 = \frac{\int_{p_o}^{\infty} \left[S(p)\, \sigma(p)\right]^2 dp.}{\left[\int_{p_o}^{\infty} S(p)\, dp\right]^2}$$

and for this instrument using the momentum spectrum of muons given by Hayman and Wolfendale (1962)

$$\sigma_{\Delta\psi}^2 = 4.46\ 10^{-5} + 0.178\ \sigma_T^2$$

with $\sigma_{\Delta\psi}$, σ_T measured in radians.

The distribution obtained from 238 muons is given in figure 3-14 and can be seen to be closely normal. The value for σ_T found is $\sigma_T = 0.3^o \pm 0.3^o$.

Fig. 3.14 The Distribution in Deflection obtained from the Zero Field Run.

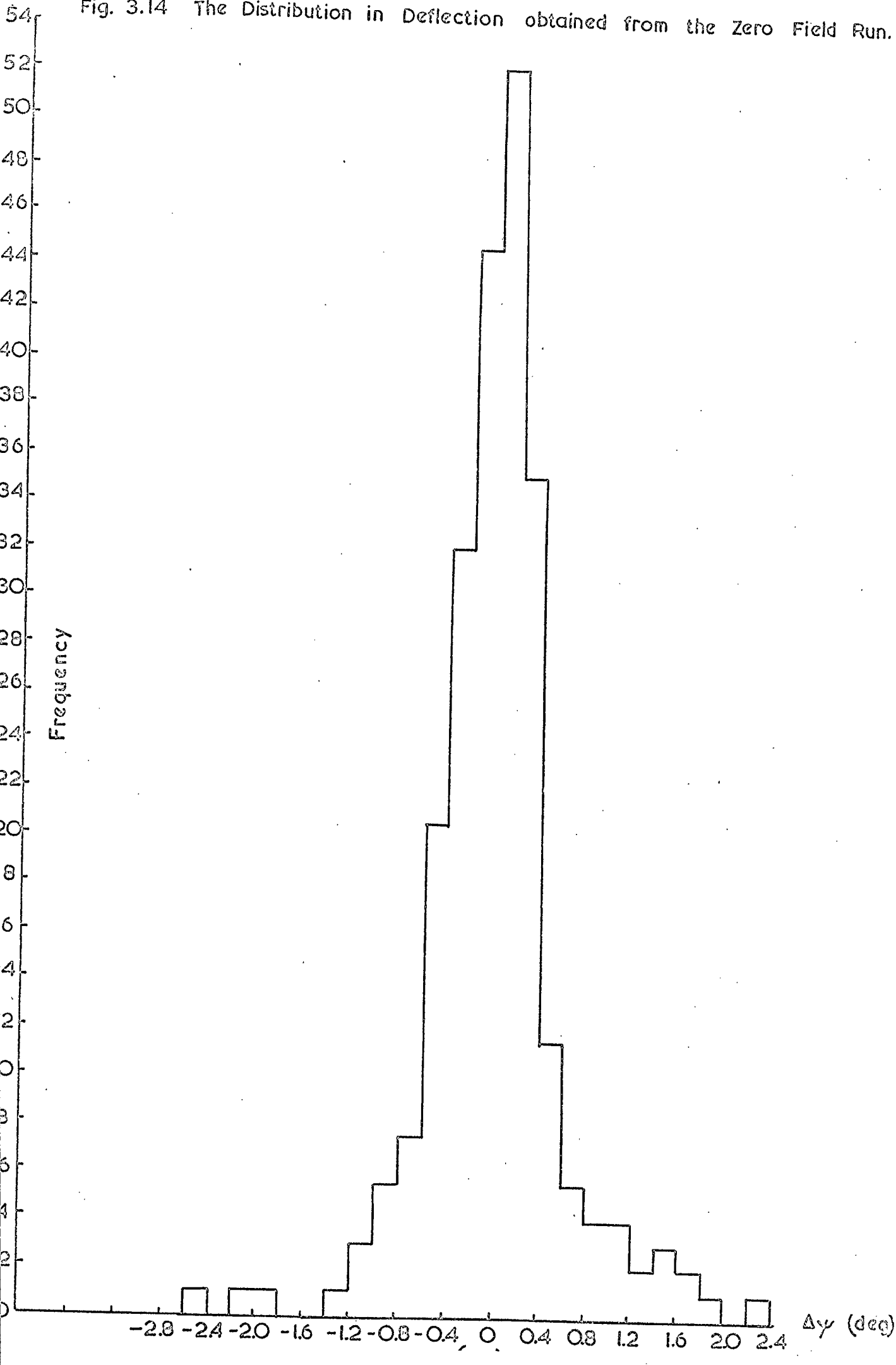

3.5.5. The Single Muon Momentum Spectrum.

The momentum spectrum of unassociated cosmic ray muons measured with the present spectrograph is given in figure 3-4 where it is compared with the spectrum of Allkofer et al., 1971. It can be seen that the spectra agree in shape up to a momentum of ~ 30 GeV/c with no corrections applied to the present data. This indicates that this spectrograph can be used, without applying corrections, to accurately measure the momentum of individual particles up to this value, corresponding to a deflection of 0.1^{o}, and so the measurement noise must be less than 0.07^{o}.

Considering the accuracy of each of these estimates of the measurement noise it was decided that the value obtained from the distributions of the lateral seperation of the tracks in the mid-plane of the magnet gave the best value and so the noise was taken to be $0.24^{o} \pm 0.03^{o}$.

3.6. Derivation of the Momentum Spectra

3.6.1. Introduction

All the information concerning momentum of NAPs obtained in this experiment is reduced to two deflection distributions, one for positive NAPs and one for negative NAPs. So, it is possible to derive the momentum spectra and intensities of two types of particle. The NAPs which might exist in cosmic rays near sea level are nucleons, anti-nucleons, pions and kaons. The relative yield of kaons to pions in proton collisions at 70 GeV is ~ 0.1 (Antipov et al., 1971) and the kaon lifetime is approximately half that of the pion, and so the number of kaons in cosmic rays at sea level will be negligble compared with the number of pions. Also, the yield of anti-protons at 70 GeV is ~2% of that of pions, (although recent evidence indicates that this yield increases with energy to ~ 15% at 1500 GeV), so that the number of anti-protons should be small, and there is very little evidence to date for the existence of anti-protons in cosmic rays near sea level. Hence it is assumed that the particles detected in the present experiment are protons and positive or negative pions. It is also assumed that, since all pions are produced in the atmosphere, the spectra of positive and negative pions are identical. With these assumptions it is possible

to derive the momentum spectra of protons and negative pions in cosmic rays at ground level.

3.6.2. Separation of Spectra of Protons and Pions

Let $K_p S_p(p)dp$, $K_{\pi^+} S_{\pi^+}(p)\,dp$, $K_{\pi^-} S_{\pi^-}(p)\,dp$ be the momentum spectra of protons, postive pions and negative pions respectively. Then the observed deflection spectra for positive particles, $N_+(\Delta\psi)\,d\Delta\psi$, and negative particles $N_-(\Delta\psi)\,d\Delta\psi$ will be

$$N_+(\Delta\psi)\,d\Delta\psi = \int_0^\infty K_p S_p(p) W_p(p,\Delta\psi)dp\,d\Delta\psi + \int_0^\infty K_{\pi^+} S_{\pi^+}(p) W_{\pi^+}(p,\Delta\psi)dp\,d\Delta\psi + \int_0^\infty K_{\pi^-} S_{\pi^-}(p) \bar{W}_{\pi^-}(p,\Delta\psi)dp\,d\Delta\psi$$

and $$N_-(\Delta\psi)\,d\Delta\psi = \int_0^\infty K_p S_p(p) \bar{W}_p(p,\Delta\psi)dp\,d\Delta\psi + \int_0^\infty K_{\pi^+} S_{\pi^+}(p) \bar{W}_{\pi^+}(p,\Delta\psi)dp\,d\Delta\psi + \int_0^\infty K_{\pi^-} S_{\pi^-}(p) W_{\pi^-}(p,\Delta\psi)\,dp\,d\Delta\psi$$

where $W_k(p,\Delta\psi)$ and $\bar{W}_k(p,\Delta\psi)$ are the probabilities of a particle of type k, of momentum p, giving a measured deflection $\Delta\psi$ with the correct and incorrect charge, respectively. But we assume $K_{\pi^+} = K_{\pi^-} = K_\pi$

and $$S_{\pi^+}(p)dp = S_{\pi^-}(p)dp = S_\pi(p)\,dp$$

for all p.

Then

$$N_+(\Delta\psi)\,d\Delta\psi = \int_0^\infty K_p S_p(p) W_p(p,\Delta\psi)\,dp\,d\Delta\psi + \int_0^\infty K_\pi S_\pi(p)\left[W_\pi(p,\Delta\psi) + \bar{W}_\pi(p,\Delta\psi)\right]dp\,d\Delta\psi$$

and

$$N_-(\Delta\psi)\,d\Delta\psi = \int_0^\infty K_p S_p(p) \bar{W}_p(p,\Delta\psi)\,dp\,d\Delta\psi + \int_0^\infty K_\pi S_\pi(p)\left[\bar{W}_\pi(p,\Delta\psi) + W_\pi(p,\Delta\psi)\right]dp\,d\Delta\psi$$

Subtracting

$$\left[N_+(\Delta\psi) - N_-(\Delta\psi)\right] d\Delta\psi = \int_o^\infty K_p S_p(p) \left[W_p(p,\Delta\psi) - \bar{W}_p(p,\Delta\psi)\right] dp \quad d\Delta\psi$$

which, when converted to a histogram, is

$$\left[N_+(\Delta\psi_i \to \Delta\psi_j) - N_-(\Delta\psi_i \to \Delta\psi_j)\right] = \int_o^\infty \int_{\Delta\psi_i}^{\Delta\psi_j} K_p S_p(p) \left[W_p(p,\Delta\psi) - \bar{W}_p(p,\Delta\psi)\right] dp \; d\Delta\psi$$

$$= \int_o^\infty K_p S_p(p) dp \left\{ \int_{\Delta\psi_i}^{\Delta\psi_j} W_p(p,\Delta\psi) \, d\Delta\psi - \int_{\Delta\psi_i}^{\Delta\psi_j} \bar{W}_p(p,\Delta\psi) \, d\Delta\psi \right\}$$

This can be solved for $S(p)\,dp$.

Then, substitution for $S(p)dp$ in either N_+ or N_- gives $S_\pi(p)dp$ with the intensities normalised to one another, but not absolutely.

3.6.3. The Weighting Factors

The functions

$$\int_{\Delta\psi_i}^{\Delta\psi_j} W_k(p,\Delta\psi) \, d\Delta\psi \qquad \text{and} \qquad \int_{\Delta\psi_i}^{\Delta\psi_j} \bar{W}_k(p,\Delta\psi) \, d\Delta\psi$$

must be evaluated for protons and pions in order to derive the momentum spectra.

They are given by

$$W_k(p,\Delta\psi) \, d\Delta\psi = \int_{\psi_o} \int_{\phi_o} A(\psi_o,\Delta\psi) \, B_k(\psi_o) \, C_k(\phi_o) \, D(\phi_o) \, P_k(p,\psi_o,\phi_o,\Delta\psi) \, d\psi_o \, d\phi_o \qquad (3.6.1)$$

where $\int_{\Delta\psi_i}^{\Delta\psi_j} W_k(p,\Delta\psi)d\Delta\psi$ and $\int_{\Delta\psi_i}^{\Delta\psi_j} \bar{W}_k(p,\Delta\psi)d\Delta\psi$ are given by integrating from $\Delta\psi_i = \pm |\Delta\psi_i|$ to $\Delta\psi_j = \pm |\Delta\psi_j|$ and $\Delta\psi_i = \mp |\Delta\psi_i|$ to $\Delta\psi_j = \mp |\Delta\psi_j|$ respectively.

$A(\psi_o,\Delta\psi)$ is the probability that a particle incident at a projected angle ψ_o will be deflected through $\Delta\psi$ and accepted assuming the neutron monitor to be uniform and neglecting the gap in the X2 flash tube tray.

$B_k(\psi_o)$ is the distribution in ψ_o for the particle type k

ϕ_o is the angle of incidence in a plane perpendicular to the measuring plane of the spectrograph and $C_k(\phi_o)$ is the distribution of ϕ_o for particle type k.

$D(\phi_o)$ is the probability of a particle incident at ϕ_o being accepted.

$P_k(p, \psi_o, \phi_o \Delta\psi)$ is the probability that a particle of type k and momentum p incident at angles $\psi o, \phi_o$ will be deflected through an angle $\Delta\psi$

Equation 3.6.1 was evaluated numerically and then integrated over the appropriate values of $\Delta\psi$ to give the required histograms.

3.6.4. Derivation of Spectral Shapes for Protons and Pions

The momentum spectra are derived using the method described by Orford (1968) in which an arbitrary momentum spectrum, $S(p)\,dp$, is taken as starting point. This spectrum is converted to a deflection spectrum using the appropriate combination of weighting factors and is then modified using the comparison between the predicted and observed deflection spectra such that

$$S_{j+1}(p)dp = \frac{\Sigma_i \left[S_j(p) \quad W(p\Delta\psi_i)\ M(\Delta\psi_i) \,/\, N_j(\Delta\psi_i) \right] dp.}{\Sigma_i\ W(p\Delta\psi_i)}$$

where $W(p\Delta\psi_i)$ is the appropriate combined weighting factor,

$M(\Delta\psi_i)$ is the observed deflection spectrum

$N_j(\Delta\psi_i)$ is the deflection spectrum predicted from $S_j(p)dp$, given by $\int S_j(p)\ W(p\Delta\psi_i)dp$ and is normalised to $M(\Delta\psi_i)$.

This process is carried out until the value of χ^2 found by comparing the predicted and observed distributions changed by less than 1% between two successive iterations. The best fit deflection distributions obtained are shown in figures 4-1 and 4-3 where they can be compared with the observed distributions.

The differential momentum spectrum was then integrated and statistical errors added to each point of the integral spectrum. Then estimates of the steepest and flattest acceptable integral spectra were drawn through the points. The intensities of these limiting spectra were then estimated and each spectrum was differentiated numerically to give the upper and lower limits of the differential intensities found above.

3.6.5. Corrections to Basic Data

Corrections were applied to the basic data to allow for the following

errors:-

(a) Losses due to incorrect identification of NAPs as muons caused by the limit applied to the scattering criterion,

(b) Loss of genuine NAPs in which the track in the lower half of the spectrograph would have passed between the 2 trays of flash tubes beneath the neutron monitor and which had no observable track in these trays.

(c) Loss of genuine NAPs which had an impact distance greater than the arbitrary limit applied.

(d) The identification of slow negative muons, which give rise to a neutron coincidence, as having a momentum > 1 GeV/c resulting from scattering in the material of the spectrograph.

(e) The loss of events through the rejection of tracks with 3 or fewer tubes in a momentum measurement flash tube tray since these would not provide a reliable track reconstruction.

(f) The loss of genuine unaccompanied NAPs which had been classed as 'F' events. (See §3.2.1).

The corrections for each of the above categories were made as follows:-

(a) From a comparison of the scattering distribution of all the "B" events with that of muons an estimate of the number of NAPs which were rejected was made.

(b) The impact distance distribution for the rejected events was compared with the distribution expected if all these events had been accidental. There was found to be an excess of observed events at small impact distances. These events were regarded as NAPs and their number was added to the $\Delta\psi$ distributions.

(c) From the theoretical impact distance distribution the number of genuine NAPs with impact distance > 15 was estimated and added to the observed $\Delta\psi$ distributions.

(d) The number of stopping negative muons which produced a detected neutron was calculated and then the fraction of these which

would be scattered so that the measured momentum was $> \frac{1}{4}$GeV/c was estimated. These were subtracted from the $\Delta\psi$ distribution of negative particles with no secondary emerging from the neutron monitor.

(e) The number of events which had been rejected through having only 3, or fewer, tubes in a flash tube tray was found. Assuming that the proportions of the various types of particle were the same within this group as within all the data, the number of NAPs which had been lost was estimated and added to the $\Delta\psi$ distributions.

(f) It was thought that the F events were caused by unassociated cosmic ray particles passing through part of the spectrograph during the sensitive time of the neon flash tubes which was quite long owing to the multiple pulsing technique. Hence the spectrograph was triggered randomly and the number of tracks which were seen was counted. This led to an estimate of the percentage of triggers which should have had an unassociated track visible in the spectrograph. Since this figure and the fraction of all the data which were classed as "F"-events were similar within experimental error, it was considered that all the "F"-events were caused by this mechanism and so were treated in the same manner as the rest of the data. These events were analysed and added to the NAP distributions before the above corrections, a - e, were applied.

Figure 3-15 gives the final $\Delta\psi$ distributions for positive and negative particles, after application of the above corrections.

3.6.6. Corrections to Spectral Shape

The method of deriving the spectral shape, described in §3.6.4, leads to a set of values of the intensity at a particular momentum. However, there are momentum dependent corrections which must be applied to the spectrum, and so these are estimated for the appropriate momentum values.

Fig 3.15 The Distribution in Angular Deflection for Positive and Negative NAPs after Correction of the Basic Data.

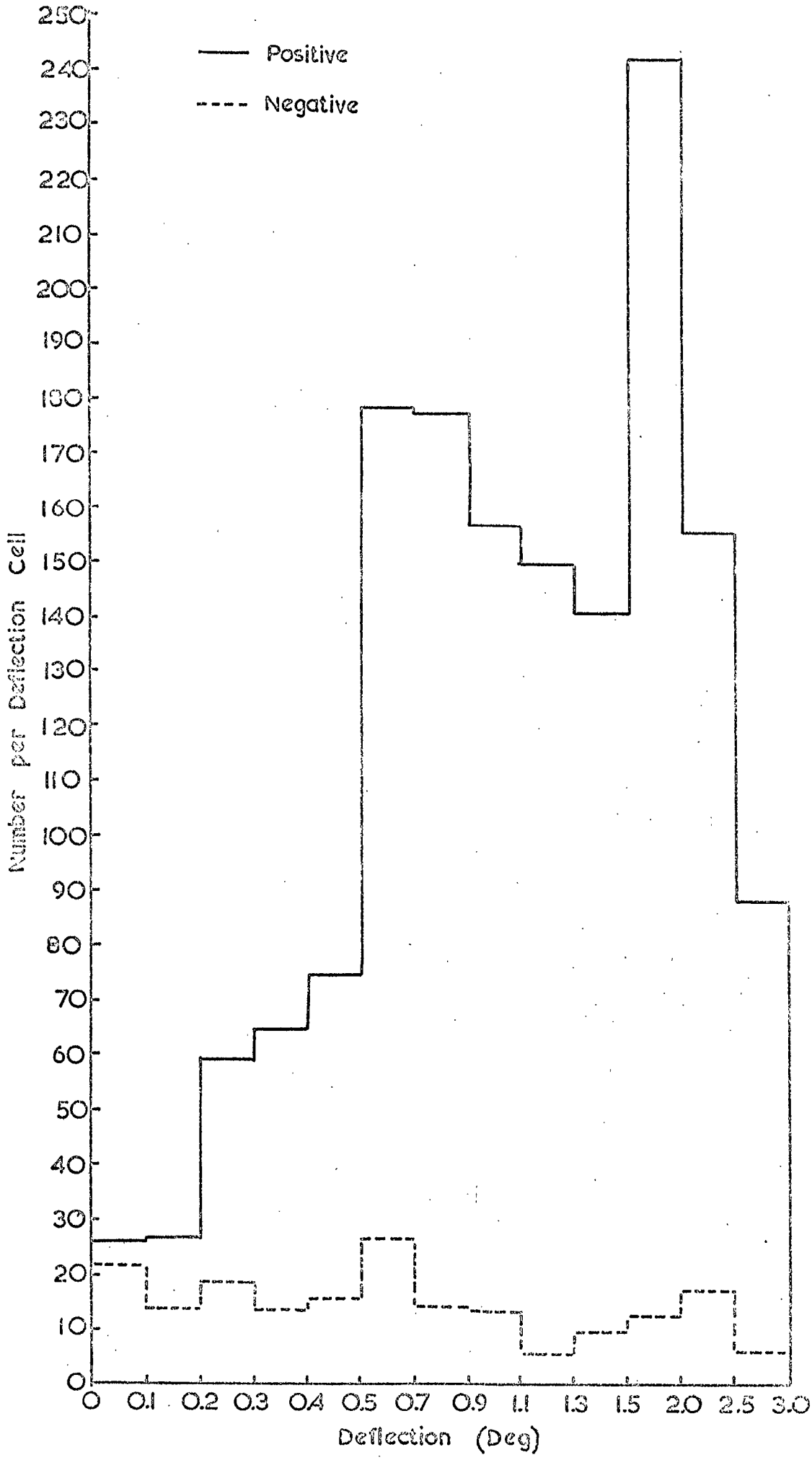

Errors are made in measuring the spectra due to

(a) loss of events due to interactions in the spectrograph,

(b) loss of events due to the low efficiency of the neutron monitor,

(c) loss of events due to the transparency of the neutron monitor.

(a) Interactions in the Spectrograph

Events which could be identified as interactions in the material of the spectrograph were rejected, and, since the probability of interaction is momentum-dependent, the correction for these losses is applied to the derived momentum spectrum. The probability of particles traversing the spectrograph without interacting was calculated as a function of momentum and particle type and is shown in figure 3-16. Both electromagnetic and nuclear interactions were included in this calculation.

(b) Neutron Monitor Efficiency

It has been shown that, if the multiplicity spectrum of evaporation neutrons produced in an interaction of a given energy follows a single exponential law, then the probability of detecting no neutrons is given by $1/\bar{m}$, where $\bar{m}$ is the average number of detected neutrons. Thus the correction to be applied to the spectral shape is $\bar{m}/(\bar{m}-1)$ where $\bar{m}$ is a function of momentum. From the observations for NAPs the variation of $\bar{m}$ with momentum was found and so the correction factor could be derived for the required values of momentum. This correction is independent of the value of efficiency of the neutron monitor and so no attempt was made to measure the efficiency.

(c) Transparency of Neutron Monitor

In order to be detected by the neutron monitor a particle must undergo a nuclear interaction in the lead target of the monitor. The probability of such interaction is a function of momentum and was estimated for a target of thickness 268 g cm^{-2} and the variation of the total interaction cross-section given by Giacomelli, 1970.

These three correction factors are combined to give the total correction factor as a function of momentum given in figure 3-17.

Fig. 3.16 The Probability of a Particle traversing the Spectrograph without Interacting

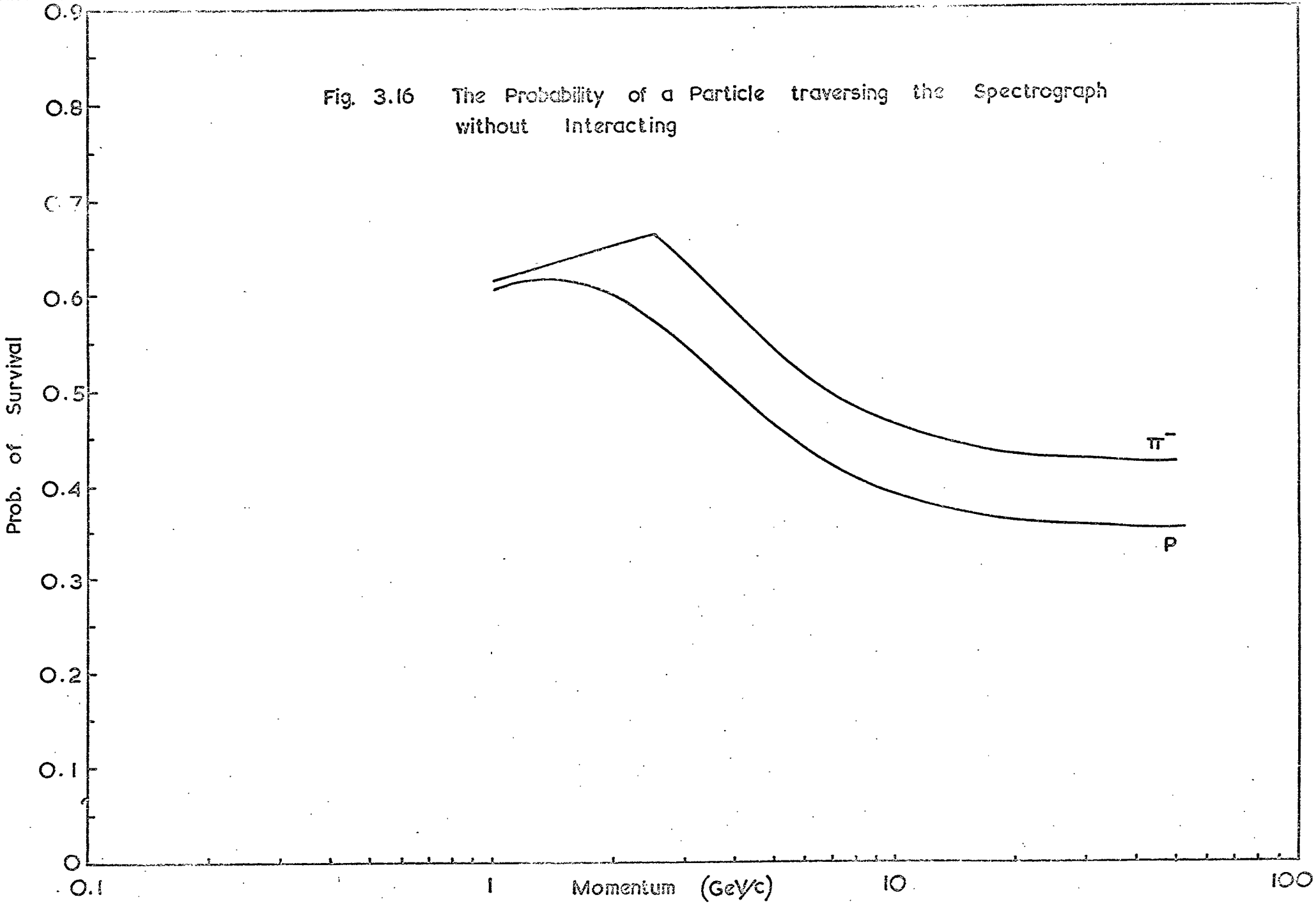

Fig. 3.17 The Total Correction Factor.

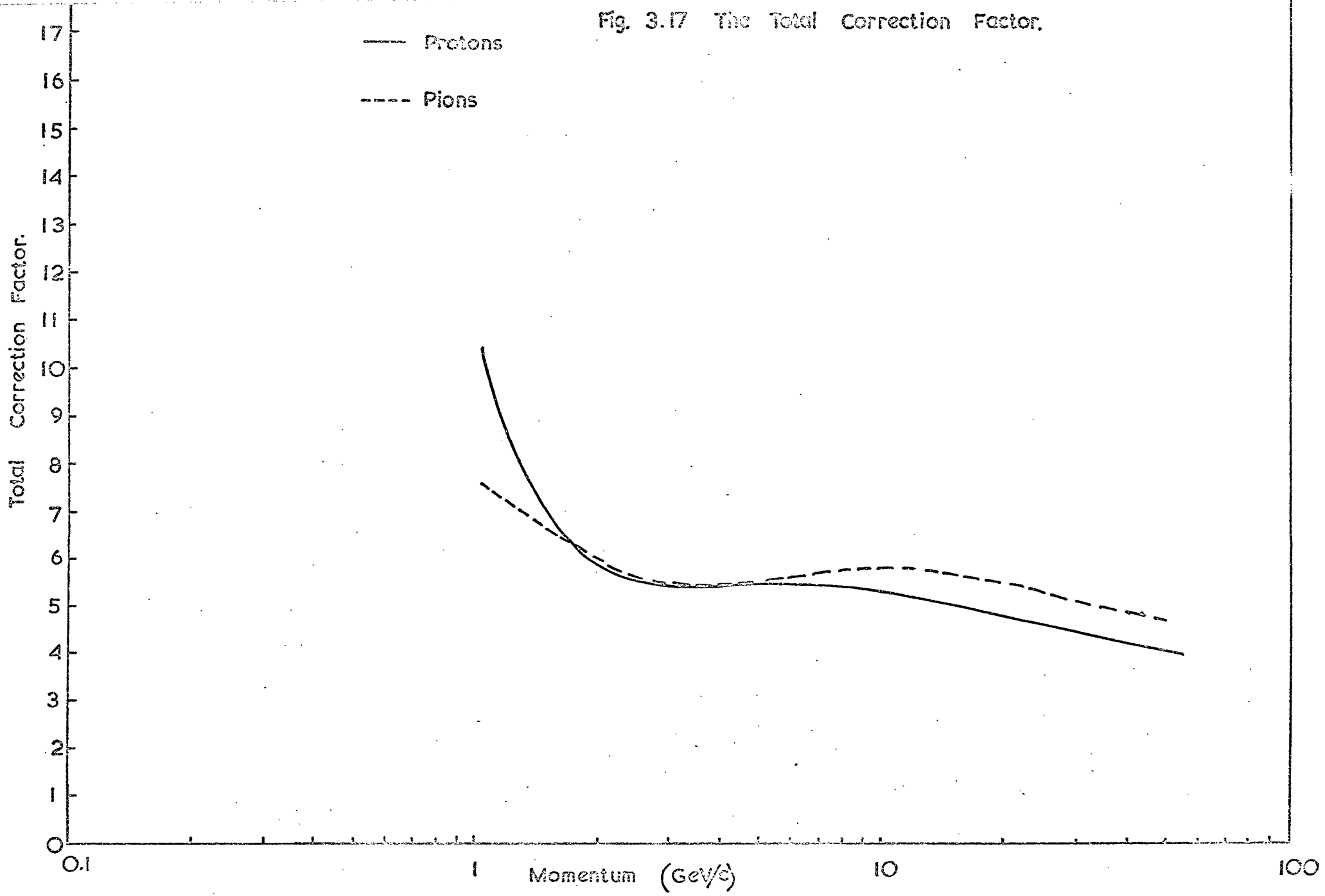

3.6.7. Normalisation

The analysis procedure described above yields the shapes of the momentum spectra of protons and negative pions at ground level together with their relative intensities, but does not give the absolute intensities. In order to obtain the absolute intensities the acceptance of the spectrograph must be evaluated accurately. This is a difficult task since GM counters were used and the effective size of each GM counter must be measured. It was thus decided to normalise thespectra to the absolute intensity of the muon spectrum available from other measurements.

When the muon momentum spectrum was measured using the present equipment the number of events with a measured momentum greater than 1GeV/c was recorded, together with the on-time of the equipment. The acceptance of the instrument can be estimated from these figures and the assumed intensity of muons of momentum greater than 1 GeV/c taken to be that given by Allkofer et al., 1971. The acceptance of the spectrograph was found to be 52 cm^2ster.

Then using this figure together with the known sensitive time of the equipment (1.56×10^6 secs) the absolute intensities could be estimated.

CHAPTER FOUR

NUCLEAR-ACTIVE PARTICLES NEAR SEA LEVEL

4.1. Unaccompanied Nuclear-active Particles

4.1.1. Introduction

Many of the previous measurements of the intensities of protons in the cosmic radiation at or near sea level have been confined to momenta below 1 GeV/c (e.g. Ogilvie, 1955, Filthuth, 1955, McDiarmid, 1959) using a technique in which NAPs were recognised by their absorption in local absorbers. This technique was also used by Mylroi and Wilson, 1951, who extended their measurements to a momentum of about 10 GeV/c. However, as pointed out by Brooke and Wolfendale, 1964, the probability of secondary particles penetrating the absorber becomes large at high energies, making this technique increasingly unreliable. This difficulty can be avoided if the interactions of the NAPs are observed as done by Pak and Greisen, 1962, who used a multi-plate cloud chamber to give a measurement at ~20 GeV/c, while Brooke and Wolfendale, 1964, identified NAPs through the production of evaporation neutrons, to complement their measurements using the absorption technique at low energies. Thus the only measurements comparable to the present data are those of Mylroi and Wilson, 1951, Pak and Greisen, 1962, and Brooke and Wolfendale 1964.

The sole measurement of pions in the cosmic radiation near sea level is that of Brooke et al., 1964b, using the same technique as Brooke and Wolfendale, 1964, for the proton measurement; an estimate of the pion to proton ratio at mountain altitude has been made by Subramanian, 1962.

4.1.2 The Momentum Spectrum of Unaccompanied Protons near Sea Level

Figure 4-1 shows the distribution of deflection of protons found in the present experiment and derived by subtracting the distribution for negative NAPs from that for positive NAPs as described in §3.6.2. Also on this diagram is the predicted deflection distribution obtained from the best fit momentum spectrum found using the technique described in §3.6.4.

Fig. 4.1 The Distribution in Angular Deflection used for Derivation of the Proton Momentum Spectrum.

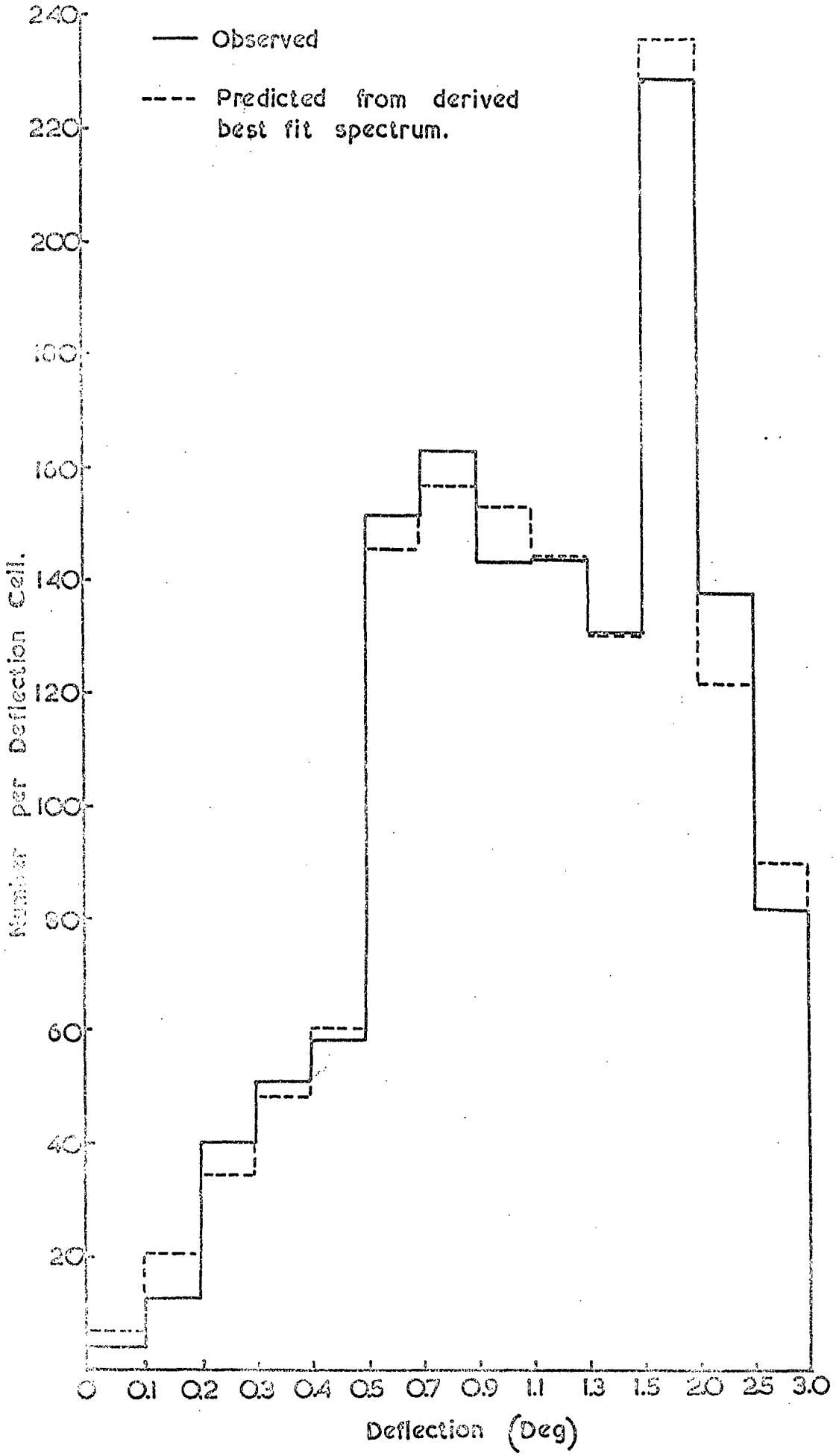

This momentum spectrum is shown in figure 4-2 where it is compared with the data of Brooke and Wolfendale, 1964. It should be noted that the previous measurements as presented here were normalised to the 1 GeV/c muon intensity of Rossi, 1948, whereas the present data were normalised to the intensity given by Allkofer et al., 1971, which is about 20% greater. Hence, for more realistic comparison, the points of Brooke and Wolfendale should be increased by ~20%. However, there is reasonable agreement between the two measurements although a somewhat different spectral shape from the power law which can be fitted to the data of Brooke and Wolfendale, is to be preferred for the present data. The curve through the present points was drawn by eye and does not represent a mathematical fit to the data.

4.1.3 The Momentum Spectrum of Unaccompanied Pions near Sea Level

The deflection distribution for negative pions obtained in the present experiment, after allowance has been made for protons which have been scattered to appear negatively charged, is shown in figure 4-3 and compared with the distribution predicted from the best-fit momentum spectrum. This momentum spectrum is presented in figure 4-4 and it is compared with the data of Brooke et al., 1964b, where the negative pion intensities were obtained by halving the published charged pion intensities. Again the absolute intensities of Brooke et al., 1964b, and the present work were obtained by normalization with the absolute muon intensities quoted by Rossi, 1948, and Allkofer et al., 1971, respectively.

The shapes of the two spectra are very similar but the intensities obtained from the present work are systematically a factor of up to 2 higher than those of Brooke et al. Part of this discrepancy can be attributed to the different normalization but there will still remain a discrepancy of more than a factor of 1.5.

In the present experiment, great care has been taken in the selection of the events and in correcting for various possible sources of error, e.g. the scattering of low energy negative muons detected by the neutron monitor

Fig. 4.2 The Differential Momentum Spectrum of Protons in the Cosmic Ray Beam near Sea Level.

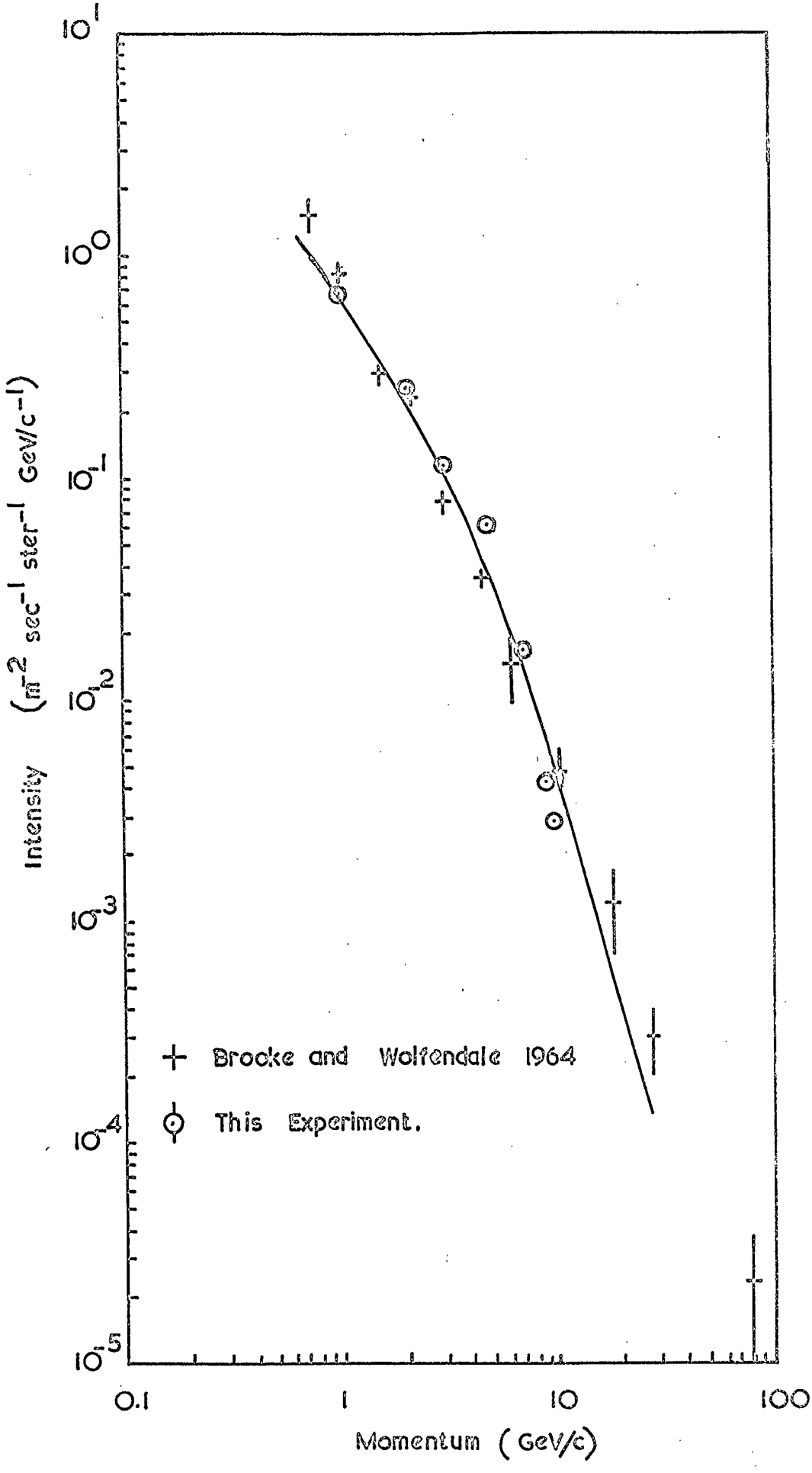

Fig. 4.3 The Distribution in Angular Deflection used for Derivation of the Negative Pion Momentum. Spectrum

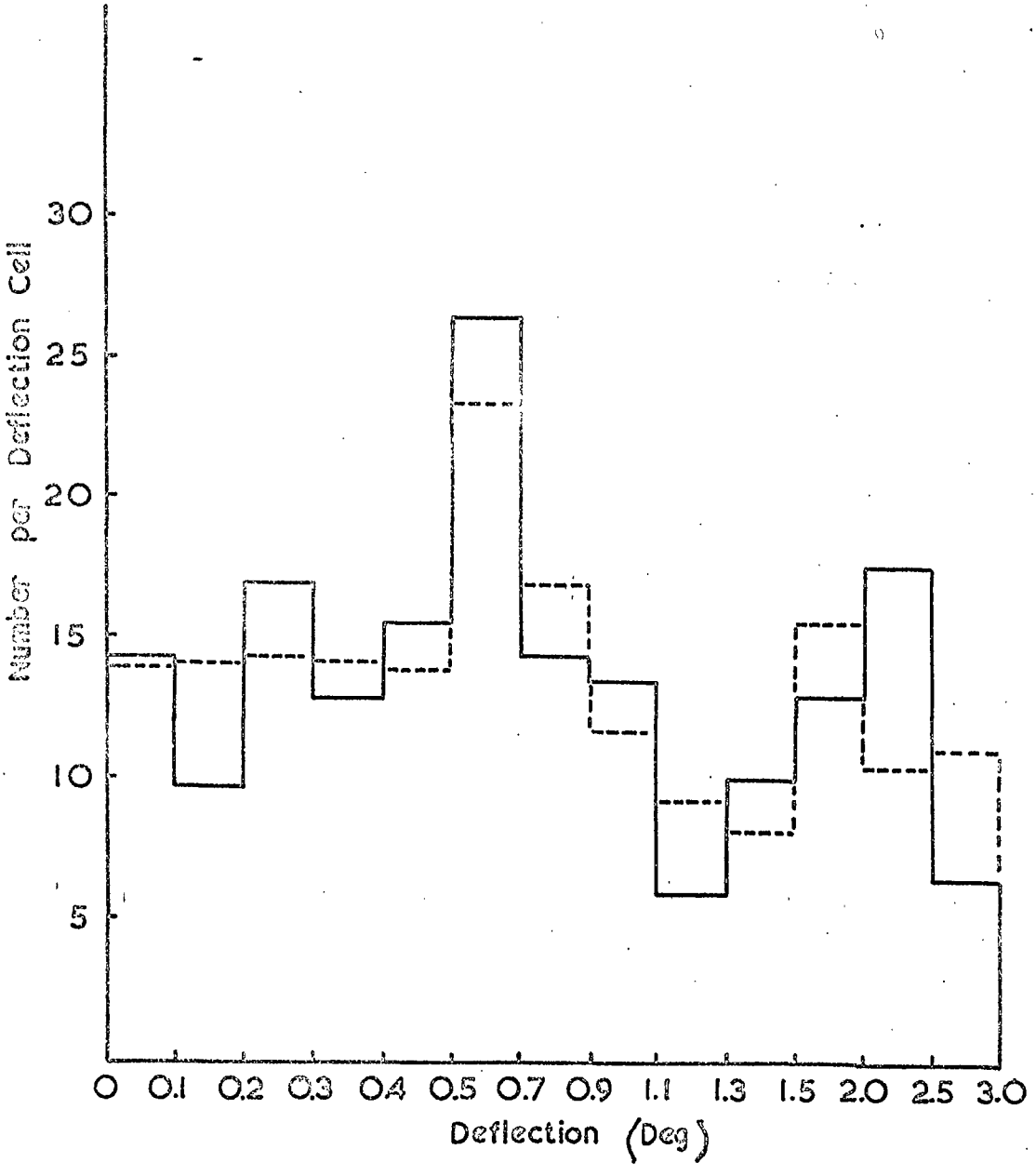

Fig 4.4 The Differential Momentum Spectrum of Negative Pions in the Cosmic Ray Beam near Sea Level.

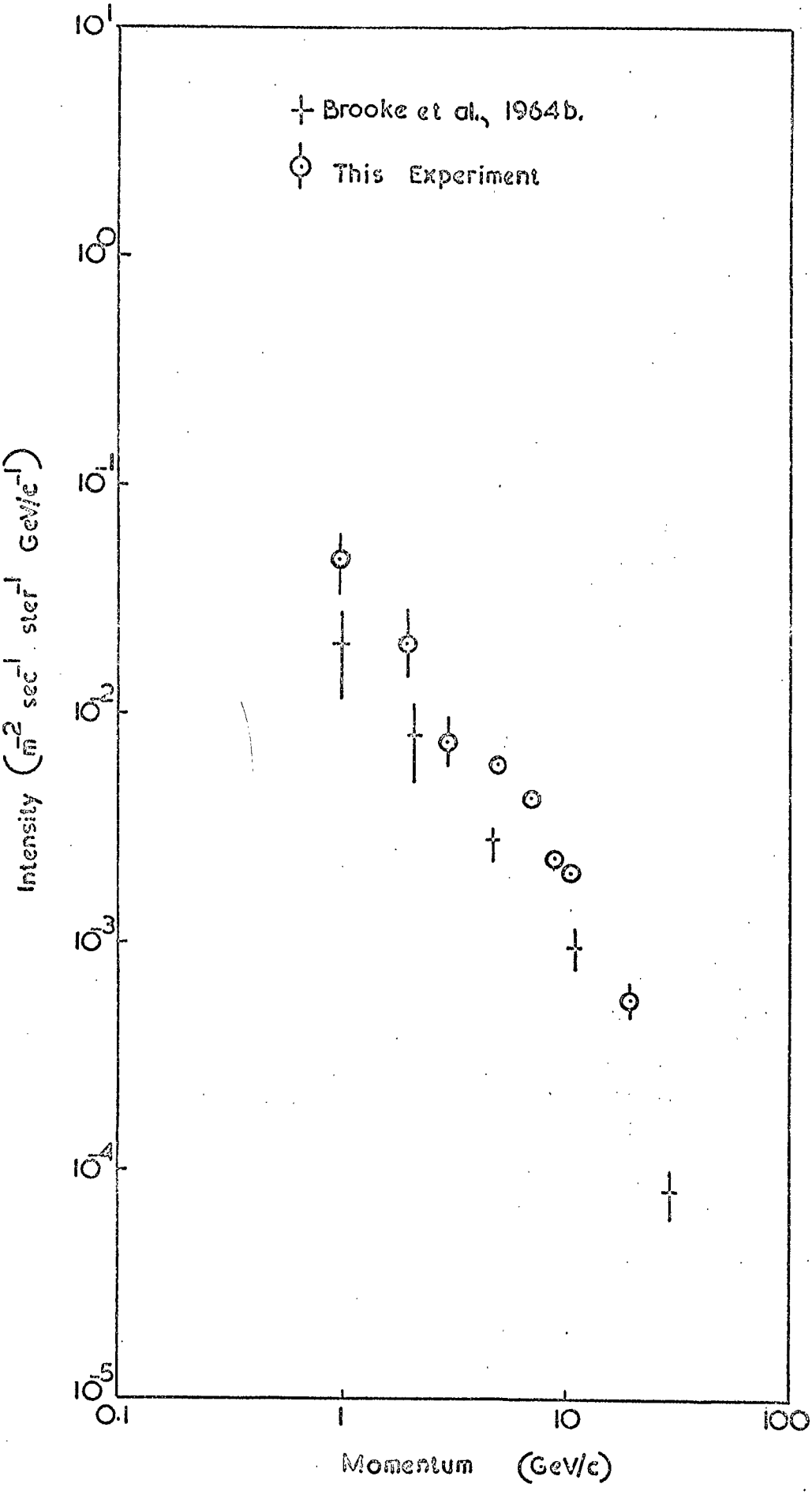

to appear to have momentum > 1 GeV/c and the scattering of positive nuclear-active particles so that they appear to be negatively charged. However, even when these corrections have been applied the apparently significant discrepancy between the two sets of data remains unexplained.

4.2. Nuclear Active Particles in Extensive Air Showers

4.2.1. Introduction

The study of nuclear-active particles (NAPs) in extensive air showers (EAS) described here comprised two parts:-

1) That undertaken with the original spectrograph and neutron monitor and using the array of water Cerenkov detectors as EAS selectors. This was reported by Hook et al. 1970.

2) That undertaken concurrently with the work on unaccompanied NAPs, as described above, by examining those events which contained more than one complete track in the visual detectors of the spectrograph.

4.2.2 The Early Work

4.2.2 (i) The Experimental Technique

The equipment used in this section of the work was different from that described in Chapter 2 in three major respects:-

a) the wall of barytes concrete bricks was not installed around three sides of the lower part of the spectrograph,

b) there were no visual detectors beneath the neutron monitor,

c) the neutron monitor consisted of six BF_3 proportional counters, as described in §2.3.2., with four shorter counters (length 45cms) arranged in pairs on either side. Also the multiplicities of detected neutrons in non-adjacent pairs of long counters were displayed, together with the total multiplicity from all four short counters.

Extensive air showers were selected by requiring coincident pulses, of a size equivalent to ten or more muons, from the central water Čerenkov detector (see §2.6) and any two of the other three detectors, together with a signal from the Geiger-Müller tubes in the magnetic field of the spectrograph, (§2.4.2). All such coincidences were recorded. Those

events which had responses from the neutron monitor, the sensitive time of which was from 50 to 720 μsecs after the EAS coincidence, were then selected from the film records and examined for analysable NAP tracks.

4.2.2 (ii) Results of the Early Work

The equipment was operated in this mode for a period of 4 months at a rate of detection of EAS of $\sim$10 hr^{-1} giving $\sim$4 hr^{-1} EAS with a response from the neutron monitor. However, it was found to be impossible to identify individual tracks unambiguously as NAPs because of contamination of the lower part of the spectrograph by the other components of the EAS so that there were alternative tracks impacting on a hodoscoped pair of BF_3 proportional counters. No information about the momentum and charge of the NAPs was obtained, although the response of the neutron monitor to the EAS could be investigated.

Figure 4.5 shows the distribution of detected neutron multiplicity from EAS initiated events compared with the distribution from particles of the cosmic ray beam, predominantly low energy neutrons. It is noted that the much higher mean multiplicity found for the EAS events reflects the much higher mean energy of the NAPs in EAS.

Using the top tray of neon flash tubes as a charged particle detector the local shower density could be estimated by counting the number of discharged tubes per layer and correcting for the effect of the discrete size of the detectors. This quantity was then related to the multiplicity of detected neutrons and the results are shown in figure 4.6. These results are compared with those of Fieldhouse et al., 1962, who used a Leeds IGY neutron monitor and GM counter EAS array and are seen to be in good agreement where comparison is possible.

4.2.3 The Recent Work

4.2.3 (i) Experimental Technique

In view of the difficulties found with the original design of the spectrograph when attempting to identify individual NAPs in EAS, the equipment was modified to the form described in Chapter 2 and used for the

Fig 4.5 Comparison of Observed Distributions of the Multiplicity of Detected Neutrons from E.A.S. and Cosmic Ray Beam initiated Events.

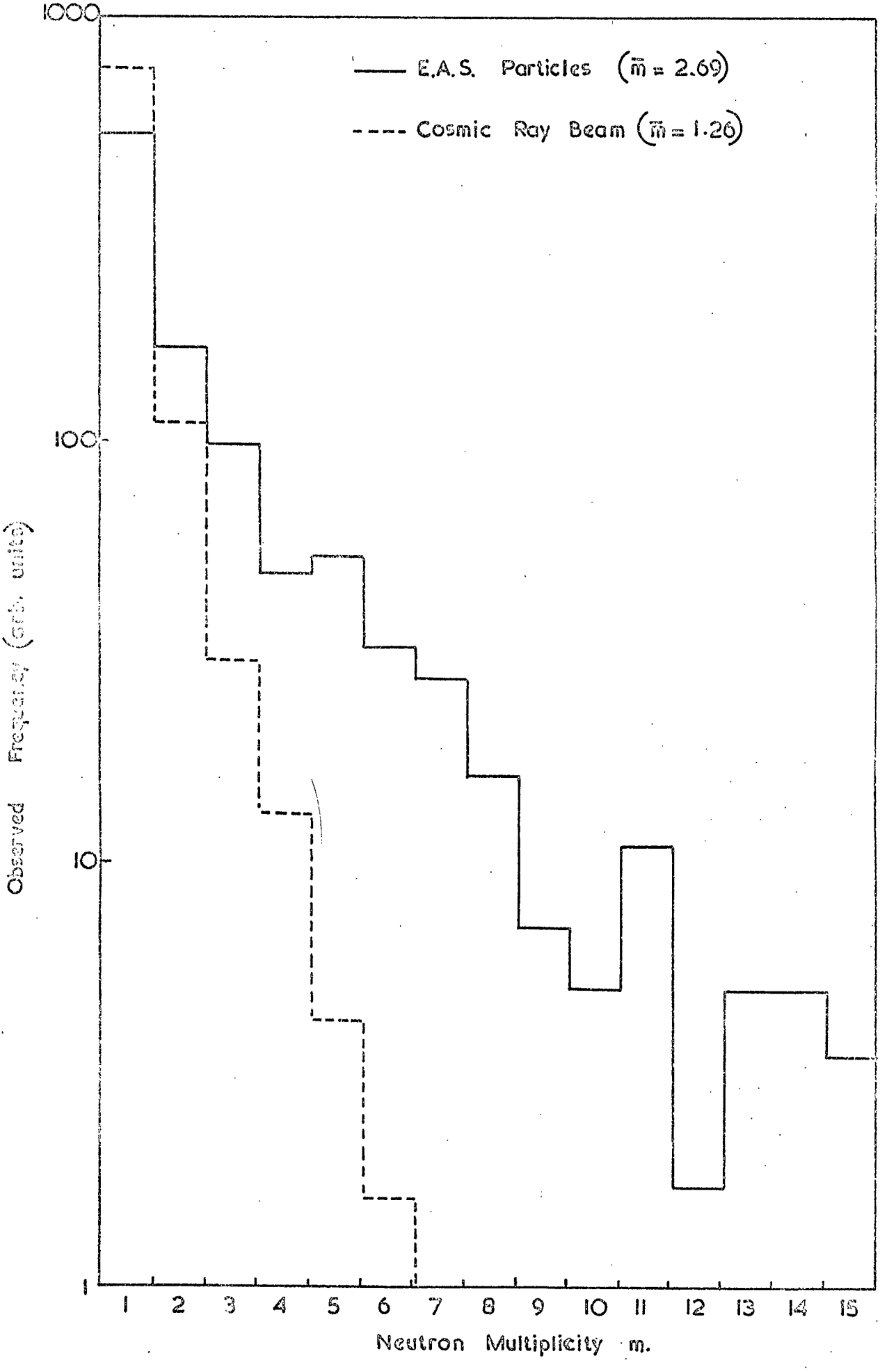

Fig 4.6 The Variation of Mean Detected Neutron Multiplicity with the Local Particle Density.

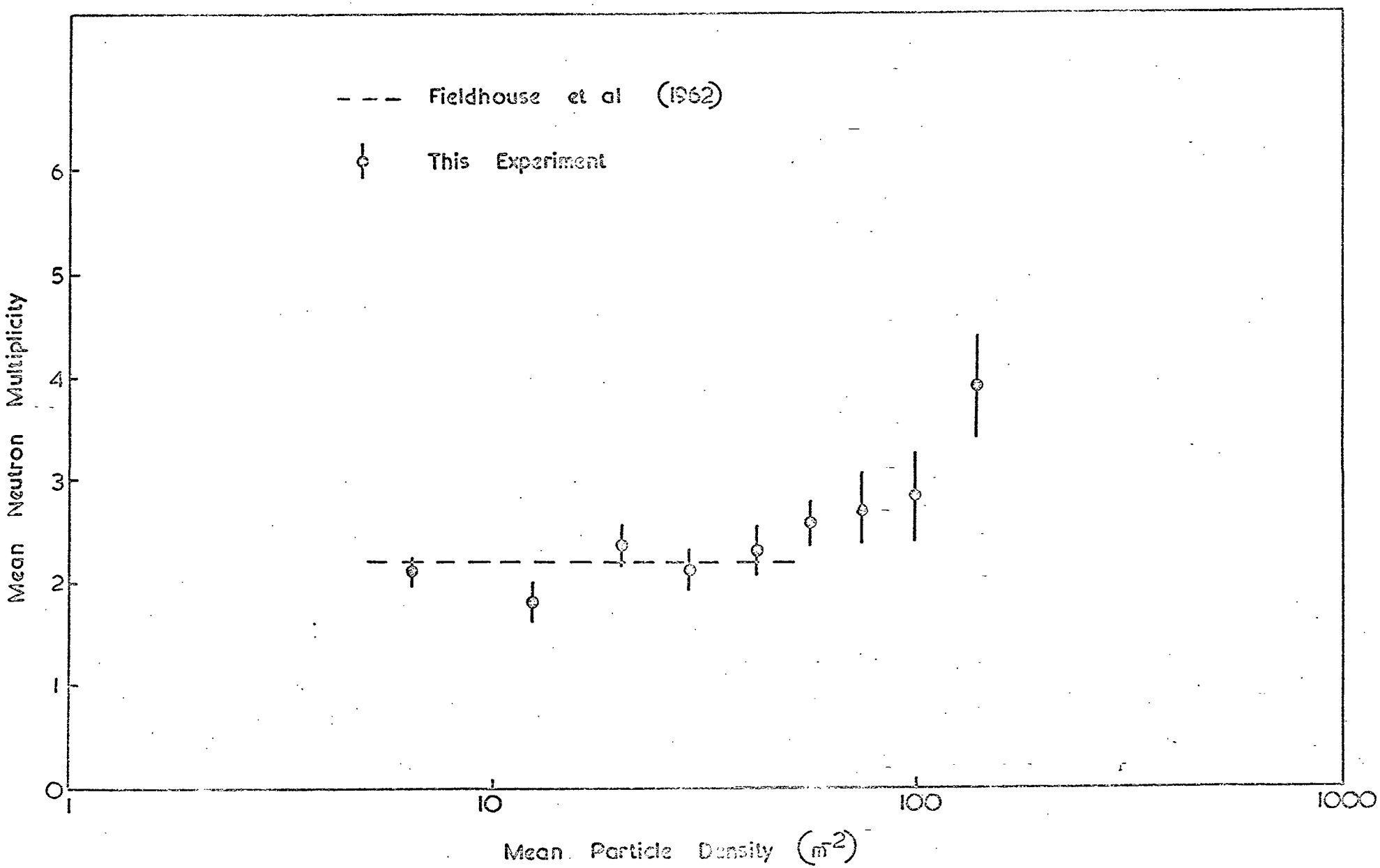

work which comprises the major part of this thesis. During the acquisition of the data for the unaccompanied NAP spectra a number of events were recorded in which more than one complete track was present in the spectrograph. These have been regarded as EAS although there was no information on the responses of the water Čerenkov detectors and hence no indication of the core location or primary energy of the EAS. From this data 28 particles, usually accompanied by only one or two other tracks, have been identified as accompanied NAPs and their characteristics determined. These particles are thought not to be due to chance coincidences between unaccompanied NAPs and other cosmic ray tracks during the live-time of the visual detectors because their frequency is significantly higher than that expected from this source.

4.2.3 (ii) The Response of the Neutron Monitor.

From the limited numbers of particles identified as accompanied NAPs the mean multiplicities of detected neutrons for positive and negative particles have been calculated. These are given in table 4.1 together with the mean multiplicity from positive and negative unaccompanied NAPs.

TABLE 4-1 Mean Multiplicity of Detected Neutrons from Accompanied and Unaccompanied NAPs.

CHARGE	ACCOMPANIED NAPs	UNACCOMPANIED NAPs
POSITIVE	2.6 ± 0.4	1.97 ± 0.04
NEGATIVE	2.3 ± 0.3	2.3 ± 0.1
TOTAL	2.5 ± 0.3	1.99 ± 0.04

The figures for these accompanied events are in good agreement with the value of 2.69 found from the earlier work, although the sensitive times of the two neutron monitors were different. The value of mean multiplicity for the positive EAS particles, is significantly higher than that for the unaccompanied NAPs indicating a harder momentum spectrum, while the values for negative particles are in agreement reflecting the hard momentum spectrum of unaccompanied negative pions.

4.2.3 (iii) The Momentum and Charge of NAPs in EAS

The 28 events identified as accompanied NAPs were analysed for their charge and momentum and the results are summarised in table 4.2, where they are compared with the corresponding values obtained for the unaccompanied NAPs.

TABLE 4-2 The Mean Momentum and Charge Ratio of Accompanied and Unaccompanied NAPs

	ACCOMPANIED NAPs		UNACCOMPANIED NAPs	
CHARGE	POSITIVE	NEGATIVE	POSITIVE	NEGATIVE
NUMBER	19	9	1298	177
MEAN MOMENTUM (GeV/c)	4.5	4.3	4.64	10.7
CHARGE RATIO	2.1 ± 0.9		7.3 ± 0.6	

The values for the momentum and charge of the unaccompanied NAPs quoted here were found from the basic data before any corrections for scattering or other momentum dependent effects had been applied since these corrections have not been applied to the accompanied events reported here.

The mean values of momentum for the positive particles can be seen to be similar but the value for the negative accompanied NAPs is smaller than that for the unaccompanied NAPs; although no errors have been evaluated it is unlikely that the discrepancy is significant. The charge ratios for the two types of event are, however, significantly different and, on the assumption that all the negative NAPs detected were negative pions and that there are equal numbers of negative and positive pions, it is possible to infer a proton to pion ratio of 0.55 ± 0.33 for the accompanied events compared with 3.17 for the unaccompanied events. This significant difference between the two types of events provides strong evidence that they are from different sources, although the momentum spectra, of limited statistical accuracy in the case of the accompanied events, are similar.

4.2.4 Conclusions

From the multiplicity distributions obtained in the earlier work it can be seen that the momentum spectrum of NAPs in genuine EAS is harder than that of unaccompanied NAPs, as is known to be the case from previous experiments.

The mean multiplicities found for the positive accompanied events in the more recent work were also found to be higher than for the unaccompanied particles, again indicating a harder momentum spectrum, although this is not borne out by the mean values of momentum. However, the statistics of the sample of accompanied events are extremely poor and the apparent contradiction could reflect a statistical fluctuation.

Although the modifications to the equipment did result in an improvement in the rate of collection of identifiable accompanied NAPs the rate still makes a succesful experiment difficult to achieve. Unfortunately, for the sample of accompanied events recorded the details of the EAS accompanying these particles are unknown.

A further experiment has been made and more events have been recorded in which a coincidence with the EAS water Čereknov detectors was also required. The results from this run are not yet available but a preliminary analysis is not encouraging.

CHAPTER FIVE

MODEL PREDICTIONS OF THE MOMENTUM SPECTRA OF NUCLEAR-ACTIVE PARTICLES AT SEA LEVEL

5.1. Introduction

There is considerable current interest in simulating the propagation of very high energy cosmic rays through the atmosphere particularly for comparison with measurements of the large extensive air showers (EAS) which are produced. The results of these simulations are used to estimate the energy of the primary particle at the top of the atmosphere so that the primary particle energy spectrum at these very high energies can be measured. A further property of considerable importance is the spectrum of the atomic mass number of the primary particles, and simulations of EAS can be used to predict those parameters which may be most sensitive to the mass of the primary particle. However, the simulations involve representations of interactions between both nucleons and pions and air nuclei at energies which are far beyond the range of direct experimental data and so depend heavily on extrapolation from low energies of the characteristics of nuclear interactions. It is expected that the unaccompanied NAPs at sea level, of momenta in the range measured in the present experiment, will arise from primary cosmic rays of energy intermediate between that of interest in the EAS simulations and that at which data on high energy interactions are available from accelerators. Thus a comparison of the measured spectra with predictions should yield useful checks of the details of high energy nuclear physics used in EAS models and of the simulation procedures themselves.

However the sea level NAP spectra depend not only on the propagation of particles through the atmosphere, but also on the energy spectrum of the primary particles. Recently several direct measurements, using satellite and balloon-borne equipment, have been made of the primary spectrum e.g. Schmidt et al., 1969, and Grigorov, 1971. These measurements are in good

agreement neither with each other, nor with the previous estimates of the spectrum e.g. Kaplon and Ritson, 1952, and a comparison of the measured sea level spectra with the present model predictions may also aid in a solution of this problem.

5.2 Previous Simulations

Several predictions of the spectra of the various components of the sea level cosmic radiation have been made by, for example, Pal and Peters, 1964, Jabs, 1968, 1972, with considerably varying models and varying success in obtaining agreement with observations.

Most representations of nuclear interactions wich have been used in these models can be classified as one of two types: (a) 'fireball' models, or (b) 'isobar' models.

a) 'Fireball' Models of Nuclear Interactions

It is assumed in these representations that, in a high energy interaction, one or more 'fireballs' are produced which are at rest or moving slowly in the centre-of-mass of the system. A 'fireball' is regarded as a highly excited cloud which returns to a ground state by emitting mesons. An analysis of a system of this kind leads to a law relating the mean multiplicity of mesons produced to the energy of the incident particle. The exact form of the law depends on the assumptions made regarding the properties and numbers of 'fireballs'. Also, these models lead to smoothly varying energy spectra for the secondary particles produced in interactions.

b) 'Isobar' Models of Nuclear Interactions

In an isobar model it is assumed that, in addition to the production of fireballs, theincident particle has a significant probability of emerging from the interaction in an excited state, an isobar. The isobar then returns to its ground state by the emission of a few high energy mesons. There is very little evidence for the production of isobars in pion-nucleon interactions and so this assumption is usually restricted to the nucleon-nucleon interactions.

Since the incident nucleon in an interaction is observed to retain a considerable fraction of its initial energy, the pions produced by the decay of an isobar will be of higher mean energy in the laboratory frame than the

mesons produced from the fireball. Then, according to Pal and Peters, 1964, because of the rapidly falling spectrum of primary cosmic rays, the products of isobar-produced pions will dominate the spectra of secondary cosmic rays in the atmosphere.

An example of an isobar model is that developed by Pal and Peters, 1964, in which a value for the mean multiplicity of pions produced by the isobar was obtained from a comparison of the predicted and observed spectra of muons.

Jabs, 1968, Adair, 1968, and O'Brien, 1971 all used 'fireball' models, but each assumed a different multiplicity law and O'Brien and Adair both neglected the secondary particles produced in the interactions of pions with air nuclei. This leads to an underestimate of the intensities of the various components at great depths in the atmosphere, as noted by Pal and Peters, 1964, and as may be seen from figure 5.1 which shows the sea level muon spectra, derived with the model to be described in this thesis, when pion-air nucleus interactions are included, curve A, and neglected, curve B. As can be seen, neglecting the pion interactions in the present model leads to an underestimate of the intensities by $\sim 20\%$.

O'Brien obtained good agreement between his predictions and observations of unaccompanied particles at sea level, but Jabs and Adair both concluded that there was a discrepancy between their predictions and the observations. Jabs suggested that agreement could be obtained if either the intensity of the primary particles at all energies were reduced by a factor of 2.5 compared with the direct measurements, or by including the production of significant quantities of baryon-anti-baryon pairs in nuclear interactions.

The predictions of these authors are compared in detail with the results of the present simulations later (Chaper 6).

5.3 Description of Model

The important parameters required for a simulation of the propagation of cosmic rays through the atmosphere using a phenomenological model are:-

a) the mean multiplicity of particles produced in interactions of pions and nucleons with air nuclei;

Fig. 5.1 The Effect on the Sea Level Muon Spectrum of excluding the Interactions of Pions in a Simulation.

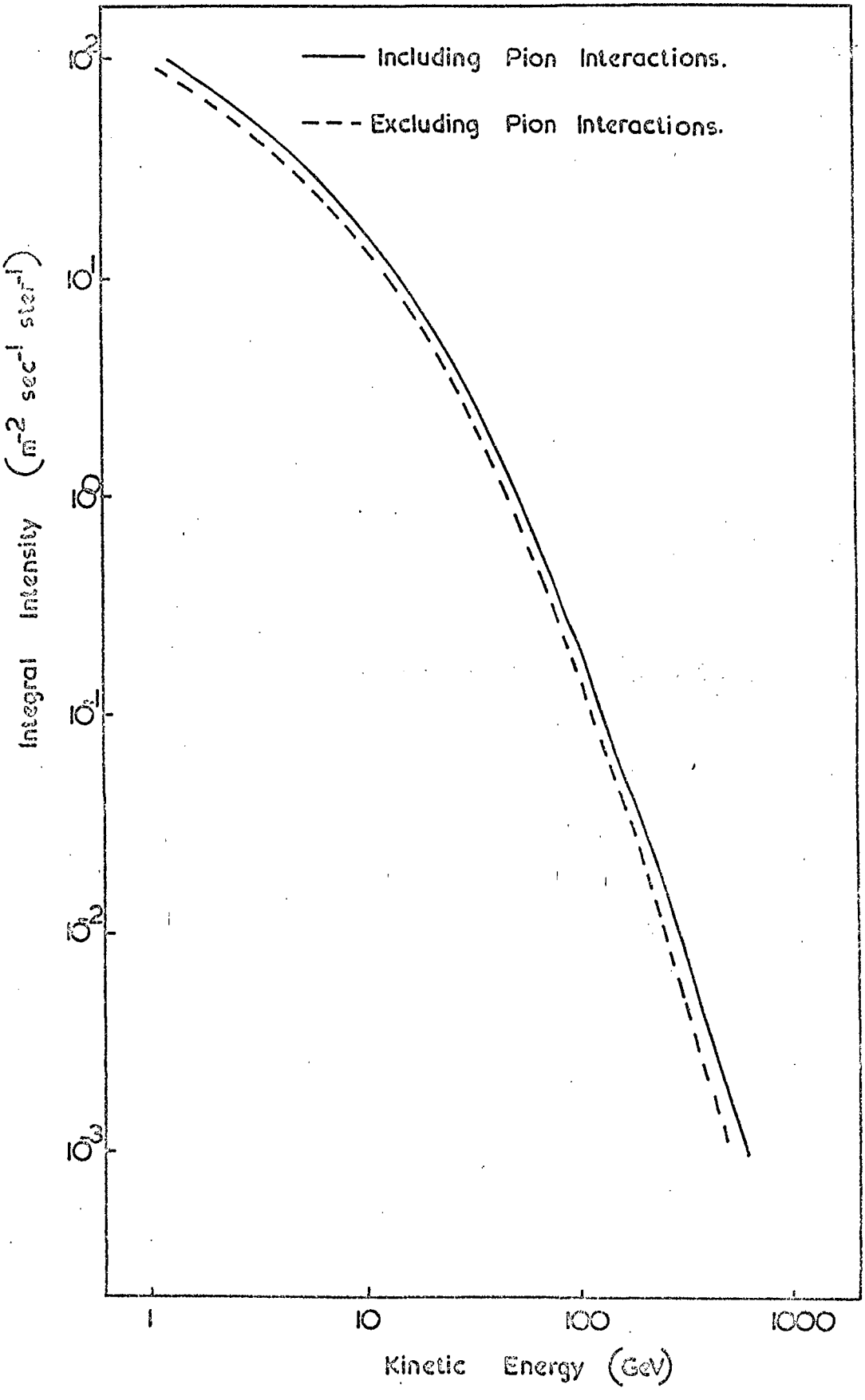

b) the fraction of the incident energy which is used to produce secondary particles, i.e. the inelasticity, in pion and nucleon interactions with an air nucleus;

c) the distribution in energy of the particles produced;

d) the interaction mean free path of nucleons and pions in air.

The values of these parameters chosen for the present model are discussed below.

a) The Multiplicity of Produced Particles

Following a recent survey of experimental data on nuclear interactions at energies from 19 GeV up to 10 TeV (J.Hough, private communication), the parameters used in this model were those considered to be the best estimates currently available. The mean multiplicity of particles produced in an interaction of a particle with an 'air' nucleus was taken to be

$$n_s = 3.85\ (KE_p)^{\frac{1}{4}} \qquad 5.3.1$$

where n_s is the number of secondaries, charged and neutral,

K is the inelasticity of the interaction (see 5.3.b), and

E_p is the kinetic energy of the incident particle in the laboratory frame of reference.

The value of the constant (3.85) arises from the value for p-p collisions (1.9) allowing for the mass, A, of the target nucleus using a relation in which $n_s \alpha A^{0.19}$.

It was assumed that all the produced particles were pions and that positive, negative and neutral pions were produced in equal numbers. The production of isobars in nucleon interactions was not allowed since the cross- section for their production appears to be a decreasing function of energy at accelerator energies up to 70 GeV and, with certain exceptions (e.g. Koshiba et al., 1970), it is considered that the data on the distribution of secondary particle energies at higher energies can be explained by fluctuations in the interactions.

b) The Coefficient of Inelasticity

The distribution of inelasticity of nucleon-nucleus interactions was taken to vary with a rectangular distribution between limits of 0.25 and 0.75, leading to a mean inelasticity of 0.5. If a distribution of inelasticity of the form considered by Brooke et al., 1964, were used, with a similar mean value, the effects on the predicted sea level spectra were shown to be negligble..

Pion interactions were taken to be totally inelastic as there is little evidence to the contrary and, as mentioned above, the product of pion interactions are not the dominant constituents of the sea level cosmic radiation.

c) The Energy Distribution of the Secondary Particles

The distribution of the secondary energies in the laboratory frame-of-reference was taken to follow the well-known formula given by Cocconi, Koester and Perkins, 1962, of the form

$$S(E)\,dE = 0.5\left[\frac{1}{G}\exp(-E/G) + \frac{1}{T}\exp(-E/T)\right]dE$$

where G, T are the mean energies, in the laboratory frame, of particles moving backward and forwards, respectively, in the centre-of-mass frame-of-reference.

d) The Interaction Mean Free Path

At energies greater than about 20 GeV the cross-section for nucleon-nucleon interactions tends to a constant value of ~38 mb (Giacomelli, 1971) Using an optical model for nucleon-nucleus interactions, this value corresponds to a cross-section consistent with a nuclear interaction mean free path of 80 g cm^{-2} in air.

From a consideration of similar accelerator data for pion interactions, the mean free path for pions in air was taken to be 120 g cm^{-2} for both positive and negative pions at all energies.

Using these parameters a one-dimensional Monte-Carlo simulation of the propagation through the atmosphere of a primary cosmic ray nucleon was carried out to predict the kinetic energy spectra at sea level of nucleons, muons and charged pions. The total number of electrons at sea level was also predicted using a solution, under approximation B, of the electromagnetic cascade equations.

Considerable development of the model has recently taken place but the improvement of many of the simple assumptions noted above has not resulted in any significant changes of relevance to the present work.

5.4 Checks of Model Predictions

As a check on the validity of the model the results of several runs at various primary energies up to 10^{14}eV were compared with the available experimental data.

All the existing EAS data express a measured parameter (e.g. the number of muons of energy $> E$ per shower) as a function of shower size, and not primary energy. This leads to difficulty when comparing predictions with data since predictions are usually performed for a fixed primary energy, for which there are large fluctuations in the shower size. Also the definition of measured shower size depends on the energy threshold, and type, of the device used for the measurement. Hence it is considered that a comparison of spectral shapes, rather than absolute numbers, is the most stringent test which can be applied to the predictions.

Figure 5-2 shows the integral energy spectrum of nuclear-active particles in a shower of primary energy 10^{14}eV compared with the data given by Greisen 1960, Chatterjee et al., 1964, and Matano et al., 1964. The data of Matano et al. and Chatterjee et al. were given for a shower size of 3.10^5 particles and have been normalised to the predicted spectra at an energy of 100 GeV, while the spectrum given by Greisen has been evaluated for a shower size of 10^4 particles, which is in the region of the value expected for a primary of energy 10^{14}eV. It can be seen that there is good agreement between the prediction and both measurements for NAP energies $\gtrsim 10$ GeV and that the point of Chatterjee et al. is in good agreement with the prediction at 1 GeV, although the spectrum given by Greisen indicates considerably more low energy NAPs.

Figure 5-3 shows the integral energy spectrum of muons compared with the expression given by Bennett and Greisen, 1961, which was derived from measurements on showers of size $\sim 10^6$ particles. It can be seen that there is good agreement between the predicted and measured spectral shapes for muon energies greater than 10 GeV even though the mean 'shower size' of the predicted

Fig 5.2 The Integral Energy Spectrum of all N.A.Ps in a Shower initiated by a Primary Proton of Energy 10^5 GeV.

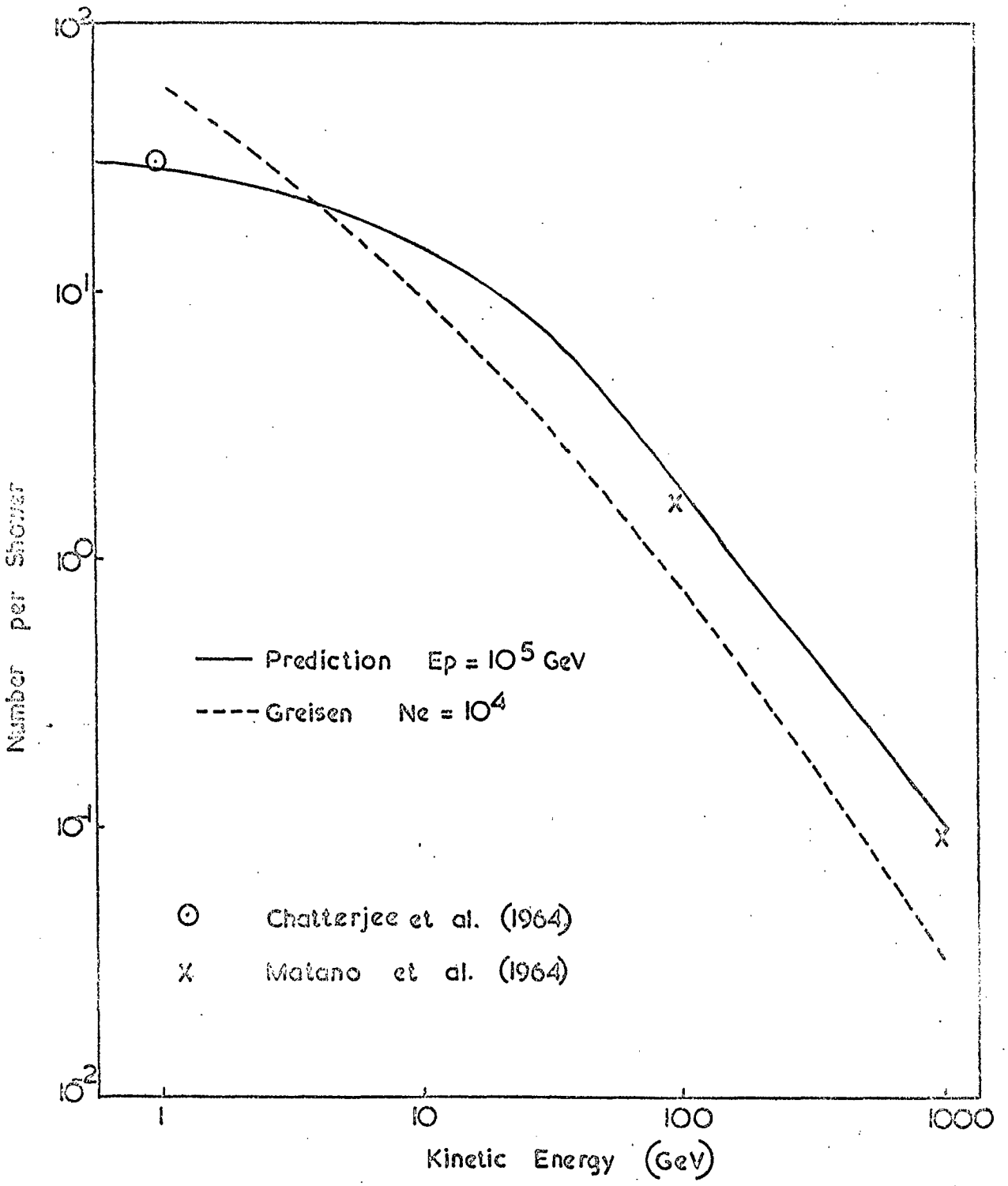

Fig 5.3 The Integral Energy Spectrum of all muons in a Shower initiated by a Primary Proton of Energy 10^5 GeV

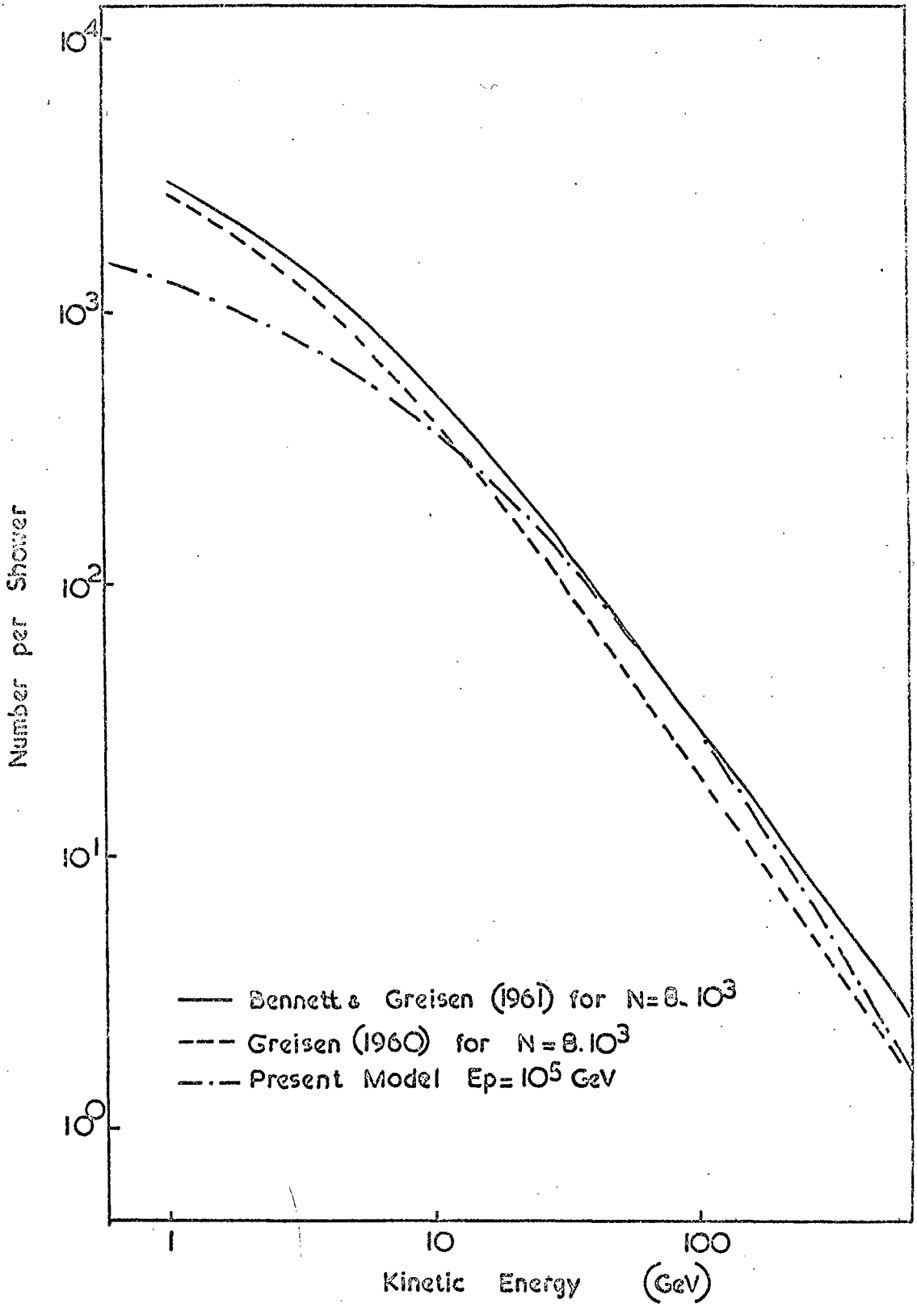

events was only 8.10^3 particles. However, below 10 GeV the measured spectrum rises considerably above the prediction.

Figure 5-4 is a comparision of the lateral distribution of muons of energy >2 GeV given by Staubert, 1969, with the distribution for muons of energy >1 GeV predicted by a 3-dimensional extension of the present Monte-Carlo model (Turver, private communication). The two distributions were normalised at a radial distance of 100m. The fit is extremely good over the entire range of measurement, indicating a satisfactory model.

It was also found that the relationship between the number of muons per primary nucleon and the 'size' of the electron shower at sea level was of the form

$$N_\mu (> 1.33 \text{ GeV}) \propto N_e^\beta \qquad 5.4.1$$

with $\beta = 0.79$, where N_μ is the number of muons of energy > 1.33 GeV and N_e is the number of electrons. This is in good agreement with the value for β of 0.75 quoted by Greisen, 1960, although, because of the large fluctuations in N_e for a particular primary energy, there is a large error associated with the predicted value of β.

From these comparisons with EAS data mainly from primary particles of energy $\sim 10^{14}$eV, and since the model is based on data from accelerators at lower energies, it may be expected that the model is adequate for deriving the sea level spectra of unaccompanied particles for comparison with measurements. If satisfactory agreement is obtained between these predictions and measurements, the model may be used with increased confidence to predict the properties of EAS from primary particles of higher energy (10^{16}-10^{17}eV).

5.5. The Procedure for the Derivation of the Sea Level Spectra

From a series of simulations using the Monte-Carlo model, the average sea level energy spectra for the various types of particle were built up at several primary energies over the range 10 GeV to 10^5 GeV. In all, about 20,000 simulations were performed to derive the nucleon and pion spectra and about 3,000 for the muon spectrum. The majority of the simulations were performed for low energy primaries since these contribute the greatest

Fig 5.4 The Lateral Distribution of Muons.

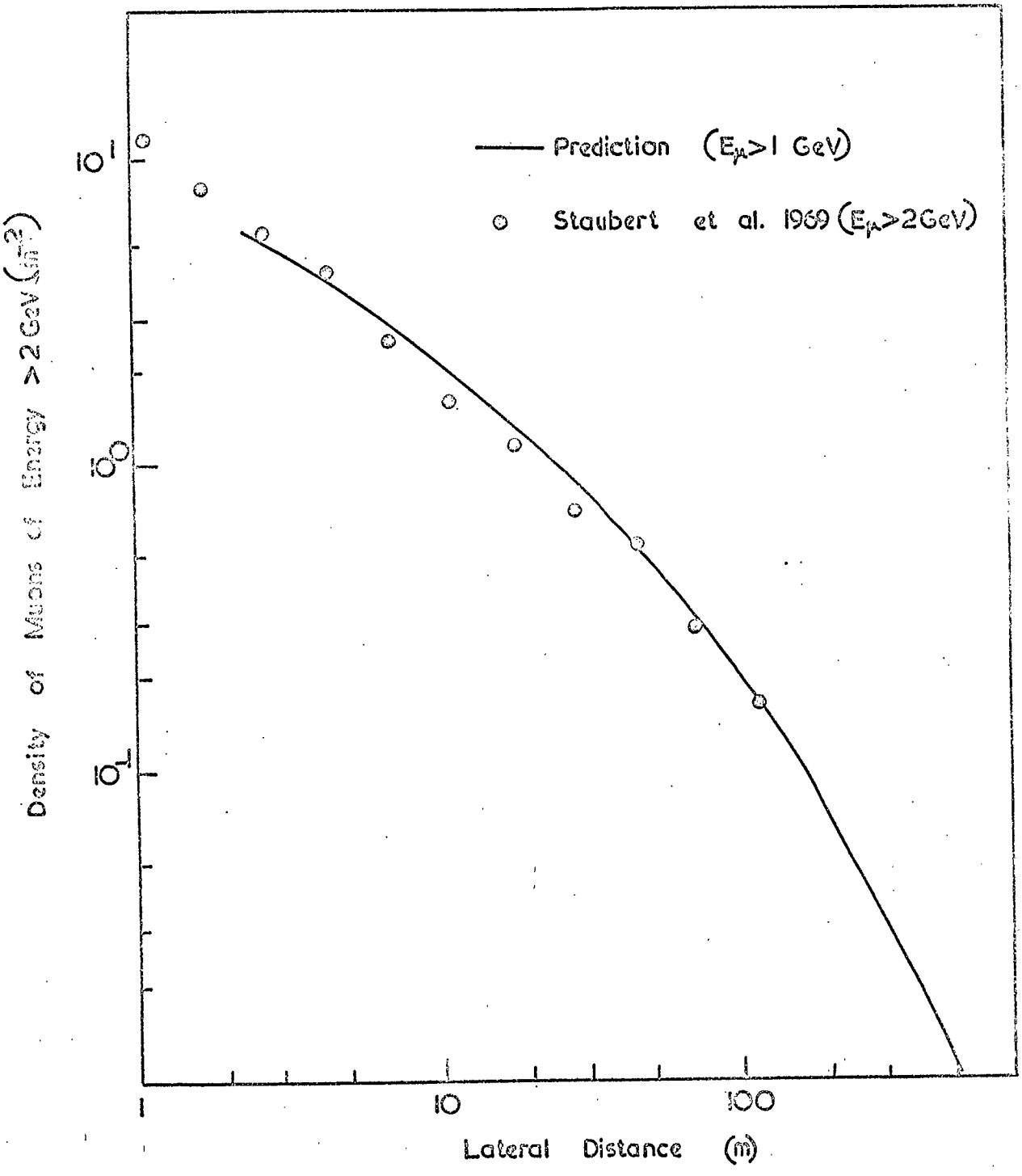

weight to the sea level spectra. To derive the intensity at a given sea level energy the yield from a particular primary energy was weighted with the primary intensity and the resulting series of values was integrated numerically over the appropriate range of primary energy.

The upper limit on this integration will be determined by the probability of detecting an accompanying particle in the instrument used for the measurement. Using the simulations to give the mean shower size for a particular primary energy, and the lateral distribution function for the electron component of the extensive air shower given by Greisen (1960), it was considered that there was a significant probability of detecting accompanying particles in the Nuclear Active Particle Spectrograph for a primary energy of $\gtrsim 6\ 10^4$ GeV. However the contribution to the sea level fluxes, at the energies considered here, from such primaries is small (see figures 5-7, 5-10, 5-13) and so the upper limit of integration was taken for convenience, to be 10^5 GeV.

The lower limit of integration is , ideally, the sea level energy under consideration but was taken to be 10 GeV since below this energy the primary spectrum is affected by geomagnetic and solar phenomena, and the contribution from primaries of energy less than this value was expected to be negligible (see figures 5-7, 5-10, 5-13).

5.6 The Primary Cosmic Ray Spectrum

A survey of recent measurements of the primary cosmic ray energy spectrum was carried out and the results are shown in figure 5-5 which shows the integral spectrum of the total radiation. The spectra of Brooke et al. (1964), Webber (1967) and Grigorov (1971) were all quoted as spectra of the total radiation while that attributed to Schmidt et al. was obtained by combining the spectrum of primary protons given by Schmidt et al (1969) with the spectrum of primary alpha particles given by Webber (1969). The contribution from heavier nuclei is negligble since the abundance of nuclei heavier than alpha particles is only 10% of the alpha particle abundance (Webber 1967).

Although the published spectra are given as integral spectra, the current work required a differential spectrum and so the following expressions were

Fig. 5.5 The Integral Spectrum of the Primary Cosmic Ray Nucleons.

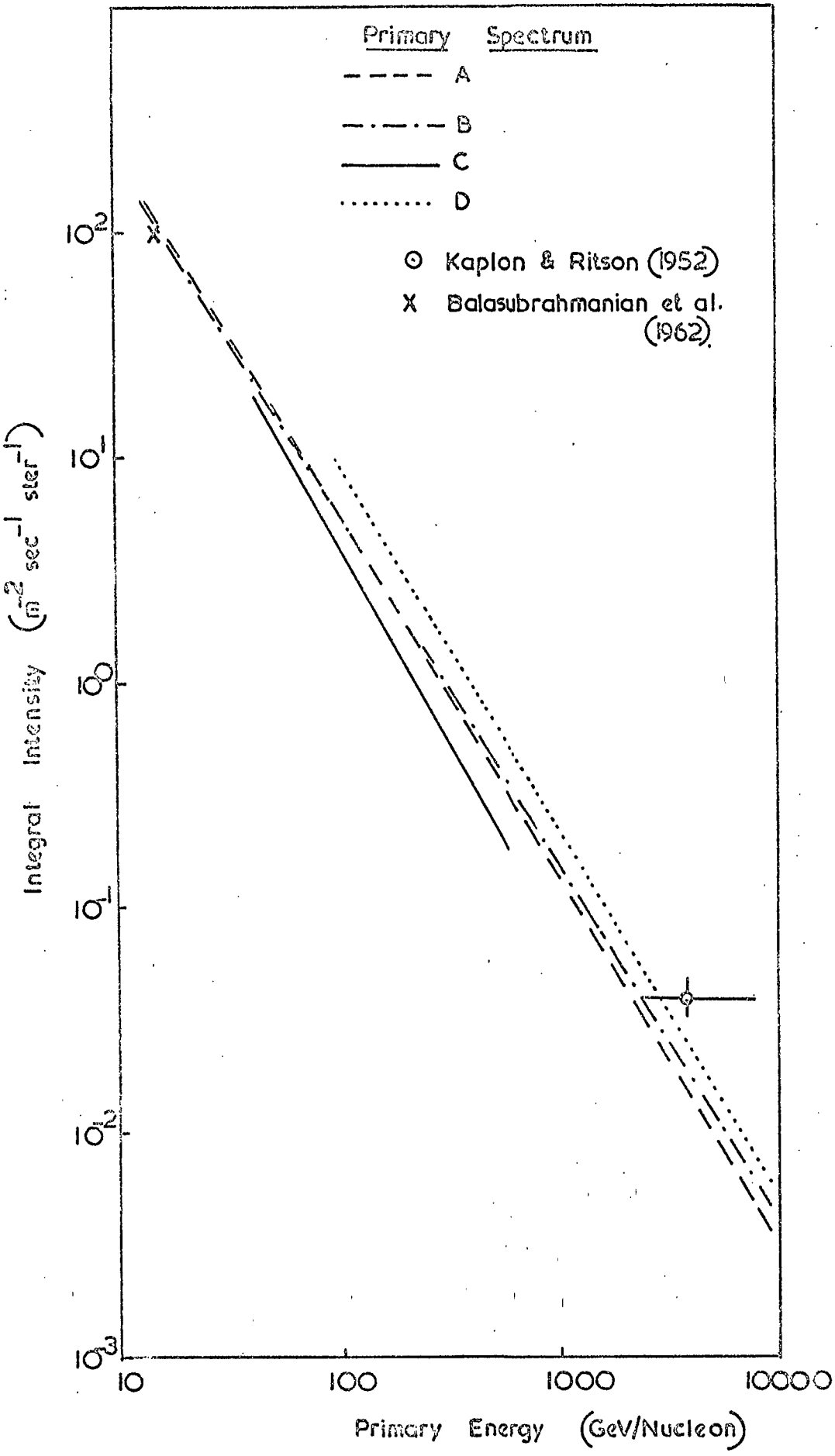

derived from expressions for the integral spectra either given by the various authors or evaluated from figure 5-5.

$$J(E)\,dE = 1.465\ 10^{4}\ E^{-2.6}\ dE\ \ m^{-2}\ sec^{-1}\ ster^{-1}\ GeV^{-1} \qquad (A)$$

from Webber (1967)

$$J(E)\,dE = 1.375\ 10^{4}\ E^{-2.58}\ dE\ m^{-2}\ sec^{-1}\ ster^{-1}\ GeV^{-1} \qquad (B)$$

from Brooke et al. (1964)

$$J(E)\,dE = 1.96\ 10^{4}\ E^{-2.7}\ dE\ \ m^{-2}\ sec^{-1}\ ster^{-1}\ GeV^{-1} \qquad (C)$$

from Schmidt et al (1969) and Webber (1969)

$$J(E)\,dE = 2.54\ 10^{4}\ E^{-2.6}\ dE\ \ m^{-2}\ sec^{-1}\ ster^{-1}\ GeV^{-1} \qquad (D)$$

from Grigorov (1971).

In addition to these spectra which were assumed to have a constant exponent from 10 GeV to 10^5 GeV, a spectrum used by Jabs (1968) in which the exponent is a function of energy of the form shown below was investigated.

$$J(E)\,dE = 10^{4}\ E^{-2.35(1+0.02\ \log_{10}E)}\ dE\ \ m^{-2}\ sec^{-1}\ ster^{-1}\ GeV^{-1} \qquad (E)$$

In practice these expressions were only used for primary energies greater than 100 GeV, with the exception of spectrum D, since below that energy there is very little difference between the various spectra. When evaluating the contribution from primaries of energy less than 100 GeV the expression for the spectrum due to Webber (equation A) was used, while the sea level intensities from spectrum D were obtained by multiplying those obtained from A at all energies by 1.7, the ratio between the intensities of the two primary spectra.

5.7. The Sea Level Proton Spectrum from Model Simulations

The present model, which is an early version of a series of models developed for EAS studies, ignores ionization energy loss of the nucleon in the atmosphere and charge exchange of the nucleon in interactions. Since the probability of charge exchange in a single interaction is high ($\sim$0.33) it is assumed that the flux of nucleons at sea level, in the energy range considered, is composed of equal numbers of protons and neutrons and so the predicted nucleon spectra have been halved to obtain the sea level spectra of protons. Also, in view of this large probability, it is assumed that,

during its passage through the atmosphere, each nucleon spends half its time as a proton and half as a neutron so that ~1 GeV of kinetic energy will be lost, through ionisation, by a nucleon between entering the atmosphere and reaching sea level. Thus a constant energy loss of 1 GeV has been assumed in each of the predicted spectra given in figure 5-6. Figure 5-6 shows the predicted momentum spectrum of protons at sea level for each of the five primary spectra considered here, compared with the measured points of Brooke et al., 1964, and those reported in this thesis.

It can be seen that the spectrum, at low momentum, is insensitive to the form of the primary spectrum and only above ~20 GeV/c is there much difference between any of the predicted spectra. The explanation can be seen in figures 5-7 and 5-8 which are curves showing the contribution of particles of various primary energy to the sea level flux of protons of momenta 5.5 GeV/c and 100 GeV/c, respectively, and indicate the response to the primary spectrum of an experiment to investigate protons of these momenta. For example, the majority of the 5.5 GeV/c protons are produced by primary nucleons of energy less than 100 GeV which is the region where the various primary spectra are very similar.

At momenta of ~100 GeV/c the difference between the predictions based on primary spectra A and C is only ~30% and so measurements of good statistical accuracy would be required at high momenta to distinguish between these primary spectra.

Fair agreement is obtained between the sea level proton spectra predicted on the basis of all the primary spectra except that of Grigorov, 1971, and the intensities measured in the present experiment.

5.8 The Predicted Sea Level Spectrum of Negative Pions

The predicted momentum spectra of negative pions corresponding to different primary energy spectra are given in figure 5-9 assuming that the charge ratio of pions at sea level is unity. It can be seen that the intensity of this component at momenta measured in the present experiment is fairly sensitive to the primary spectrum but, because of the low flux of pions compared with

Fig. 5.6 A Comparison of Measured Proton Fluxes with Model Predictions.

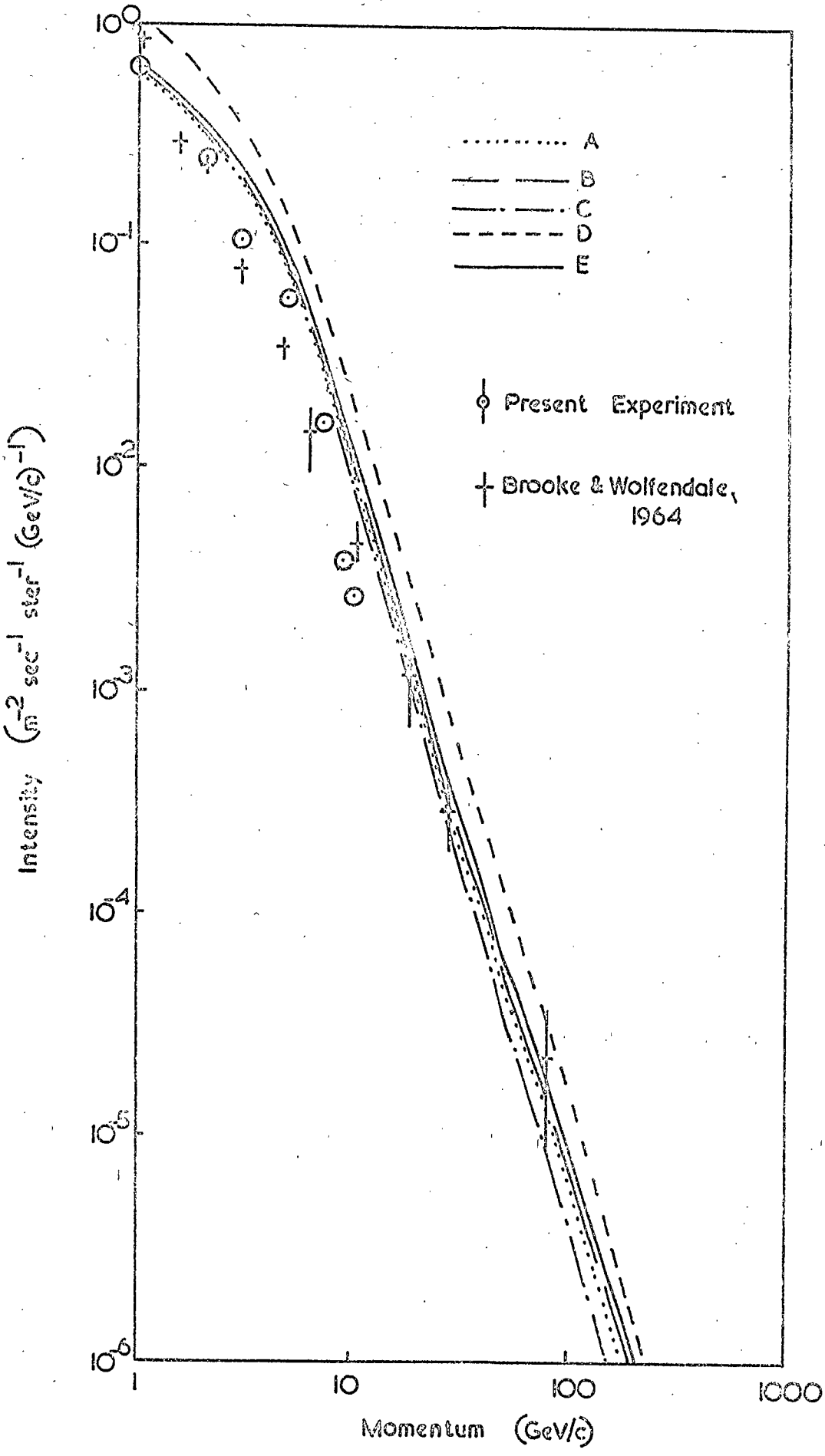

Fig. 5.7 The Contributions of Primary Particles of Energy Ep to the Sea level Flux of 5.5 GeV/c Protons

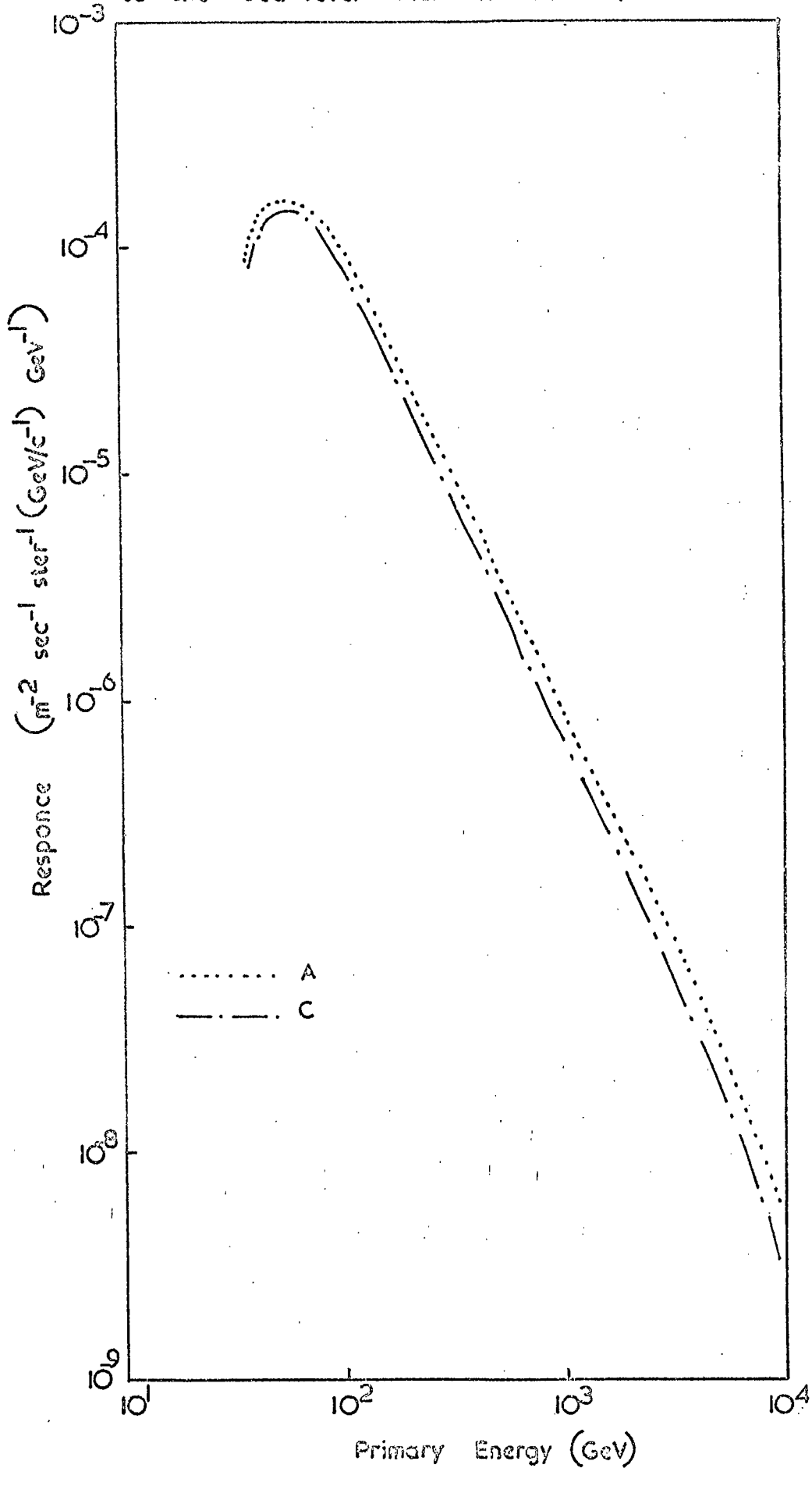

Fig. 5.8 The Contribution of Primary Particles of Energy Ep to the Sea level Flux of 100 GeV/c protons

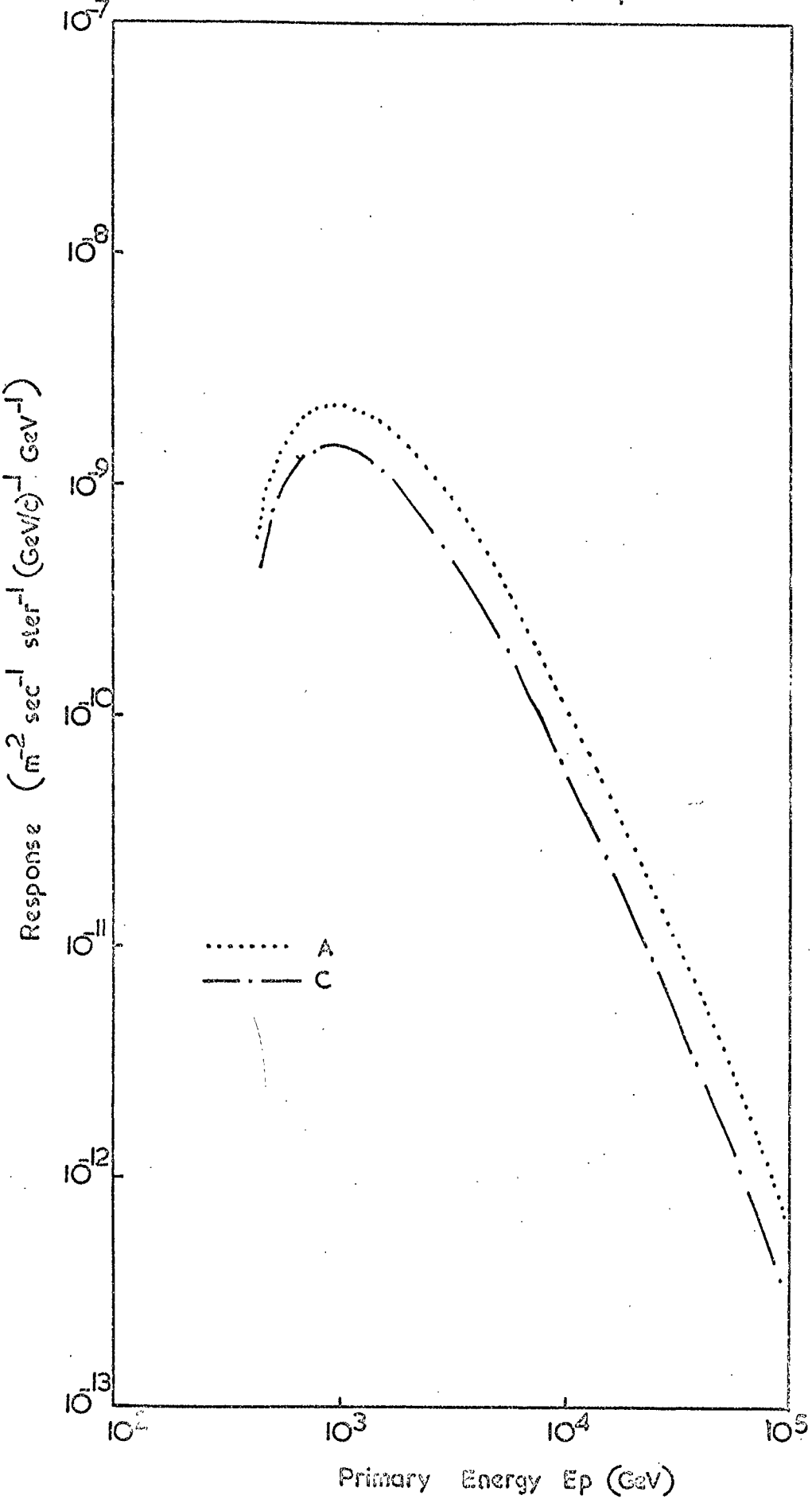

Fig. 5.9 A Comparison of Measured Negative Pion Fluxes with Model Prediction.

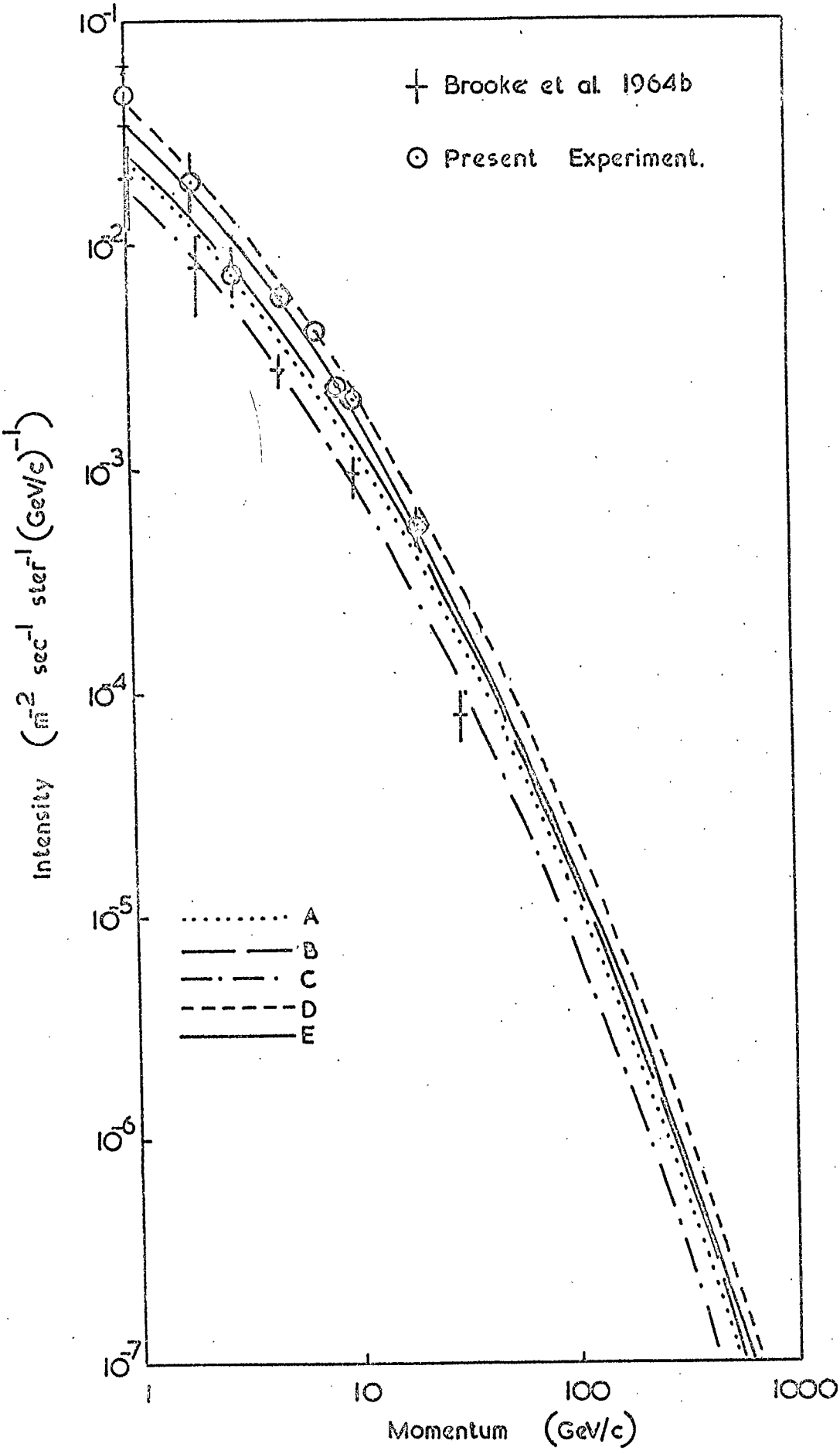

that of muons and protons, an accurate measurement is difficult. The relatively large sensitivity to the form of the primary spectrum can be explained by the response curves given in figures 5-10 and 5-11 for 5.6 GeV/c and 100 GeV/c negative pions respectively. These curves show that these pion intensities are determined predominantly by the intensity of primaries of energy greater than 100 and 1000 GeV respectively. At these energies the primary spectra considered here are significantly different.

Also shown in figure 5-9 are the experimental intensities determined in the work described in this thesis and those of Brooke et al., 1964b. Agreement between both measurements and a prediction can be obtained by varying the primary spectrum. However, the spectrum found in the present experiment is in agreement only with the prediction from the present work based on the highest primary energy spectra. As noted in §5-7, the predictions based on these primary spectra give poor agreement with the momentum spectrum of protons which is statistically much more accurate than the pion spectrum. This must cast some doubt on the validity of the present measurement unless the model gives an underestimate of the pion spectrum. Some evidence for this possibility has been found from a more recent version of the model in which the multiplicity of particles produced in nuclear interactions was taken to vary with energy according to a relation derived from results from the I.S.R. rather than the relation described in §5-3.

5.9 The Predicted Spectrum of Muons

Figure 5-12 shows the integral momentum spectra at sea level of muons, predicted using primary spectra A and C, compared with the recent measurement of Allkofer et al., 1971, and figures 5-13 and 5-14 are the response curves for muons of momentum greater than 7.5 GeV/c and 133.4 GeV/c respectively. The predictions are seen to be in good agreement with the measurement only for momenta $\gtrsim$ 50 GeV/c and at lower momenta are significantly high. This discrepancy must suggest an insufficiency of the model since this spectrum is the most accurately known of those considered in the present work.

Fig. 5.10 The Contribution of Primary Particles of Energy Ep in the Sea level Flux of 5.5 GeV/c Negative Pions.

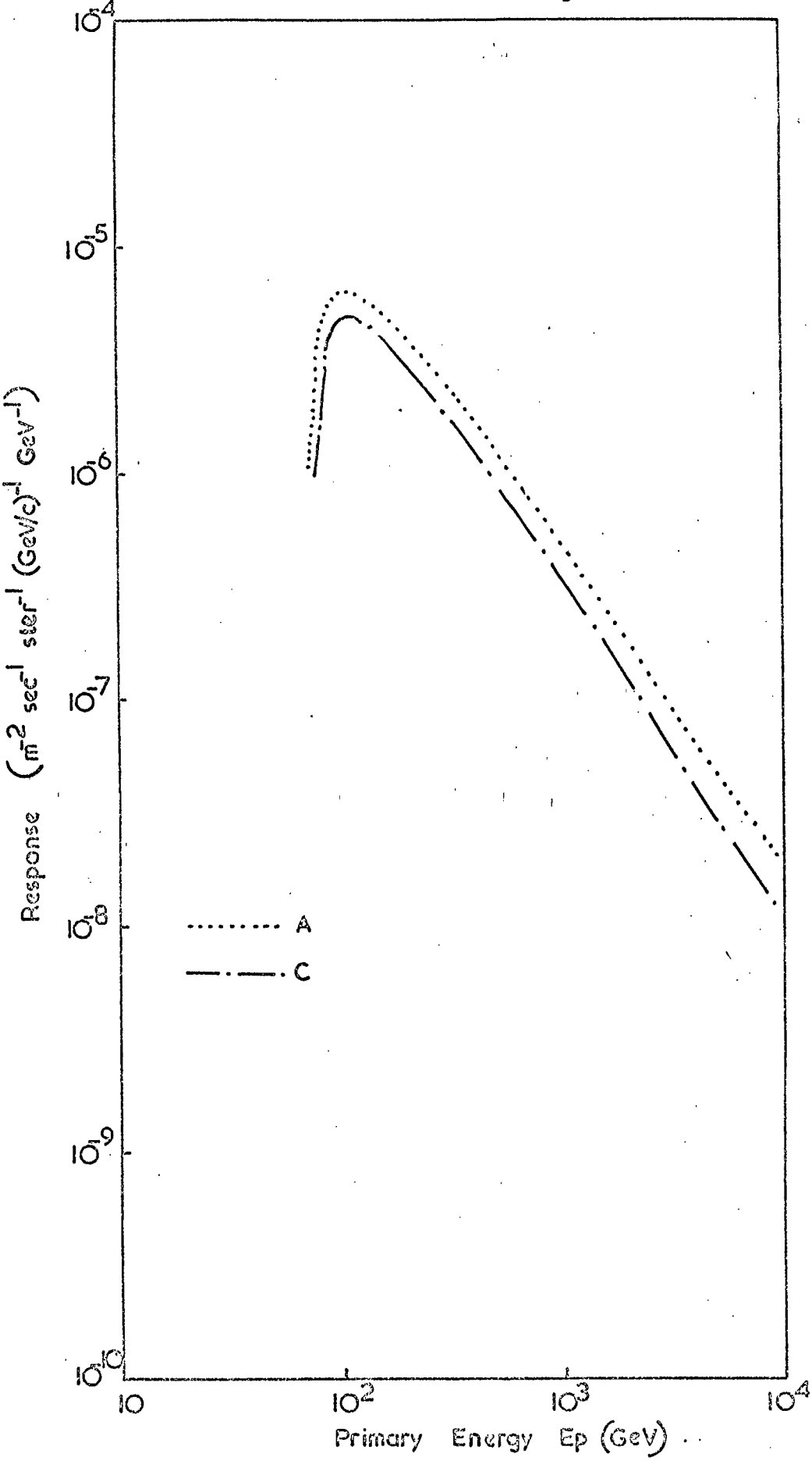

Fig. 5.11 The Contribution of Primary Particles of Energy Ep to the Sea level Flux of 100 GeV/c Negative Pions.

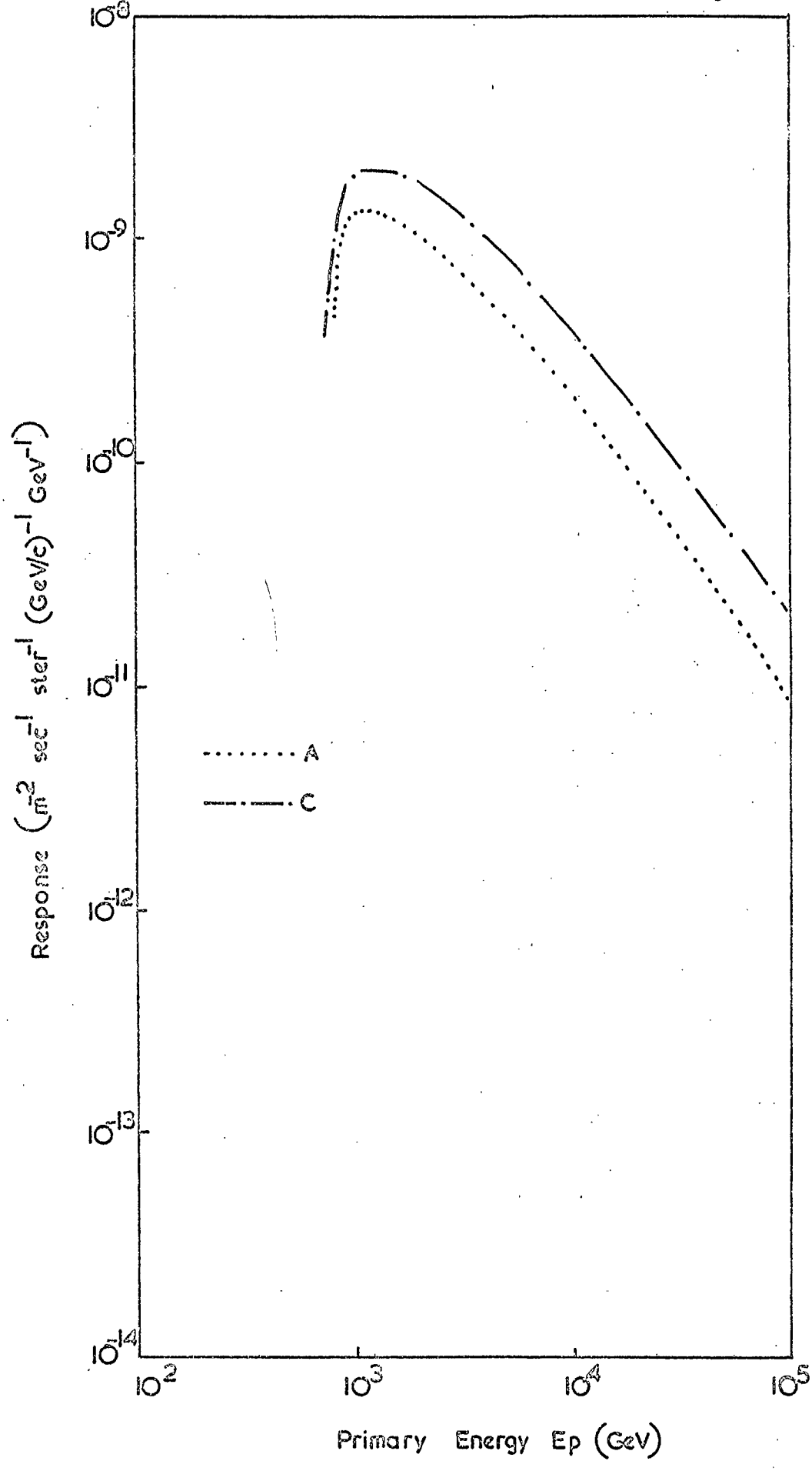

Fig. 5.12 A Comparison of Sea level Muon Fluxes with Model Predictions.

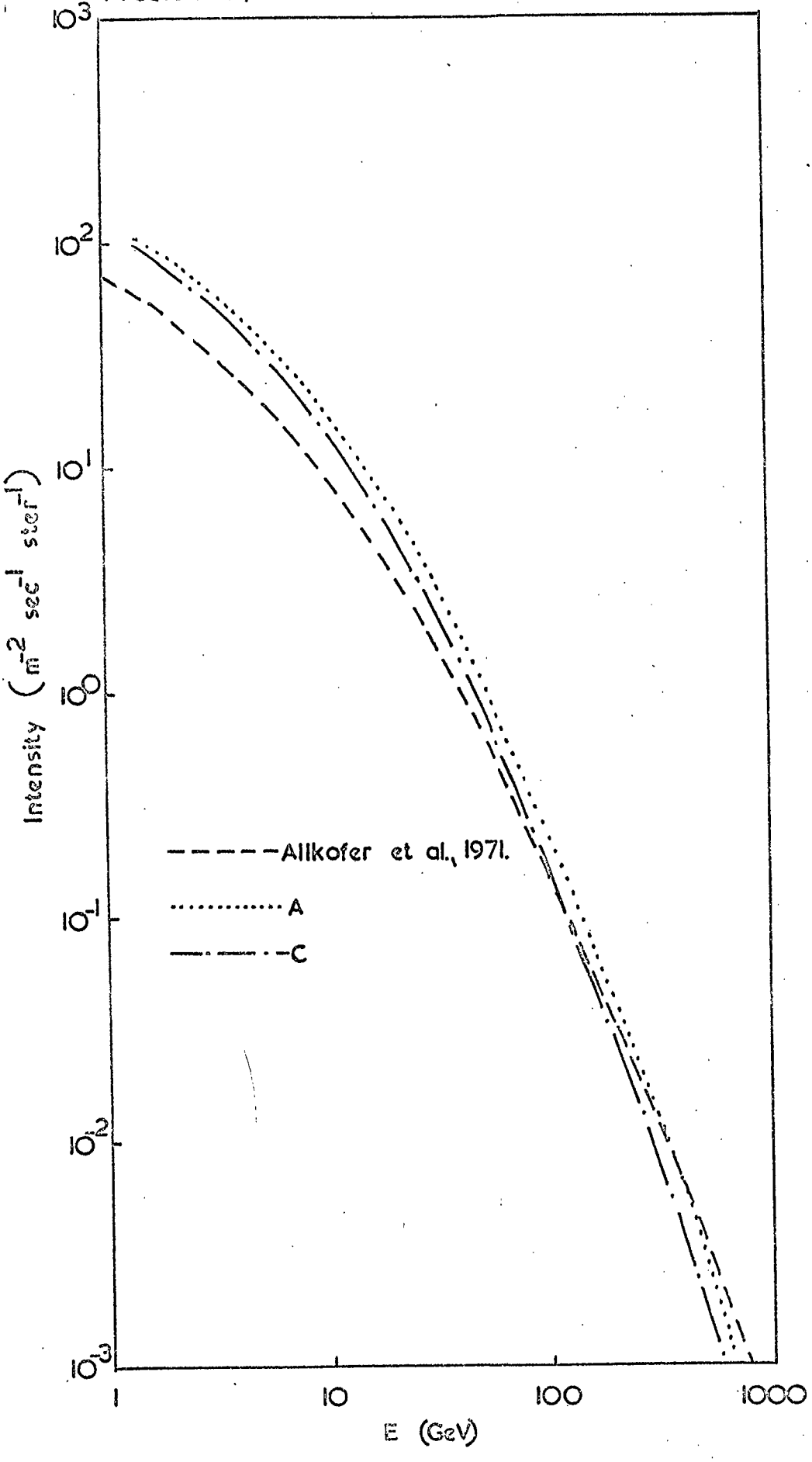

Fig. 5.13 The Contribution of Primary Particles of Energy Ep to the Sea level Flux of Muons of Energy > 7.5 GeV.

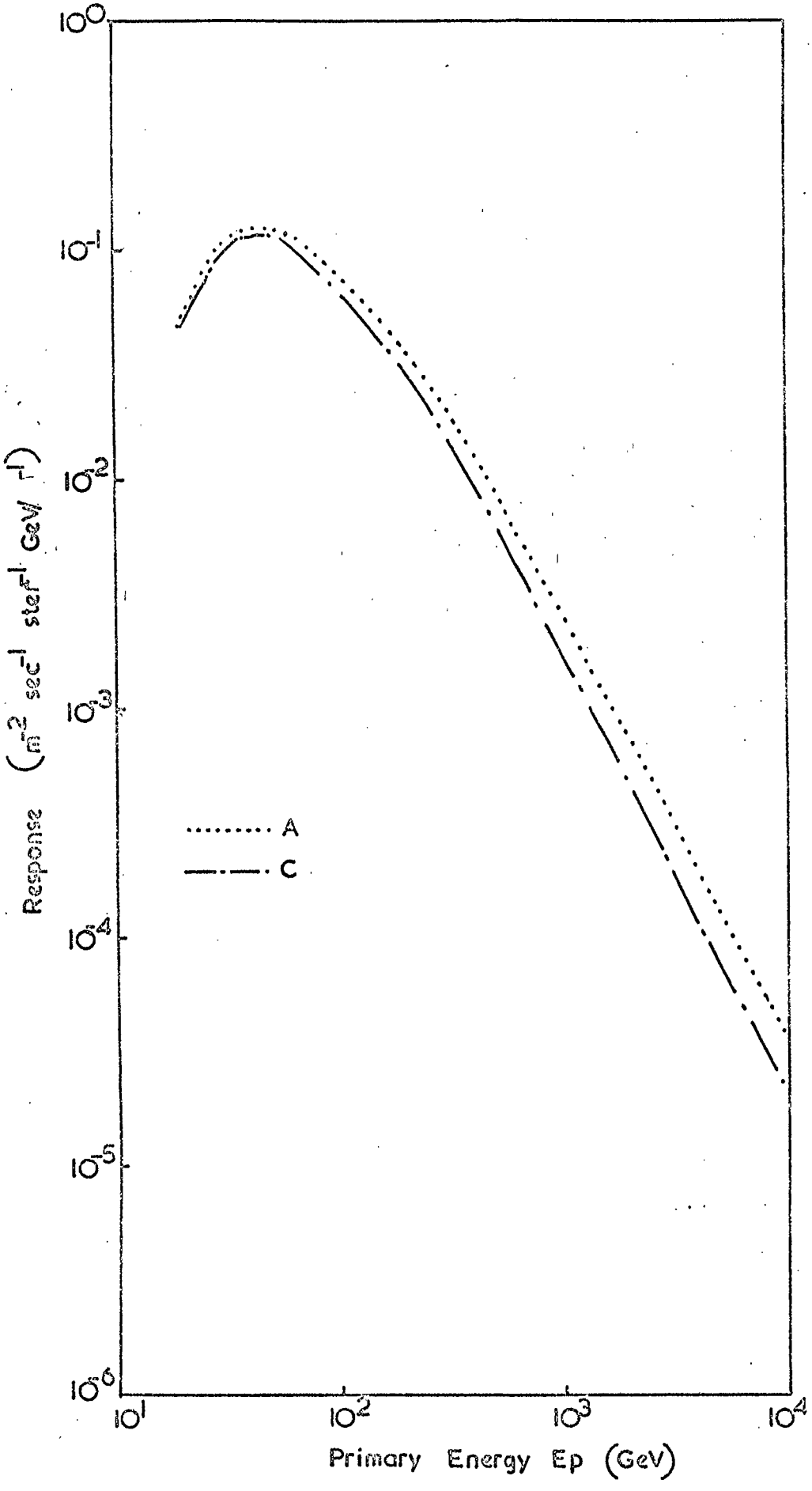

Fig. 5.14 The Contribution of Primary Particles of Energy Ep to the Sea level Flux of Muons of Energy > 133.4 GeV.

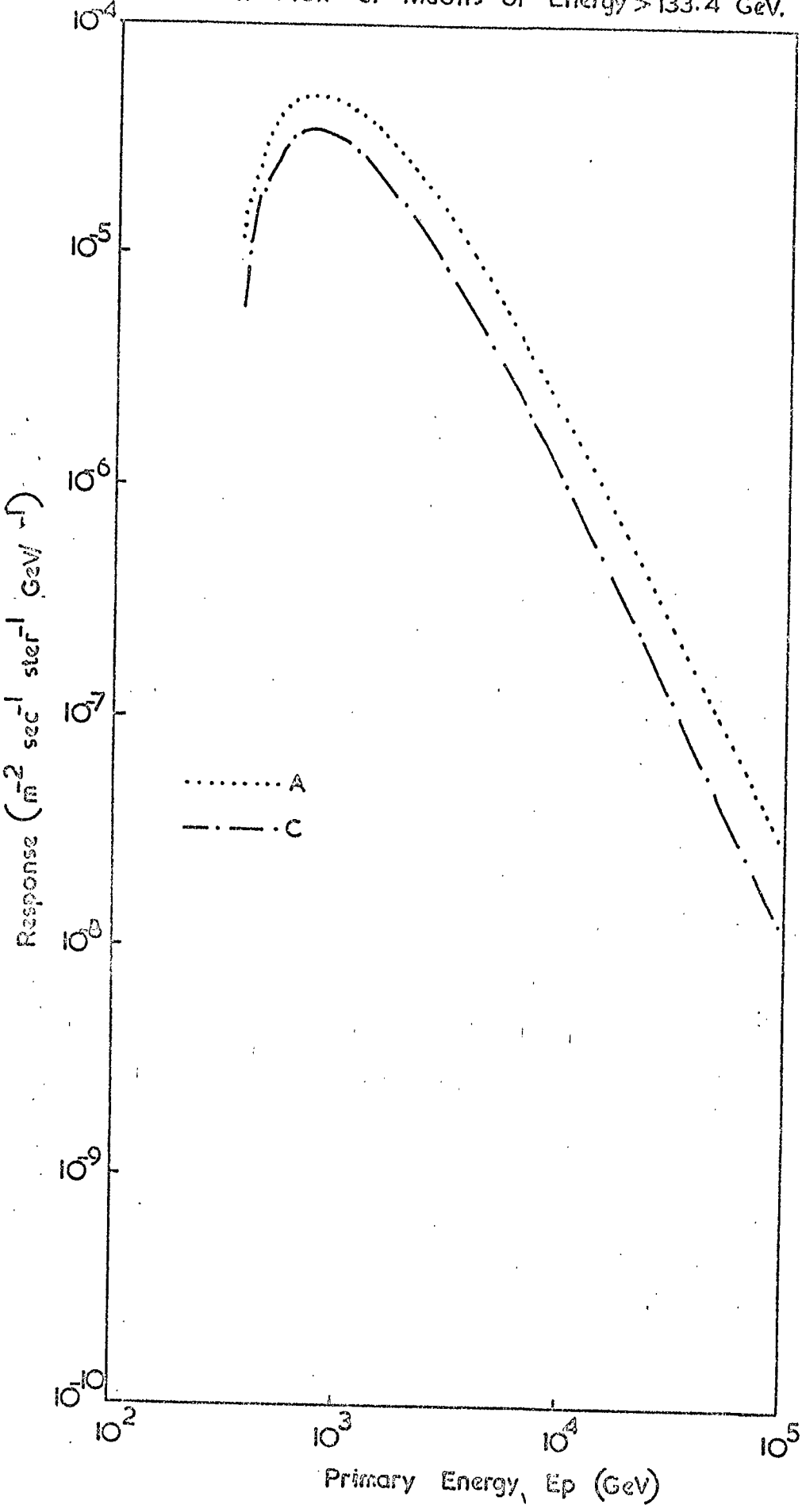

The response curve for $P_\mu > 7.5$ GeV/c (figure 5-13) shows that the intensity of the low energy muons is determined largely by primaries of energy <100 GeV. Although the model was based on experimental data at energies predominantly in this region, various approximations made may give rise to inaccuracies in the treatment of interactions in this region of energy. However, investigations with a more accurate version of the model do not indicate any discrepancy as large as is observed.

Since the muons are secondary largely to low energy primary nucleons they must be produced at great heights in the atmosphere, and thus undergo considerable scattering and ionisation energy loss before reaching sea level. Thus the error introduced by ignoring scattering, and the resultant increased energy loss will be greatest for these low energy muons, and so this omission could contribute to the discrepancy. Also, the energy loss for the muons is taken to be constant at 2 MeV/g cm^{-2} which is not valid over the entire range of momentum and should be increased for muons of momentum greater than 1 GeV/c. On the basis of these limitations, the energy of the muons at sea level will be over-estimated, and corrections for both these sources of error will reduce the intensity at a particular momentum and so tend to remove the observed discrepancy. It is at present not known whether such limitations are of sufficient magnitude to cause the full discrepancy.

The effect of using the multiplicity of produced particles as given by the I.S.R. has also been investigated. This modification led to no significant change in the sea level spectrum because, in the region of primary energy of importance to the muon spectrum (< 100 GeV), the multiplicities given by the two relations are similar.

5.10 Conclusions

Fair agrement is obtained between the observed and predicted spectra of protons, with the exception of that derived from the primary spectrum measured by Grigorov. Thus the treatment of inelasticity used in this model appears to be adequate to describe nucleon interactions, at least in the region of energies up to 100 GeV since the proton intensities are

largely dependent on primary particles up to this energy.

Although there is a large discrepancy between the measurements of the spectrum of negative pions it is still possible, by varying the primary spectrum, to obtain agreement between a prediction and each of the observations. However, each measurement agrees with an extreme primary spectrum and, in particular, that due to Grigorov must be regarded as dubious because of the poor agreement between the prediction of the sea level proton spectrum derived from it and the measured spectrum. This must cast some doubt on the accuracy of the present measurement and hence it is important that further measurements should be made of the flux of pions at sea level as this should help to resolve the discrepancy between the two measurements and also be quite sensitive to the form of the primary spectrum.

Reasonable agreement can be obtained between the measurements of sea level cosmic ray spectra and the predictions from a one-dimensional Monte Carlo model with the exception of the low energy muon spectrum which is dependent on interactions of comparatively low energy particles. Also good agreement was obtained between the predictions of the model and observations of small extensive air showers (primary energy $\sim 10^{14}$eV). Hence the simple model of nuclear interactions used here should form the basis for satisfactory simulations of EAS at much higher primary energy. Furthermore, the general agreement between the model predictions and measurements supports the recent estimates of the primary spectrum with the exception of that suggested by Grigorov.

CHAPTER SIX

6.1 Introduction

Over the past few years the results of several simulations of the propagation of cosmic rays through the atmosphere have been published (e.g. Brooke et al., 1964a, Pinkau, 1964, Pal and Peters, 1964, Bull et al., 1965) and have used various models of the characteristics of nuclear interactions. In this chapter a comparison is made of typical predictions from each of several models in an attempt to determine whether agreement can be obtained between the predictions and measurements of the momentum spectra of the various components of the unaccompanied cosmic radiation at sea level. Four different models are considered here: those of Adair, 1968, Jabs, 1968, 1971, O'Brien, 1971 and that described in chapter five of this thesis.

These four models vary considerably in their assumptionsand a brief summary of the more important features is given in §6.2. In addition to using different models of nuclear interactions, different forms of the spectrum of primary cosmic rays were used by the different authors making a satisfactory comparison of the results difficult. However, predictions have been made with the model described in this thesis using several different forms of the primary spectrum. Thus the predictions of the other models can be compared with the appropriate predictions of the present model to determine the sensitivity of a particular prediction to the form of the model of nuclear interactions assumed.

6.2 Brief Description of Other Models

The models, the predictions of which are compared in this Chapter, vary considerably in the details of their representation of nuclear interactions, and in the method of solution of the equations describing the propagation of the cosmic rays through the atmosphere. Some of the more important parameters used by the various authors to describe nuclear interactions are given in Table 6-1.

TABLE 6-1 PARAMETERS OF NUCLEAR INTERACTION MODELS

PARAMETER	PRESENT MODEL	JABS, 1968	ADAIR, 1968	O'BRIEN 1971
Nucleon Interaction Length, $\lambda_N (g.cm^{-2})$	80	70	88	80
Pion Interaction Length, $\lambda_\pi (g.cm^{-2})$	120	74	110	80
Mean Nucleon Inelasticity, $\bar{K}$	0.5	0.4	Not specified	0.5
Mean Pion Inelasticity, K_π	1	0.4	-	-
Mult. Law n(E)	$E^{0.25}$	ln(E)	see §6.2.3	E^{ℓ}
Dist. of Inelasticity g(K)dK	Rectangular between 0.25 and 0.75	$K^2 \exp\left[-\frac{3}{\bar{K}} K\right] dK$	-	Fixed
Energy Spectrum of Secondaries $f(E, E_p)dE$	C.K.P*	C.K.P*	$\exp\left[-E/E_o\right]$ E_o = 400 MeV	Power Law

* After Cocconi et al. 1961

6.2.1 The Model used by Jabs, 1968

The various interaction parameters were chosen to fit the experimental data obtained from experiments using accelerators and cosmic rays as sources of high energy particles. In addition to the parameters listed in Table 6-1 a fraction (0.2) of the secondary particles produced were considered to be kaons.

Differential equations describing the propagation through the atmosphere of cosmic rays were set up and solutions were obtained using the method of successive generations and a primary spectrum denoted by "E" in §5.6.

6.2.2 The Model used by O'Brien, 1971

The multiplicities of secondary particles produced in nuclear interactions used in this model were predicted by a power law model (see O'Brien, 1969, 1971) which includes an arbitrary parameter, ℓ (see table 6.1). The best value of ℓ was selected to be 0.216 on a least squares criterion from a consideration of experimental values of the multplicity as a function of incident energy. Good agreement was obtained between predictions of multiplicities and the experimentally observed values, but the representation of the energy spectrum of secondaries is simple. Kaon production was not considered and all pion interactions were regarded as absorptions, leading to an underestimate of the sea level muon spectrum estimated from the present work to be ~20% (see §5-2)

Atmospheric cosmic ray fluxes were obtained as analytic solutions to an approximate form of the Boltzmann equation describing the nucleonic cascade in the atmosphere. The form of the primary spectrum used was not specified by O'Brien, 1971, but it is considered to be that given by Peters, 1958, for energies greater than 10 GeV/c nucleon, and is of the form

$$\log N = 6.73 - 0.0495\ (11.7 + \log(1.7+E_p))^2\ \text{cm}^{-2}\text{sec}^{-1}\text{ster}^{-1}$$

for proton primaries where N is the intensity of protons of kinetic energy $>E_p$. This spectrum is in good agreement with the spectra used for the present model at energies ~10 GeV/nucleon, but becomes significantly higher at larger energies. Spectra with the same shape but with different constant

terms were used for primary nuclei heavier than protons. None of the primary particle spectra used with the other models considered here are directly comparable with this spectrum; spectrum 'E',(see §5-6) is the nearest and is used for the comparison.

6.2.3. The Model used by Adair, 1968

Adair constructed a model of very high energy nucleon-nucleon interactions assuming that the dominant processes could be described in terms of the production of two centres of excitation (fireballs). On the basis of this model, meson production multiplicities and nucleon inelasticity factors were derived and found to be in accord with experimental observations of nucleon-nucleon interactions.

A one-dimensional Monte Carlo simulation of the propagation of cosmic rays was made, neglecting kaon production and treating all meson interactions as absorptions.

The spectrum of primary nucleons used was

$$S(E_p)\, dE_p = 2.65\ 10^4\ E_p^{-2.67}\ dEp\ \ m^{-2}sec^{-1}st^{-1}GeV^{-1}$$

The most similar spectrum used in the present work was that of Schmidt et al. denoted by spectrum C (see §5-6) which is used for comparison with Adair's model.

6.3 The Predicted Proton Spectrum at Sea Level

The energy spectrum of primary cosmic rays is generally taken to be represented by a power law in energy with an exponent which is either a constant over the whole range of energy considered or only a slowly varying function of energy. It has been suggested by Pal and Peters, 1964, that the nucleon spectrum will not be changed by diffusion through the atmosphere. However, this will only be true if ionisation-energy loss of protons and fluctuations in the inelasticity of nucleon-nucleus collisions are ignored and if the mean inelasticity is independent of collision energy. Allowance for these factors, in particular the ionisation-energy loss, will change the form of the nucleon spectra in the atmosphere and will lead to a reduction

in intensity at momenta of a few GeV/c, where the typical ionisation energy loss of 1 GeV is significant. Thus, at low momenta, it is not expected that the observed proton spectra will follow the shape of the primary spectrum, and, for momenta less than 10 GeV/c, it is considered that on this basis the spectrum measured in the present experiment will be a better representation of the actual spectrum at such low momenta than that of Brooke and Wolfendale, 1964.

Figure 6.1 gives the predicted momentum spectra of protons at sea level derived from the models of Jabs and O'Brien and from the present model with the primary spectrum 'E'. It can be seen that the predictions of Jabs and the present model are in good agreement at momenta less than 10 GeV/c although the flattening of the spectrum at low momenta is not so pronounced in Jabs prediction because ionisation energy loss was neglected. However, the prediction of O'Brien appears to be significantly lower than the present model at momenta less than ~50 GeV/c. This discrepancy is difficult to explain since the spectrum of nucleons depends only on the values of interaction length and inelasticity assumed for the nucleon-nucleus interactions used in the model. From table 6.1 it can be seen that the values used in the model of O'Brien and the present model are identical. However, O'Brien uses a fixed value of inelasticity while Jabs and the present model allow the value of inelasticity in an interaction to fluctuate. The effect of the form of thedistribution of inelasticity on the sea level proton spectrum has not been investigated and so it is not known at present whether this discrepancy can arise from such a cause.

The transparent overlay of figure 6-1 shows the proton spectrum as measured in the present experiment. As noted in Chapter 5, there is reasonable agreement between this measurement and the prediction of the present model and hence also reasonable agreement with the prediction of Jabs over the range of momenta in which there is reliable experimental data. However, the spectrum of O'Brien can be seen to be in poor agreement with the measurement and to have a significantly different spectral shape.

Fig. 6.1 The Spectrum of Protons

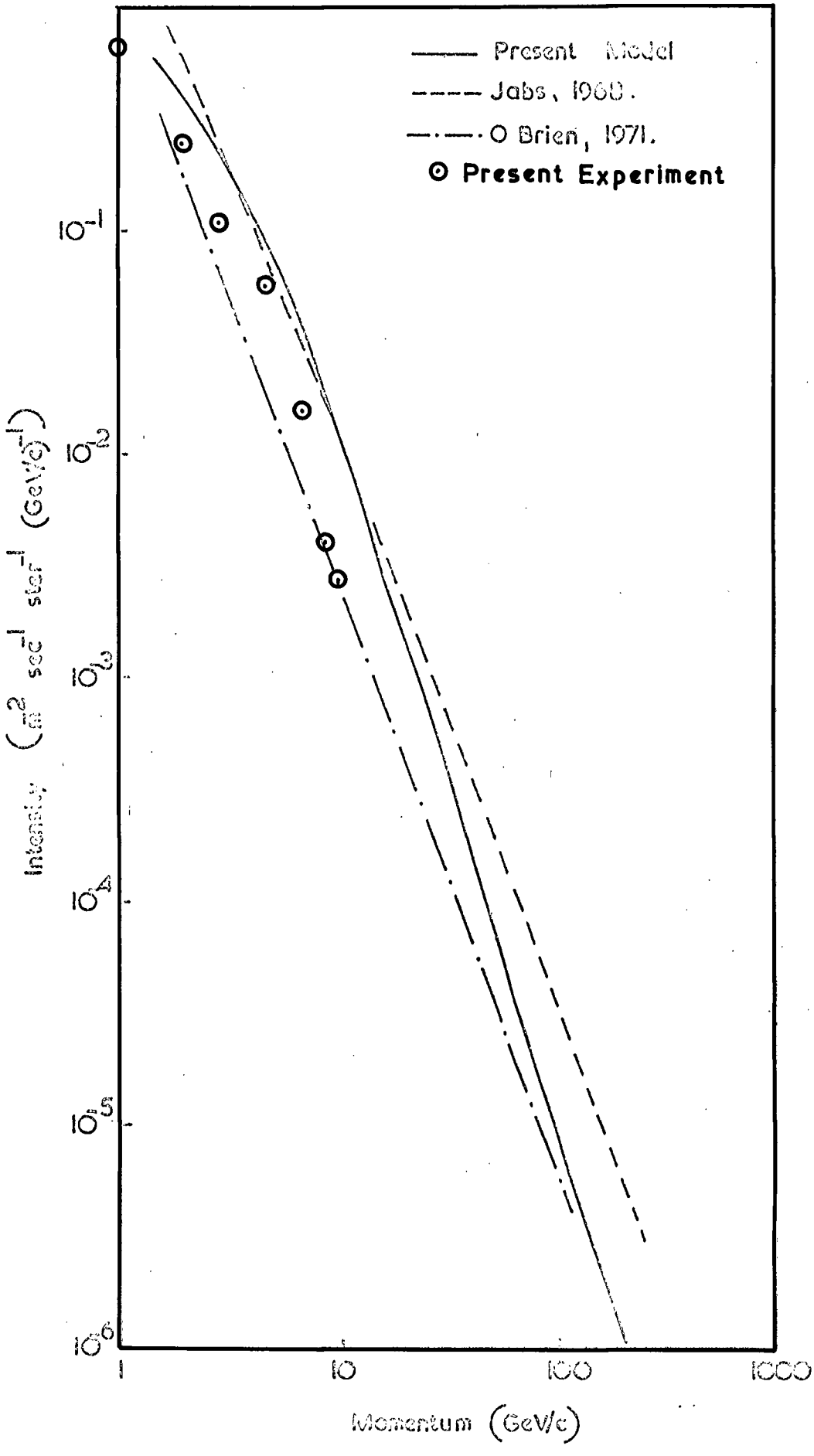

6.4. The Predicted Pion Spectrum

Figure 6-2 shows the momentum spectra of negative pions predicted by the various models discussed above. It can be seen that the three models do not produce consistent predictions over the whole range of momentum although the present model is in good agreement with that of Jabs at low momenta. However as the momentum increases the prediction of Jabs falls below that of the present model to an increasing extent. It should be noted that the spectral shapes predicted by O'Brien and the present model are very similar but the spectrum of O'Brien is a factor of ~2.5 lower in absolute intensity.

The most important difference between the model of Jabs and that described in this thesis is in the law relating the mean multiplicity of particles produced in a nuclear interaction to the kinetic energy of the incident particle. Jabs used a law of the form

$$n_s(E) = 1.69 \ln (0.3E + 1.4)$$

compared with a power law with exponent 0.25 as used in the present model. The mean multiplicities produced by these two expressions are virtually identical for interactions at energies which are of importance for the pions of low momenta. However, as the incident energy increases the discrepancy between the two laws increases so that good agreement should not be expected over the whole range of momentum considered here.

The multiplicity laws used by O'Brien and the present model are rather similar and so it is not unreasonable that the spectral shapes should be the same. However, from the comparison of the predicted proton spectra from the two models (§6.3), there is seen to be a discrepancy between the prediction from the two models. This discrepancy may also account for part, or all, of the discrepancy between the predicted pion spectra; in addition O'Brien ignores pions produced by pion-nucleus interactions. It is shown in figure 5.1 that this has only a small (~20%) effect on the predicted muon spectrum. However, because of their shorter lifetime and shorter interaction length pions which survive to sea level will be secondaries of interactions which occur much deeper in the atmosphere than will muons of the same momentum. Thus surviving pions are

produced in regions of the atmosphere where the primary particles have already been considerably degraded in energy and in which pions, of an energy sufficient to produce secondaries of a few GeV/c, constitute a significant fraction of the cosmic radiation. Thus it is expected that the effect on the sea level pion spectrum of neglecting pion interactions will be greater than on the sea level muon spectrum. The precise magnitude of this effect is not, at present, known; it is likely that the predicted pion spectrum of O'Brien is an underestimate.

The overlay to figure 6-2 gives the experimental data measured in the present experiment and those reported by Brooke et al., 1964b. As noted earlier, there is a large discrepancy between these measurements, although the data of Brooke et al., should be increased by ~30% to allow for the different normalisation used in the two experiments. It can be seen that O'Brien obtained good agreement with the measurement of Brooke et al. although, as mentioned above, the prediction is probably an underestimate. Thus, since both the earlier measurement and prediction of O'Brien are underestimates it is possible that better agreement may be maintained when both are corrected. The predictions from the present model and that of Jabs are seen to be midway between the two sets of experimental data. It has been noted in §5-8 that there is some evidence that the present model gives an increased intensity of pions if the effects of 'scaling' distributions and the appropriate multiplicity law are considered; a preliminary investigation indicates that this leads to an increase of ~10% in the intensity at 5.6 GeV/c.

6.5 The Predicted Muon Spectra

Figure 6.3 shows the sea level momentum spectra of muons predicted by the various models described above. It can be seen that the predictions of Jabs and from the present model are in good agreement over most of the range of momentum considered here, although the discrepancy between the two predictions is largest at high momenta. This is as expected from a consideration of the energies of the primary particles which give rise

to these energetic muons. From figure 5.13, 5.14 it can be seen that the low energy muons are generated predominantly by low energy primary particles and the characteristics of the interactions of such particles are identical in both models.

The model of O'Brien predicts intensities which are significantly lower than predicted by the model of Jabs and that described here, as does the simulation of Adair. The magnitude of the discrepancy decreases as the muon momentum increases.

The measured spectrum of Allkofer et al., 1971, is shown on the transparent overlay. As noted in §5.9 , this spectrum is in reasonable agreement with the predictions from the present model at momenta greater than ~50 GeV/c. The agreement between the prediction of O'Brien and the measured spectrum is good at all momenta, especially if the prediction is increased to account for those muons produced in pion-nucleus interactions.

The discrepancy between the predictions of the present model, and that of Jabs, and the observed spectrum at low momenta is difficult to explain other than as was suggested in §5.9. The use of 'scaling' distributions is not expected to affect the low momentum muons because of their relation to comparatively low energy primary particles. If a three-dimensional treatment of the present model leads to a significant improvement in the agreement between the prediction and observations, it should be noted that the predictions of O'Brien, to which a similar correction must be applied, will not be in such good accord with the observed data.

6.6 Conclusions

From the results discussed in the previous sections it can be seen that the predictions of the present model and of the model developed by Jabs are in good agreement with each other where this may be expected, i.e. in regions of secondary particle energy where the products of low energy primary particles are dominant.

It has been indicated (§6.2.2) that the primary spectrum used by O'Brien gives higher primary intensities, at energies greater than 10 GeV/nucleon, than the spectrum used for the other predictions; it may thus be expected that the predictions of O'Brien would indicate greater intensities for all particle fluxes at sea level. However, it is noted that O'Brien predicts lower intensities than the other models for all components.

The momentum spectrum of protons, as predicted by the present model and that of Jabs, is in good agreement with the observed spectrum as measured in the present experiment at low momenta. The intensities predicted by O'Brien are rather too low to be regarded as in acceptable agreement with this measurement.

The pion spectra predicted with the present model and the model of Jabs are in good agreement at low momenta, but both are significantly higher than that predicted by O'Brien. However, because of the large discrepancy between the two experimental observations no definite conclusion concerning the validity of the various models can be reached on the basis of this spectrum. Further experimental work will be required to resolve this discrepancy.

The measured sea level muon spectrum of Allkofer et al., 1971, is in reasonable agreement with all the predictions at high momenta and agrees very closely with the prediction of O'Brien at all momenta.

Thus, there is no single model of the propagation of cosmic rays through the atmosphere, which, when combined with a not implausible spectrum of the primary radiation, is, at present, sufficient to explain completely the momentum spectra of all components of the unaccompanied cosmic rays at sea level. The failure of the models to satisfactorily explain simultaneously both the proton and muon momentum spectra (especially the muon spectrum) must be regarded as a serious failing of the models as these spectra are well known experimentally.

CHAPTER SEVEN

SUGGESTIONS FOR FURTHER WORK.

7.1 The Unaccompanied Nuclear Active Particle Spectra

Reasonable agreement has been obtained between the measurements of the momentum spectrum of unaccompanied protons at sea level made in the present experiment and those of Brooke and Wolfendale, 1964. However, the intensity of the spectrum of pions measured in the present experiment is a factor of $\lesssim 2$ greater than that found by Brooke et al., 1964b. Thus the most obvious need is for a further measurement of the pion spectrum in order to resolve the large discrepancy between the two measurements.

In both experiments which measured the momentum spectra of unaccompanied nuclear-active particles (NAPs) it was assumed that all the negative NAPs at sea level were pions. In view of the recent results of Tonwar et al., 1971, and from the CERN I.S.R. experiments indicating that the cross-section for production of nucleon-anti-nucleon pairs in nucleon-nucleon interactions increases with the energy of the incident particle, it is important that the validity of this assumption should be checked. The best technique for the detection of anti-protons in the cosmic radiation is probably the use of a threshold Čerenkov light detector together with a measurement of the charge of the particle. A gas Čerenkov detector will distinguish anti-protons from negative pions at momenta up to ~30 GeV/c, while a water Čerenkov detector will be sensitive over a more limited range around 1 GeV/c. The addition of a water Cerenkov detector to the magnet spectrograph described in this thesis should be able to identify unaccompanied anti-protons of momentum ~1 GeV/c; such a detector has been recently installed (Diggory - private communication).

7.2 Nuclear-active Particles in Extensive Air Showers.

The results of the studies of NAPs in extensive air showers (EAS) described here indicate that measurements of the particle momentum and

charge are very difficult when a neutron monitor is used to identify the NAPs. The major drawback to the use of this technique is the diffuse nature of the response of the neutron monitor to the NAPs. This is illustrated in figure 3-8 , the impact distance distribution due to unaccompanied NAPs, which indicates that in 10% of cases the interaction which produced the response ocurred more than 30 cms away from the point of detection of the neutron. In an instrument of the size of the neutron monitor this leads to a sensitive area of ~0.3 m^2 and, in most EAS at small core distances there will be several tracks which would be NAP candidates. Thus a more precise technique for locating the nuclear interactions, e.g. multi-plate spark chamber or hodoscoped ionisation calorimeter, would probably give a significant improvement in the rate of acquisition of reliable data.

7.3 The Energy Spectrum of Primary Particles

The present data on unaccompanied NAPs near sea level are insufficient to enable any definite conclusions to be drawn concerning the energy spectrum of the primary cosmic radiation, although the primary spectrum measured by Grigorov et al., 1971, seems, on the basis of the present calculations, to be inconsistent with the measured proton spectrum near sea level. However, the results of the theoretical analysis presented in chapter 5 indicate that the sea level measurements which will be most sensitive to the primary energy spectrum in regions of high energy are the momentum spectrum of negative pions and the spectrum of protons at momenta >100 GeV/c. Good statistical accuracy will be required in both these measurements in order to distinguish between the alternative primary spectra, and this will lead to considerable experimental difficulty because of the very low fluxes of particles of these types and energies.

7.4 Models of Atmospheric Propagation

Good agreement was obtained between the predictions of the present model and the measured spectra of protons, but the predicted muon spectrum was significantly higher than the measured spectrum at momenta $<$ 50 GeV/c.

Various possible limitations of the model of the propagation of particles through the atmosphere used here have been noted in chapter 5, i.e. approximations in the treatment of interactions, the one-dimensional propagation, and constant energy loss of muons. These limitations can be removed and may lead to a better prediction of the sea level momentum spectrum of muons which must be adequately predicted by any acceptable model since the experimental data are the most accurate available.

Recent experimental data from the CERN I.S.R. experiments indicate that the variation of the mean multiplicity of particles produced in a nuclear interaction with the energy of the incident particle is better represented by an expression which rises somewhat more slowly than that used in the present work up to an energy of 1500 GeV. Some preliminary work has been done using this multiplicity law although conclusions are not possible at present.

The results of the experiments of Tonwar et al., 1971, in EAS and those using the CERN I.S.R. system indicate an increased production of nucleon-anti-nucleon pairs and of kaons in interactions at high energies. Although pions will still be the most commonly produced particles, the increased proportions of these alternative particles will absorb a fraction of the available energy so that the details of the propagation of particles through the atmosphere will be altered. Clearly, to obtain the most accurate simulation of cosmic ray propagation, the production of particles other than pions should be allowed in the model. In principle, all these modifications can be included in the Monte Carlo model although the computing time for each simulation will be increased. However, because of the steep primary spectrum, this should not be a great limitation since simulations of low energy primary particles will be of considerable interest. Thus the theoretical studies described here could be extended, but with greater statistical accuracy and a more realistic model, to give predictions of the fluxes of anit-protons and kaons, as well as protons, pions and muons at sea level.

APPENDIX A

THE DISTRIBUTION OF LATERAL SEPARATION OF THE TRACKS IN THE MID-PLANE OF THE SPECTROGRAPH

From figure A1 it can be seen that the distribution in the lateral separation, Δ, is given by

$$f(\Delta) = \bar{x}_1 - r_1 \tan \bar{\psi}_1 - F(\bar{x}_1 - x_1) - r_1 P (\bar{\psi}_1 - \psi_1)$$

$$- \bar{x}_o + r_o \tan \bar{\psi}_o + G(\bar{x}_o - x_o) + r_o Q (\bar{\psi}_o - \psi_o)$$

where $\bar{\psi}_o$, $\bar{x}_o$, $\bar{\psi}_1$, $\bar{x}_1$ are the parameters of the actual trajectory and ψ_o, x_o, ψ_1, x_1 are the parameters of the best fit estimate of the trajectory and F, G, P, Q are the distributions of the differences between the actual and estimated parameters. But

$$\bar{x}_o - r_o \tan \bar{\psi}_o = \bar{x}_1 - r_1 \tan \bar{\psi}_1$$

$$\therefore f(\Delta) = G(\bar{x}_o - x_o) + r_o Q (\bar{\psi}_o - \psi_o) - F(\bar{x}_1 - x_1) - r_1 P (\bar{\psi}_1 - \psi_1)$$

Thus the distribution of Δ will have a standard deviation, σ_Δ, given by

$$\sigma_\Delta^2 = \sigma_{x_o}^2 + \sigma_{x_1}^2 + r_o^2 \sigma_{\psi_o}^2 + r_1^2 \sigma_{\psi_1}^2$$

where σ_{ψ_o}, σ_{ψ_1} are the standard deviations of the distributions of $(\bar{\psi}_o - \psi_o)$ and $(\bar{\psi}_1 - \psi_1)$ and σ_{x_o} and σ_{x_1} are the standard deviations of $(\bar{x}_o - x_o)$ and $(\bar{x}_1 - x_1)$ respectively.

But σ_{ψ_o} and σ_{ψ_1} are made up of two parts; errors due to scattering in the material of the spectrograph, σ_c, and errors due to instrumental noise, σ_n.

$$\therefore \sigma_{\psi_o}^2 = \sigma_c^2 + \sigma_n^2 \quad \text{and} \quad \sigma_{\psi_1}^2 = \sigma_c^2 + \sigma_n^2$$

since there is the same material in each half of the spectrograph

But $\sigma_c^2 \propto \frac{1}{p^2} \propto |\Delta\psi|^2$

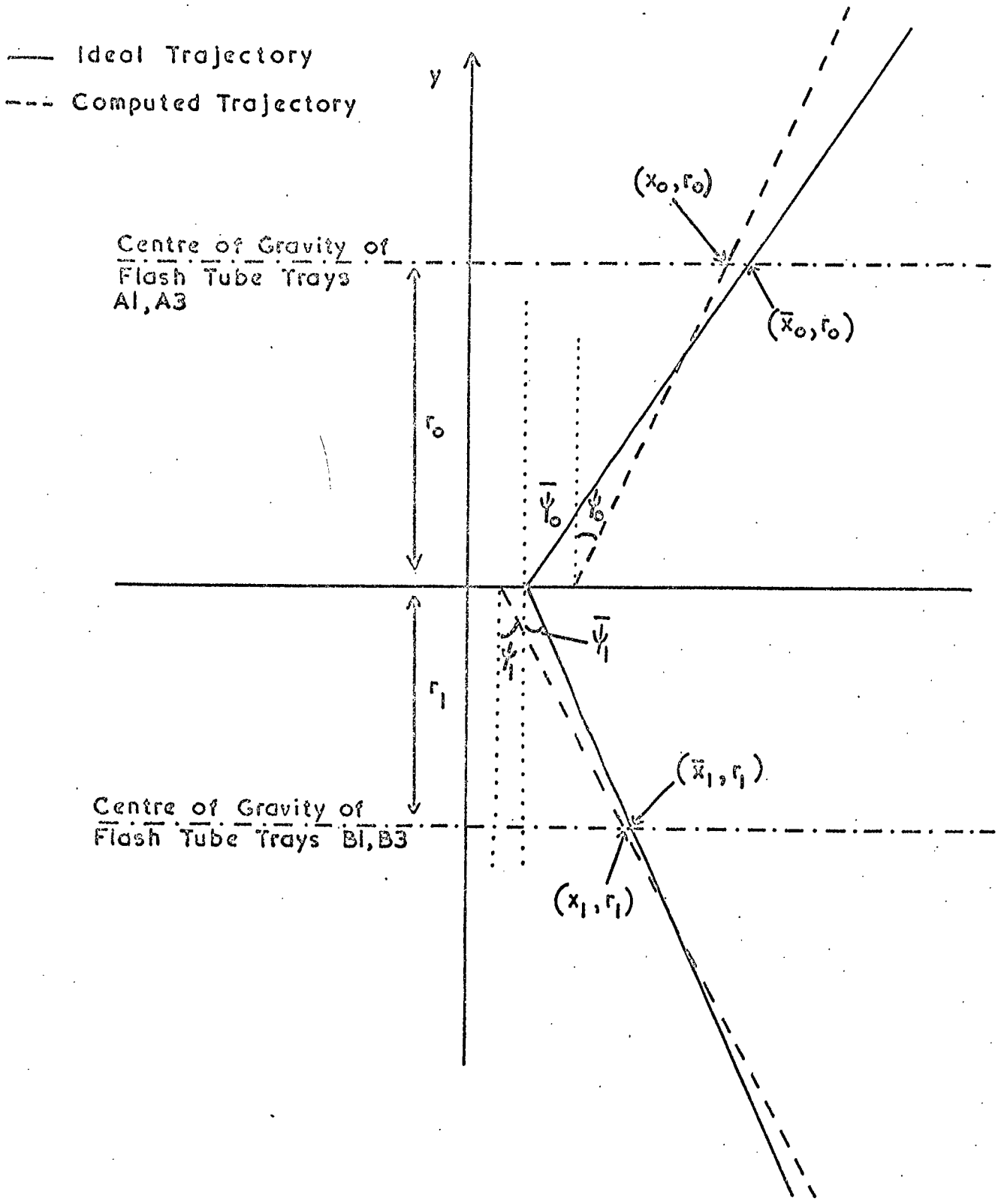

Fig. A1 The Co-ordinate System Used For The Determination of The Instrumental Noise

$$\therefore \quad \sigma_{\Delta}^{2} = K(r_o^2 + r_1^2) \ |\Delta\psi|^2 + (r_o^2 + r_1^2) \ \sigma_n^2$$

$$= C \ |\Delta\psi|^2 + (r_o^2 + r_1^2) \ \sigma_n^2$$

neglecting σ_{x_o} and σ_{x_1} compared with $(r_o^2 + r_1^2) \ \sigma_n^2$.

Thus a graph of σ_{Δ}^2 against $|\Delta\psi|^2$ should be a straight line with an intercept on the σ_{Δ}^2-axis of $(r_o^2 + r_1^2) \ \sigma_n^2$.

REFERENCES

ALLKOFER, O.C., CARSTENSEN, K. AND DAU, W.D., 1971, Proc. 12th Int. Conf. on Cosmic Rays, Hobart, 4, 1314.

ADAIR, R.K., 1968, Phys. Rev., 172, 5, 1370-1380.

ADAMS, N. and BRADDICK, H.J., 1951, Z. Naturf., 6a, 592.

ANTIPOV, Yu. M., et al., 1971, Phys. Letters, 34B, 2, 164.

BALASUBRAHMANIAN, V.K., et al., 1962, Proc. Int. Conf. Cosmic Rays, Kyoto, III, 8.

BENNETT,S., and GREISEN, K., 1961, Phys. Rev., 124, 1982-1987.

BRADT, H., La POINTE, M. and RAPPAPORT, S., 1965, Proc. 9th Int. Conf on Cosmic Rays, 2, 651.

BRADT, H.V. and RAPPAPORT, S.A., 1967, Phys. Rev., 164, 5, 1567-83.

BROOKE, G. and WOLFENDALE, A.W., 1964, Proc. Phys. Soc. 83, 843

BROOKE, G., HAYMAN, P.J., KAMIYA, Y. and WOLFENDALE, A.W., 1964a. Proc. Phys. Soc., 83, 853.

BROOKE, G., MEYER, M.A. and WOLFENDALE, A.W., 1964b, Proc. Phys. Soc., 83, 871.

BULL, R.M., COATES, D.W., NASH, W.F. and RASTIN, B.C., 1962, Nuovo Cim., (Suppl.) 23, 39.

BULL, R.M., NASH, W.F. and RASTIN, B.C., 1965, Nuovo Cim., 40A, 365.

CHATERJEE, B.K., et al., 1965, Proc. Int. Conf. on Cosmic Rays, London, 2, 734.

COCCONI, G., KOESTER, L.J., PERKINS, D.H., 1961, UCRL-10022, 167-190.

COCCONI, G., COCCONI-TONGIORGI, V.C. and WIDGOFF, M., 1950, Phys. Rev., 79, 768.

CONVERSI, M., FOCARDI, S., FRANZINETTI, C., GOZZINI, A. and MURTAS, P., 1955, Suppl. Nuovo Cim., 4, 234.

CONVERSI, M. and GOZZINI, A., 1955, Nuovo Cim., 2, 1, 189-91

COXELL, H. and WOLFENDALE, A.W., 1960, Proc.Phys. Soc., 75, 3, 378.

EARNSHAW, J.C., ORFORD, K.J., ROCHESTER, G.D., SOMOGYI, A.J., TURVER, K.E. and WALTON, A.B., 1967, Proc. Phys. Soc., 90, 91-108.

FIELDHOUSE, P., HUGHES, E.B., and MARSDEN, P.L., 1962, J. Phys. Soc. Japan, 17, Suppl. A2, 318.

FILTHUTH, H., 1956, Z. Naturf., 10a, 219.

GARDENER, M., KISDNASAMY, S., ROSSIE, E., and WOLFENDALE, A.W., 1957, Proc. Phys. Soc. B, 70, 687.

GIACOMELLI, G., 1970, Progress in Nucl. Phys. 12, 2, 77.

GREISEN, K., 1960, Ann. Rev. Nucl. Sci., 10, 63.

GRIFFITHS, W.K., HARMAN, C.V., HATTON, C.J. and RYDER, P., 1966, Proc. Int. Conf. Cosmic Rays. London, 1, 475.

GRIGOROV, N.L., GUBIN, Yu.V., RAPPOPORT, I.D., SAVENKO, I.A., YAKOVLEV, B.M., AKIMOV, V.V. and NESTEROV, V.E., 1971, Proc. 12th Int. Conf. Cosmic Rays Hobart, 5, 1746.

GUNN, J.E., and OSTRIKER, J.P., 1969, Phys. Rev. Letters, 22, 14, 728.

HATTON, C.J., 1971, Prog. in Elem. Part and Cosmic Ray Physics, X, 1.

HATTON, C.J. and TOMLINSON, E.V., 1968, Nuovo Cim., 53B, 63.

HAYMAN, P.J. and WOLFENDALE, A.W., 1962, Proc. Phys. Soc., 80, 710.

HOOK, J.R., MASLIN, G.C., ORFORD, K.J. and TURVER, K.E., 1970, Acta. Phys. Acad. Scient. Hung., 29, Suppl. 3, 475.

HUGHES, E.B., MARSDEN, P.L., BROOKE, G., MEYER, M.A. and WOLFENDALE, A.W., 1964, Proc. Phys. Soc., 83, 239.

JABS, A., 1968, Zeit, fur Physik, 212, 222-234.

JABS, A., 1971, To be published.

JOSEPH, P.M., 1969. Nucl. Inst. and Methods, 75, 13-17.

KAPLON, M.F., and RITSON, D.M., 1952, Phys. Rev., 88, 386.

KAPLON, M.F., RISTON, D.M. and WOODRUFF, E.P., 1952, Phys. Rev., 85, 933.

KOSHIBA, M., NOZAKI, T., TOTUSKA, Y. and YAMADA, S., 1967, Proc. 10th Int. Conf. on Cosmic Rays, Calgary, Canad. J. Phys., 46, 10, 3, 671-4.

MATANO, T., NAGANO, M., SHIBATA, S., SUGA, K. and HASEGAWA, H., 1965. Proc. 9th Int. Conf. Cosmic Rays, London, 2, 672.

McDIARMID, I.B., 1959. Canad. J. Phys., 37, 79.

MYLROI, M.G., and WILSON, J.G., 1951, Proc. Phys. Soc. A, 64, 4o4.

O'BRIEN, K., 1969. Nucl. Instr. Meth., 72, 93.

O'BRIEN, K., 1971, Nuvov Cim., 3A, 3, 521-547.

O'CONNOR, P.V. and WOLFENDALE, A.W., 1960, Nuovo Cim., (Suppl 2), 15, 202.

OGILVIE, K.W., 1955, Canad. J. Phys., 33, 746.

ORFORD, K.J., 1968, Ph.D Thesis, University of Durham.

PAK. W., and GREISEN, K., 1962, Phys. Rev., 125, 1668.

PAL, Y. and PETERS, B., 1964, Mat. Fys. Medd. Dan. Vid. Selsk, 33, 15.

PETERS, B., 1958, Cosmic Rays in Handbook of Physics, Eds. Condon, E.U., and Odishaw, H. (New York).

PINKAU, K., 1964, Fortschr, Phys., 12, 139.

ROSSI, B., 1948, Rev. Mod. Phys., 20, 537.

SCHMIDT, W.K.H., PINKAU, K., POLLVOGT, U., and HUGGETT, R.W., 1969. Phys. Rev., 184, 5, 1279.

SIMPSON, J.A., 1949a, Echo Lake Conf. on Cosmic Rays, 175.

SIMPSON, J.A., 1949b, Echo Lake Conf. on Cosmic Rays, 252.

SIMPSON, J.A., 1957, Ann. I.G.Y., (London: Pergamon Press) Part VII.

SIMPSON, J.A., FONGER, W. and TREIMAN, S.B., 1953, Phys. Rev., 90, 93.

STAUBERT, R., TRÜMPER, J., WIEDECKE, L., WOLTER, W., BÖHM, E., FRITZE, R., MIE, F., SAMORSKY, M., 1970, Acta. Phys. Acad. Scient. Hung, 29, Suppl. 3, 661.

SUBRAMANIAN, 1962, Ph.D Thesis, University of Madras.

TONGIORGI, V.C., 1949, Phys. Rev., 75, 1532.

TONWAR, S.C., NARANAN, S. and SREEKANTAN, B.V., 1971, Lett. Al. Nuovo Cim., 1, 13, 531.

WEBBER, W.R., 1967, HANDBUCH DER PHYSIK, XLVI, 2, 181.

WEBBER, W.R., 1969, Proc. 11th. Int. Conf. Cosmic Rays. Budapest, Invited Papers and Rapporteur Talks (Central Research Ints. for Phys).

WILSON, J.G., ALLEN, H.R., LILLICRAP, S.C., REID, R.J.O., and TURVER, K.E. 1963, Proc. 8th Int. Conf. Cosmic Rays, Jaipur, 4, 27.

ACKNOWLEDGEMENTS

I would like to thank the following for their help in various ways:-

Professor G.D. Rochester, F.R.S., for the provision of the facilities of his laboratories which made this study possible.

Dr. K.E. Turver, my supervisor, for his advice and encouragement at all times.

My Colleagues, Mr. I.S. Diggory, Mrs. H.E. Dixon, Dr. J.C. Earnshaw, Mr. I.A. Jenkins, Mr. G.C. Maslin and Dr. K.J. Orford for their contributions to the construction and operation of the equipment and analysis of the data.

Miss A.M. Bevils for her patient work during the arduous task of data reduction and for drawing the diagrams for this thesis.

The technical staff of the Department of Physics, particularly Mr. W. Leslie and Mr. H. Davison, for their ready assistance in the constructional work.

Mrs. D.A. Anson for typing this thesis.

The Science Research Council for the provision of a Research Studentship during the course of this work.